Structure, properties and function of viscin from berries of European mistletoe (*Viscum album* L.)

vorgelegt von
M. Sc.
Nils Horbelt

an der Fakultät III – Prozesswissenschaften
der Technischen Universität Berlin
zur Erlangung des akademischen Grades

Doktor der Ingenieurwissenschaften
– Dr.-Ing. –

genehmigte Dissertation

Promotionsausschuss:

Vorsitzender:	Prof. Dr. Dietmar Auhl
Gutachterin:	Prof. Dr. Claudia Fleck
Gutachter:	Prof. Dr. Peter Fratzl

Tag der wissenschaftlichen Aussprache: 12. März 2021

Berlin 2021

Abstract

Viscin is a term used for an adhesive mucilaginous tissue covering the seeds of most mistletoe species which plays a crucial role in the seed dissemination of this hemiparasitic plant. The dissemination usually occurs with the help of birds which feed on the mistletoe berries. During feeding or the subsequent defecation the adhesive seeds are deposited onto a potential host tree where the seed can successfully germinate. This work deals with the analysis of structure-function-relationships of berries from the European mistletoe (*Viscum album* L.) with a specific focus on the viscin tissue. The viscin of some *V. album* L. subspecies shows the remarkable ability to form long adhesive fibers of more than a meter in length as well as the formation of adhesive films, both supporting a successful seed-host attachment. This work aims to get a better understanding of this film and fiber formation process and to investigate viscin as a potential role model for the development of new bio-inspired materials.

At first the berries of two closely related subspecies of *V. album* L. will be investigated, one growing exclusively on conifers, the other one on deciduous trees, where only the latter shows the characteristic formation of adhesive fibers. With the help of histological investigations and mechanical examination of different tissue types within the berry it could be shown, that the capacity for fiber formation can be localized to a specific tissue type found exclusively in the tissue of the subspecies growing on deciduous trees, which was completely absent in the other subspecies. Microscopic investigations showed that this tissue mainly consists of elongated so-called viscin cells densely packed into bundles or clusters. The cell walls of these cells consist of cellulose fibrils with an unusual orientation – perpendicular to the cell long axis – which are embedded into a non-cellulosic matrix. These cells can be mechanically drawn into micron sized filaments which co-align in parallel in the drawing direction to form the macroscopic viscin fibers.

In the second section the rapid fiber formation process is investigated in more detail. To follow this highly dynamic process we developed protocols and drawing devices for controlled manual and semi-automated fiber drawing which allowed us to investigate the structural changes in the transition zone between native viscin cell bundle and the emerging fiber. Applying synchrotron based X-ray diffraction and in situ polarized light microscopy we could show, that cellulose microfibrils inside the viscin cell walls undergo a dramatic reorganization upon mechanical load and align almost perfectly along the drawing direction. Micro-mechanical investigations under controlled climatic conditions showed an impressive tensile stiffness (~14 GPa) of dried viscin fibers and also revealed that the stiffness highly depends on the fiber moisture content. Indeed, the fibers revealed a 35x reduction in stiffness between the dry (0% relative humidity) and the wet state (90% relative humidity). An in-depth structural examination with synchrotron based X-ray diffraction revealed new insights on the fiber ultrastructure: highly aligned slender cellulose microfibrils showed the presence of crystalline domains with a high aspect ratio. Furthermore, the microfibrils revealed a highly regular interfibrillar spacing which increased during water uptake, probably

due to a swelling of the matrix, and decreased fully reversibly during water loss. Based on a model we discuss the possible impact of our ultrastructural findings on the macroscopic fiber properties and the fiber formation process. It is suggested that the matrix plays a crucial role which acts like a lubricant in the wet state allowing the cellulose microfibrils to slide past one another and firmly cements them in the dry state.

The last part of this work we demonstrate and discuss possible application of the adhesive viscin. Here we examine the viscin from the perspective of a versatile, fiber-reinforced natural adhesive. Investigations with polarized light microscopy and scanning electron microscopy reveal how freshly formed hydrated viscin fibers can self-adhere and how this can be used to build more complex 2D and 3D structures. Furthermore, we show how the adhesive properties of dried fibers (non-sticky) can be reactivated by simple rehydration which enables the viscin fibers to weld via the in-built adhesive. Apart from the self-adhesive properties and its natural function to glue the seed onto the host tree, we could show that viscin is able to adhere (under load) to a broad range of different materials like wood, metals, glass and polymers (e.g. PP, PE, PTFE) as well as biological materials such as skin and cartilage. Finally, we demonstrate how mechanically isolated viscin can be drawn into freestanding, quickly drying and dimensionally stable 2D films. Based on these findings and following ancient traditions, we demonstrate potential application of viscin as a fast-drying liquid wound sealing to treat skin injuries.

Zusammenfassung

Als Viscin wird ein klebrig schleimiges Gewebe bezeichnet, welches die Samen der meisten Mistelarten umgibt und das entscheidend an der Verbreitung der Samen dieser halbparasitären Pflanzen beteiligt ist. Die Verbreitung erfolgt in der Regel durch Vögel, die sich von den Beeren der Misteln ernähren und beim Fressen oder der anschließenden Ausscheidung den klebrigen Samen auf einem potentiellen Wirtsbaum hinterlassen, wo er erfolgreich keimen kann. Diese Arbeit beschäftigt sich am Modellsystem der Weißbeerigen Mistel (*Viscum album* L.) mit der Strukturanalyse der Mistelbeeren mit speziellem Fokus auf dem Viscingewebe und seinen funktionellen Eigenschaften. Das Viscin einiger Unterarten dieser Mistelspezies weist die besondere Eigenschaft auf, in meterlange klebrige Fäden sowie Filme ausgezogen werden zu können, welche die Wahrscheinlichkeit der erfolgreichen Samenanheftung auf dem Wirt entscheidend unterstützen. Ziel dieser Arbeit ist es, diesen Entstehungsprozess von adhäsiven Fäden und Filmen besser zu verstehen und das Viscin ferner auf sein Potential als biologisches Modellsystem für die Entwicklung neuer biologisch inspirierter Materialien zu überprüfen.

Zu Beginn wurden die Beeren zweier engverwandter Unterarten von *V. album* L. untersucht, von denen eine exklusiv auf Nadelbäumen und die andere auf Laubbäumen wächst, jedoch nur Letztere die charakteristischen, klebrigen Fäden aufweist. Durch histologische Untersuchungen und mechanische Prüfungen einzelner Gewebetypen im Inneren der Beere konnte gezeigt werden, dass die Entstehung der Fäden auf einen Gewebetyp im Viscin der Laubholzmistel zurückzuführen ist, der in der Nadelholzmistel schlicht fehlt. Mikroskopische Untersuchungen ergaben, dass dieses Gewebe hauptsächlich aus langgestreckten sogenannten Viscinzellen besteht welche in dichtgedrängten Bündeln oder Clustern organisiert sind. Die Zellwände dieser Zellen besitzen Zellulosefibrillen mit einer ungewöhnlichen Orientierung quer zur Faserlängsachse, eingebettet in eine zellulosefreie Matrix und lassen sich mechanisch in lange, wenige Mikrometer dicke Filamente ausziehen, welche sich in Zugrichtung parallel aneinanderlagern und so die makroskopischen Viscinfäden bilden.

Im zweiten Abschnitt wird der Entstehungsprozess dieser Fäden genauer Untersucht. Zur Verfolgung dieses höchst dynamischen Prozesses wurden Protokolle und Zugeinrichtungen für ein kontrolliertes manuelles und semi-automatisches Fadenziehen entwickelt. Dies ermöglichte die Untersuchung der strukturellen Veränderungen im Übergangsbereich zwischen dem nativen Viscinzellbündel und des daraus entstehenden Fadens. Mit Hilfe synchrotronbasierter Röntgenbeugung und in situ Polarisationsmikroskopie wurde gezeigt, dass sich die Zellulosemikrofibrillen in den Viscinzellen bei mechanischer Last reorientieren und hochgradig entlang der Zugachse ausrichten. Mikrozugversuche an handgezogenen Fäden unter klimatisch kontrollierten Bedingungen ergaben eine beindruckende Zugsteifigkeit (~14 GPa) der getrockneten Viscinfäden, zeigten aber zugleich, dass die Steifigkeit der Fäden stark von ihrem Feuchtegehalt abhängt. Diese zeigten eine dramatische Reduzierung der Steifigkeit um Faktor 35 zwischen 0% und 90% relativer Luftfeuchtigkeit. Eine

eingehende strukturelle Untersuchung mittels synchrotronbasierter Röntgenbeugung lieferte neue Erkenntnisse über die Ultrastruktur der Fäden: Hochgradig ausgerichtete schlanke Zellulosemikrofibrillen weisen kristalline Domänen mit einem hohen Längen-/Breitenverhältnis auf. Zudem weisen die Mikrofibrillen untereinander stark regelmäßige Abstände auf, welche sich bei Feuchteaufnahme, vermutlich durch ein Quellen der Matrix, vergrößern und bei Feuchteabgabe vollständig reversibel wieder verringern. In einem Modell diskutieren wir, wie sich die Erkenntnisse über die Ultrastruktur und deren Änderung in Abhängigkeit der Feuchtigkeit auf die makroskopischen Eigenschaften der Fasern und den Prozess des Fadenziehens auswirken könnten. Eine entscheidende Rolle dürfte hier die Matrix einnehmen, welche im feuchten Zustand das Abgleiten und Ausrichten der Zellulosefibrillen ermöglicht und sie im trockenen Zustand fest miteinander verklebt.

Im letzten Teil der Arbeit werden mögliche Anwendungsbeispiele des Viscins demonstriert und diskutiert. Dieser Teil beleuchtet das Viscin aus der Perspektive eines vielseitigen, faserverstärkten natürlichen Klebstoffs. Polarisations- und elektronenmikroskopische Untersuchungen zeigten, wie frischgezogene, hydrierte Viskinfäden in der Lage sind, miteinander zu verkleben und wie daraus komplexere 2D und 3D Strukturen hergestellt werden können. Zudem wird gezeigt, wie die adhäsiven Eigenschaften getrockneter (nicht klebender) Fäden durch einfaches Wiederbefeuchten reaktiviert werden können, was es ermöglichte, Viskinfäden durch ihren eingebauten Klebstoff miteinander zu verschweißen. Neben seinen selbstklebenden Eigenschaften und der natürlichen Funktion, den Samen am Wirtsbaum festzukleben, konnten wir zeigen, dass Viscin in der Lage ist, an zahlreichen unterschiedlichen Materialien wie Holz, Metallen, Glas, Kunstoffen (z.B. PP, PE und Teflon) sowie biologischen Materialien wie Haut und Knorpel unter Last zu haften. Schließlich zeigen wir, dass mechanisch isoliertes Viscin in freistehende, schnell trocknende und dimensionsstabile 2D Filme ausgezogen werden kann. Darauf aufbauend und in Anlehnung an antike Überlieferungen demonstrieren und diskutieren wir die potentielle Verwendung von Viscin als schnell trocknendem Flüssigverband zur Behandlung von Hautverletzungen.

Contents

1 Introduction and motivation

The European mistletoe (*Viscum album* L.) may be considered the most famous parasitic plant due to its special place in European history and folklore. The mistletoe plant grows in the canopies of predominantly broadleaved host trees. In European winter, it calls for people's attention when the orb-like evergreen shrub with its shining white berries can be seen from afar against the naked silhouette of the leafless host tree (Fig. 1-1).

Figure 1-1: The habitat of *Viscum album* ssp. *album*. Top: European mistletoe shrubs growing on poplar trees near Golm, Potsdam. Bottom left: heavily infected numerous mistletoe shrubs on leafless poplar trees. Arrows: individual shrubs may grow up to more than 2 m in diameter. Bottom center: single evergreen mistletoe shrub in winter on a leafless host (apple tree); Bottom right: mature mistletoe berries in winter/spring.

Mistletoe plants are intertwined with the history of human civilization in Europe, in particular for their perceived medical value and their role in religious practices and ceremonies. In the early Pre-Roman Britain mistletoe was worshipped by druids, an order of priests in Gaul, Ireland and Britain, as a sacred plant and its evergreen leaves and the mid-winter fruiting were seen as symbols for immortality and fertility (Calder 1983). During New Year celebrations the plant was cut by a druid with a golden sickle and caught in a white cloth. The branches were used in a subsequent ceremony in which animals (and occasionally humans) were sacrificed at the base of the host tree to request the goodwill of the gods. A modern tribute to this ancient ritual can be found in the cartoons of Asterix, the Gaul: Getafix, the Gallic druid, cuts the mistletoes with a golden sickle and uses the plant as the secret ingredient of his magic potion providing superhuman strength (Goscinny and Uderzo

1961). Consistent with its modern Gaelic name which means "All-heal", the mistletoe was also reported throughout history as a cure against a variety of diseases including epilepsy, vertigo, spasm, rheumatism and pertussis (LeStrange 1977), only to name a few. Infusions or concoctions from leaves and berries were prescribed to assist conception. Interestingly, in Austria it was believed to serve a contraceptive function. In Scandinavia and Britain mistletoe branches were nailed onto roof ridges and stable doors to protect people and cattle against diseases, thunder, fire and evil spirits, but also to bring good luck (Tubeuf 1923). From this it is assumed evolved the English tradition to decorate the house with mistletoe for Christmas where mistletoe shrubs or branches are nailed onto the ceiling, chandeliers or door frames. As tradition holds, on Christmas Eve one may kiss a person standing under a mistletoe. A common meaning here is that mistletoe stands again as a symbol for fertility and life. A young woman standing under the mistletoe who is not kissed was believed to stay unmarried for the year to come. This tradition has its origin in England where it can be traced back to the 17th century (Bull 1864). Later, this tradition spread to other countries and regions including Germany, France, Japan and North America where the "originally" used species *V. album* was substituted by the locally occurring lookalike *Phoradendron serotinum*. Although the modern kissing tradition cannot be traced to a specific druidic ritual, there is no doubt that the ancient pagan New Year ceremonies have somehow survived for more than two millennia and fused with one of the most prominent modern Christian festivals. A more detailed discussion of mistletoe related myth, legends and other folklore can be found in Kuijt (1969) and Tubeuf (1923).

Apart from the folklore and the attributed mystical properties, the mistletoe has been fascinating people for millennia due to the rather unique means by which the mistletoe seeds are spread and propagated. Already nearly 2500 year ago, Theophrastus (371-287 BC), a student of Aristotle reported that mistletoe seeds were disseminated with the help of birds to whom the berries serve as winter food source. This happens in one of the following ways: 1) Berries are picked by birds which successively try to feed on the pulp of the berry. Pecking into the berry leads to an instant adhesion of the bird's beak to the viscin, a sticky mucilaginous tissue which surrounds the seed. When the bird withdraws the beak the entrapped seed is pulled out of the berry. The "annoyed" bird typically tries to dislodge the sticky seed by wiping it off onto a nearby branch whereas small sticky threads are formed from the viscin that help to secure the seed onto the branch where it can germinate (Kuijt 1969; Heide-Jorgensen 2015). 2) Whole berries are swallowed by the bird and the seeds are regurgitated only a short time after. The sticky seeds, which are removed from most of the surrounding berry pulp and skin, are left on a nearby branch where they can germinate (Kuijt 1969; Heide-Jorgensen 2008). 3) Berries are swallowed by birds as a whole. Within only minutes, they pass through the bird's digestive system after which numerous seeds are excreted onto lower branches to which the seed adheres based on the sticky nature of the viscin. This often results in formation of long cellulosic adhesive fibers, connecting numerous seeds hanging loose like a string of pearls (Tubeuf 1923; Heide-Jorgensen 2008; Azuma et al. 2000), which by shaking in the wind may come into contact with a nearby branch where they adhere and germinate. The Greeks used this knowledge of mistletoe

propagation to produce birdlime (Latin – *viscum*), a natural glue made from the mistletoe berries which was spread on branches to capture birds for food. The irony of the poor bird actively spreading the seeds of a plant, which is then used to capture it later is succinctly captured in a Latin proverb about the mistle thrush (*Turdus viscivorus*), a bird whose scientific as well as its common name refers to its feeding habit: *Turdus ipse sibi cacat malum* (Plautus 254-184 BC). This was later translated by Robert Bland (1814) into a more poetic form: "The Thrush when he defiles the bough, Sows for himself the seeds of woe." But also the common English name of the mistletoe itself is thought to have its origin in this close relationship between birds and plants. According to some, the word mistletoe originates from the word mistiltan, a combination of the old German word “mist” (dung) and the old Anglo-saxon word “tan” (twig) leading to the literal translation of the “dung twig” (Calder 1983), which gives a very colorful description of the typical mistletoe lifecycle.

And although this ancient knowledge is well documented, it was forgotten or falsely rejected later, as demonstrated by Jean Bauhin, a reputated botanist from the 17th century who denied the parasitic lifestyle and rather believed mistletoes developed from the tree itself like warts from a human body (Docters van Leeuwen 1954). Kuijt (1969) assumes that Bauhin simply voiced the general opinion of his time. However, starting from the second half of the 19th century, numerous works confirm the intimate relationship between birds and mistletoes again, which is summarized by Tubeuf (1923, p. 609). While there was a renaissance of the interest in the mistletoes and their peculiar lifestyle, part of the knowledge about the bio-inspired birdliming got lost. Although Tubeuf (1923) collected numerous recipes on the making of birdlime from mistletoe, most attempts to reproduce the birdlime glue failed either due to missing or confusing information on either the correct ingredients (leaves, stalks, stems, berries) or even the proper mistletoe species.

In more recent years, there has been a renaissance in the interest of potential medical applications of mistletoe (e.g. thousands of publications dealing with complementary or even alternative anti-cancer treatment based on mistletoe extracts, reviewed in: Kleijnen and Knipschild 1994; Büssing 2000; Ernst et al. 2003; Horneber et al. 2008; Nazaruk and Orlikowski 2016). However, there is comparably little understood about mistletoe from the materials science perspective arising from a very limited number of publications on the topic. Yet, based on reports in the literature dating back to the ancient Greek philosophers concerning the adhesive prowess of mistletoe viscin and its tendency for spontaneously forming cellulosic fibers, this topic certainly deserves further examination. Therefore, the present work focuses specifically on the study of mistletoe viscin – the mucilaginous adhesive material surrounding the seed within mistletoe berries, understanding it both as a biological material whose properties have presumably evolved to facilitate seed dispersal of this hemiparasitic plant and as an exciting model system for sustainable bio-inspired adhesives and high-performance fiber. Indeed, apart from the fascinating biological implications for a possible co-evolution between host and mistletoe and between host and vector, mistletoe viscin serves as an intriguing model system for understanding the processing of cellulose-based materials under ambient conditions, which is especially relevant in light of

recent efforts to process nanocellulose isolated from biological sources (e.g. plant tissues, algae, bacteria, tunicates) into high-performance composite materials (Eichhorn et al. 2010; Klemm et al. 2011; Moon et al. 2011; Jonoobi et al. 2015). Additionally, the adhesive properties of mistletoe viscin provide a relatively untapped model system for bio-inspired glues and are certainly worthy of further scrutiny based on the ancient reports of the efficacy of birdlime in immobilizing birds. Indeed, biological adhesives ranging from mussel byssus (Waite 2017) and velvet worm slime (Baer et al. 2017) to sandcastle worm (Stewart et al. 2004) and barnacle cement (Kamino 2010) have provided novel chemical adhesion mechanisms that are being applied in some cases for development of new technical and medical glues (Lee et al. 2011; Zhao et al. 2016).

Thus, the work described in this thesis will examine in great detail the dynamic formation of adhesive films and fibers from mistletoe berry viscin, and will pose a deceivingly complex research question - how does this work? This is important from two different perspectives.

1) Biological viewpoint: Can we get a better description of the successful dissemination principle or to cite Darwin from the *Origin of Species*:

"In the case of the misseltoe [sic], which draws its nourishment from certain trees, which has seeds which must be transported by certain birds, and which has flowers with separate sexes absolutely requiring the agency of certain insects to bring pollen from one flower to another, it is especially preposterous to account for the structure of this parasite, with its relations to several distinct organic beings, by the effects of external conditions or of habit, or of the volition of the plant itself. [...] It is therefore, of the highest importance to gain a clear insight into the means of modification and coadaptation." (Darwin 1859, p. 3-4)

2) Materials viewpoint: Can we get mechanistic insights on the origin of the extremely unusual material properties of mistletoe viscin leading to multifunctionality such as easy fiber drawing and film formation, reversible easy switching between viscous and rigid states and multimaterial adhesion? Such information is expected to have strong relevance and value for efforts to generate next-generation sustainable plastics and composites, as well as for developing effective bio-inspired adhesives.

To achieve these aims, I undertook a multiscale structural and mechanical investigation of the viscin tissue using a broad range of materials characterization methods including tensile testing, X-ray diffraction and a variety of microscope techniques. The thesis consists of three data chapters that explore different aspects of the mistletoe viscin structure and function from the two perspectives described above. In chapter 4, I performed a comparative anatomical and functional investigation of two related subspecies of *Viscum album* L., allowing me to clearly localize the capacity for fiber formation to a specific anatomical fea-

ture – the viscin cell bundles and viscin cell clusters. In chapter 5, I mechanically and structurally characterized the fiber formation process by the viscin cell bundle using in situ X-ray diffraction methods, providing deep insights into the hierarchical structure of crystalline cellulose and swellable matrix, and their role during viscin processing. In chapter 6, I explored the potential of the viscin as a source of bio-inspiration by examining its processability and adhesive properties, revealing the ability to form 3D fiber scaffolds via wet-welding, free-standing films via biaxial drawing and demonstrating the versatility of the adhesive behavior on a broad range of surfaces including wood, glass, metal, engineering polymers and even biological tissues. This last surface is especially interesting revealing the potential biomedical applications of the viscin material. Thus, as a whole, this work has its foundation in the biological origins of this fascinating material, which caught even the attention of Charles Darwin, and further expands to future applications by elucidating fundamental structure-property relationships using advanced materials characterization techniques.

2 State of the art

Mistletoe viscin is a material based on plant cell wall which is the essential way for plants to build their complex tissues providing them with material characteristics. This chapter first describes wood as a prototypical plant material with hierarchical structure. Then the basic building blocks of plant cell walls as well as the structure of primary and secondary cell walls are briefly introduced. The specific hierarchical structure of mistletoe berries and the viscin they contain will be addressed in 2.2.

2.1 Structure and function of plant cell walls

Higher plants and their individual plant organs (e.g. stem, leaves, roots and flowers and fruits) reveal a sophisticated hierarchical organization typically covering several orders of magnitude which is typical for natural materials (Fratzl and Weinkamer 2007). In the following section the wood tissue found in the stems of softwoods will be used as a well-studied model system (Speck and Burgert 2011) to depict the structural organization of plant tissue.

2.1.1 Hierarchical organization of wood as an example of plant cell wall

As illustrated in Figure 2.1 wood can described as a complex multicellular tissue with several structural levels covering up to 12 orders of magnitude (Speck and Burgert 2011). The integral level of the stem (Fig. 2.1A+B) scales from only a few mm for the width of a young plant shoot up to a length of more than 100 m for the tallest trees on earth. The next level is the macroscopic level of the tissue structure. The wood tissue of softwoods predominantly consists of only one cell type, called tracheids or fibers which typically scale from several µm in diameter up to a few mm in total length (Fengel and Wegener 1989). These elongated cells can be described as hollow cylinders with a central lumen where the cell walls of the individual cells are glued together via a middle lamella located between two adjacent cells (Fig. 2-1D+E). Like many other plant cells, softwood fibers are multifunctional cells: On the one hand the cell walls provide the tissue with mechanical stability. On the other hand the hollow central lumen allows water transport along the stem. In temperate zones softwoods are able to adapt the cell wall growth during different periods of the growing season. At early stages of the growing season the plant produces rather thin walled fibers (early wood) with large lumen which are well-suited for water conduction. Towards the end of the growing season the plant produces so-called late wood fibers with gradually increasing cell wall thickness and decreasing lumen which stiffen the wood tissue (Fengel and Wegener 1989). In order to understand these adaptation mechanisms and the cell wall assembly it is necessary to examine the plant cell wall in more detail. Our current understanding on the cell wall fine structure largely bases on the intensive study on a few plant model systems (e.g. *Arabidopsis thaliana, Nicotiana tabacum*, *Populus* ssp. and *Picea* ssp.) and is far from being complete. In the next section the basic principles of the ultrastructural

assembly will be briefly discussed before the layered substructure of the cell wall will be further explored.

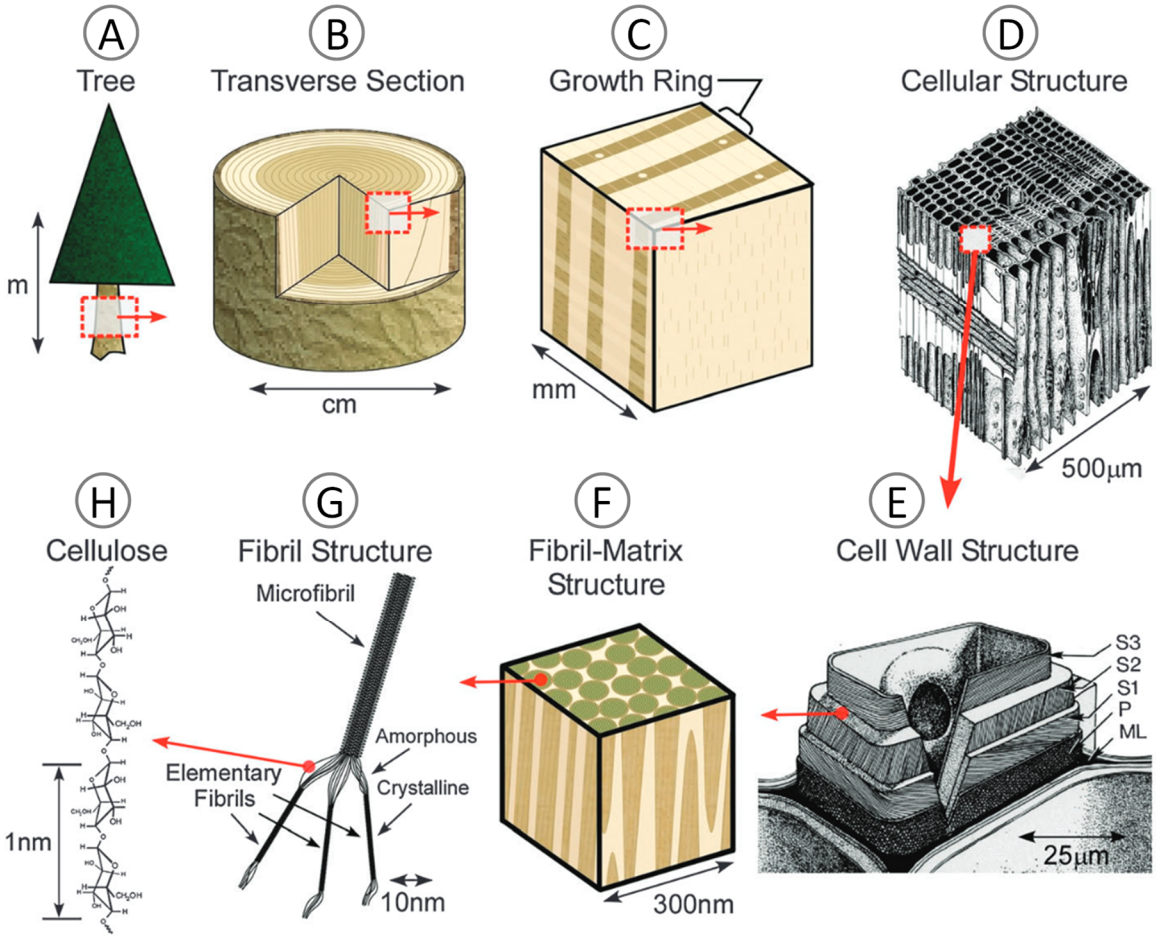

Figure 2-1: Schematic hierarchical structure of wood. Reprinted with permission from (Postek et al. 2011) Copyright 2011 IOP Publishing Ltd.

2.1.2 Plant cell wall composition

Plant cell wall are composite materials which are mainly build of only four basic groups of biopolymers: cellulose, hemicellulose, pectin and lignin. Together they form the carbohydrate extracellular matrix that surrounds plant cells. Simplified, the cell wall can be described as a fiber-reinforced composite where stiff crystalline cellulose fibrils are embedded into a soft matrix of amorphous hemicellulose and either pectin or lignin (Gibson 2012; Cosgrove and Jarvis 2012) where the latter is characteristic for woody tissue.

Cellulose

Cellulose microfibrils are composed of β-1,4-linked glucan chains (Fig. 2-1G), synthesized by cellulose synthase protein complexes (Fig. 2-2) which are located in the plasma membrane of the plant cell (Cosgrove 2005; Li et al. 2016). The individual glucan chains of

indefinite length aggregate closely after synthesis in a parallel manner to form the microfibrils. This is achieved via intra- and intermolecular bonds between the glucan chains as well as Van der Waals forces (Nishiyama 2009) and results in a crystalline conformation with an impressive longitudinal stiffness in the range of 110-220 GPa (Moon et al. 2011). The crystalline conformation of plant cellulose was determined to be of cellulose I (Nishiyama et al. 2002). Microfibrils are often described to consist of crystalline domains in series with less crystalline or even amorphous regions along the microfibrils (Fig. 2-1G, Nishiyama 2009). The typical width of plant microfibrils heavily depends on the species, cell type or location within the cell wall and ranges between 2-4 nm which equals 18 to 36 glucan chains (Cosgrove 2014). The degree of crystallinity is typically rather low due to the rather small number of glucan chains forming the crystalline core compared to the greater number of surface chains usually interacting with their local chemical environment which disturbs the crystalline conformation (Newman et al. 2013). Multiple microfibrils may aggregate into larger macrofibrils or bundles (Fig. 2-1E+F).

Matrix polymers

When the cellulose microfibrils are synthesized they are deposited into a partially preexisting cell wall matrix (Albersheim et al. 2011). The matrix polymers hemicellulose and pectin are considered to be partially assembled inside the cell from where they are transported to the plasma membrane in secretory vesicles and then finally released into the cell wall (Driouich et al. 2012; Kim and Brandizzi, 2016) where the polymers interact with each other to make the final wall architecture.

Hemicelluloses are a heterogeneous group of polysaccharides with a characteristic backbone comprising of β-1,4-linked sugar residues, namely glucose, mannose and xylose (reviewed in Scheller and Ulvskov 2010), similar to the linkage of cellulose. In contrast to cellulose (only glucose-residues) these structures are usually branched and may contain various side chains which prevents a fibril assembly. Hemicelluloses with partially unbranched surfaces are able to bind with cellulose surface chains via hydrogen-bonds to build the so-called cellulose-hemicellulose network (Fig. 2-2) which is considered to be mainly responsible for the mechanical stability of the cell wall. Hemicelluloses also act as a coupling agent between cellulose and lignin (Fengel and Wegener 1989).

Pectins are highly heterogeneous family of polysaccharides traditionally characterized by containing large amounts of galacturonic acid residues (Atmodjo et al. 2013). Pectins have a broad spectrum of functions such as the mediation of cell-cell adhesion between the middle lamella and the primary cell walls (Albersheim et al. 2011). They are also considered to provide structural support in soft tissues comprising of primary cell walls where they interact with cellulose (Fig. 2-2A; Voragen et al. 2009). They influence the formation of secondary cell walls and are involved in the lignification of fibers and other woody tissues (Höfte et al. 2012). Pectins and hemicelluloses can be covalently linked via proteoglycans (Tan et al. 2013).

Lignin is a complex phenolic polymer which is incorporated at a later stage of the cell wall assembly. Within the existing framework of the cellulose-hemicellulose network lignin surrounds the cellulose microfibrils and the matrix (Fig. 2-2B) and provides rigidity and compressive strength.

2.1.3 Plant cell wall fine structure

A common motif in cell wall structural models is the structural organization into concentric cell wall layers with distinct differences in either the volumetric proportions or the structural arrangement of the main biopolymers (Albersheim et al. 2011) where the individual layers scale from ~10 nm up to a few µm (Fig. 2-1E). The first layer which is produced after the middle lamella is formed, is called the primary cell wall (Fig. 2-2A). This thin layer comprises celluloses fibrils without pronounced preferential orientation with respect to the cell long axis. Freshly formed primary walls (PW) are typically rich in pectin (30%), with similar amounts of cellulose and hemicellulose (20-30%) and may also contain a minor percentage of proteins (1-10%) (Albersheim et al. 2011). The pectin-rich matrix is assumed to provide the cell with a moderate mechanical stability but still allows newly formed cells to expand during initial cell growth (Cosgrove 2018). After the cell has finished expansion some cell types like softwood fibers start to add successive layers which are designated as the secondary cell wall. The secondary cell wall is typically divided into two or eventually three sublayers (S1, S2, S3, Fig. 2-1E) which significantly differ from the adjacent PW in size, chemical composition and structural arrangement (Cosgrove and Jarvis 2012, Fig. 2-2B).

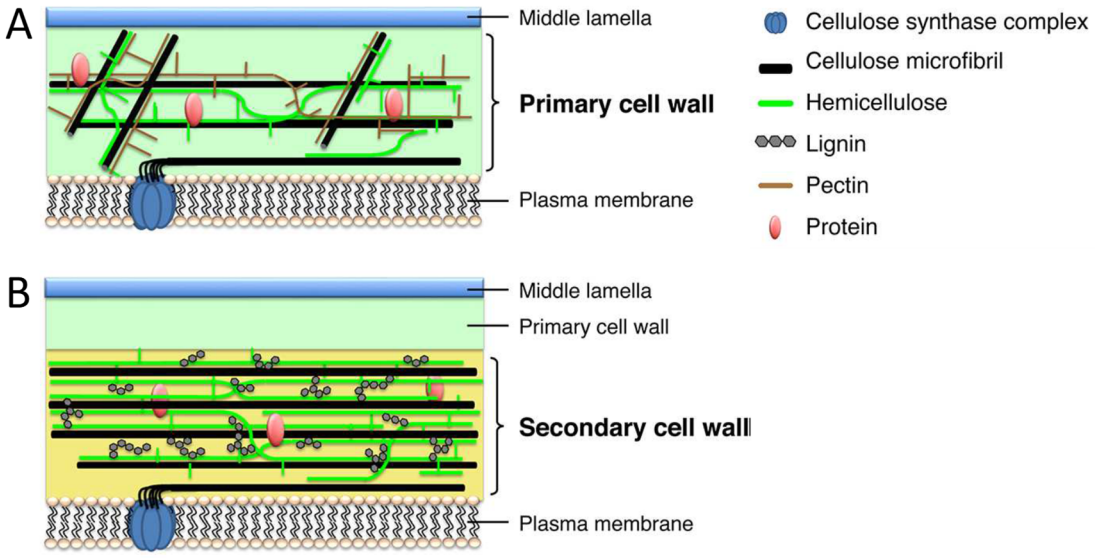

Figure 2-2: Schematics of primary and secondary cell wall structure. Reprinted from Nakano et al. (2015) with permission from Frontiers under a CC BY 4.0 license, Copyright 2015.

From a chemical point of view the pectin content usually decreases in the secondary wall (SW) while the cellulose content rises with respect to the PW. Both PW and the SWs may additionally be impregnated with lignin to rigidify the cell wall as it typically occurs in fibers to during late stages of cell development (Albersheim et al. 2011). A further very important structural difference is the preferred orientation of the cellulose fibrils within the SW layers. The angle at which the cellulose microfibrils are helically wound around the cell long axis is commonly known as the microfibril angle (MFA) where a cellulose orientation parallel to the cell long axis equals a low MFA (~0°) and a transverse orientation equals a high MFA (~90°). The MFA is frequently determined with X-ray diffraction (Cave 1997; Lichtenegger et al. 1999a). In the thin S1-layer of fibers the MFA is typically low (close to 90°) (Fengel and Wegener 1989) while the MFA of the thick S2-layer of normal wood fibers is typically around 10-20° (Lichtenegger et al. 1999b). The MFA of the S2-layer, which makes up to 80% of the entire cell wall volume of fibers (Fengel and Wegener 1989), was found to be a crucial parameter for the mechanical properties of the wood cell wall and superordinate wood tissue (reviewed in Eder et al. 2013). It could be shown that the tensile stiffness is highest for low MFA close to 0° and is reduced by roughly one order of magnitude for MFA around 45° (Reiterer et al. 1999) which are characteristic for compression wood fibers of softwoods. Fiber stiffness was found to be mainly determined by the properties and the orientation of cellulose with only little influence of the mechanical properties of lignin and hemicelluloses (Bergander and Salmén 2002). Based on modelling approaches it was concluded that the amorphous matrix polymers rather influence the cell wall properties in the transverse direction than in the longitudinal direction of the cellulose microfibrils (Salmén 2004). The mechanical properties of microfibrils are considered to be barely affected by presence of water due to the crystalline character (Salmén 2018). In contrast, the amorphous matrix substances are highly hygroscopic which affects their mechanical properties when the water content of the cell wall changes due to drying or rehydration, taking into consideration, that natural condition of the native cell wall would be fully hydrated. While lignin seems barely affected by changes of the moisture content at ambient conditions, the mechanical properties of hemicellulose are dramatically reduced during water uptake (Salmén 2004). For hydrated compression wood fibers with a large MFA (~45°) it was suggested that at large deformations the soft matrix is able to slide along the microfibrils contributing to plastic flow and a Velcro-like stick-slip mechanism was suggested (Keckes et al. 2003). However, recent investigations have shown that water is also able to access the interfaces between microfibrils (Lindh and Salmén 2017) leading to the hypothesis that water molecules may act as a lubricant promotion sliding between molecules (Salmén 2004). This might also explain the significant decrease in fiber stiffness observed between dry and wet fibers with a rather low MFA (Kersevage 1973; Eder 2007).

2.2 Structure and function of mistletoe viscin

This chapter will guide the reader starting from an introduction into the characteristic lifestyle of mistletoes via the most common seed dispersal mechanisms towards the state of art regarding the ultrastructural and chemical characterization of viscin, an adhesive tissue found in berries of *V. album* L. ssp. *album* involved in the seed-host attachment.

2.2.1 What makes a mistletoe?

The term mistletoe is generally applied to a diverse group of plants sharing a hemiparasitic lifestyle which can be found on all continents except Antarctica (Kujit 1969; Barlow 1983; Hawksworth 1983; Calder 1983; Nickrent 2011). Taxonomically they all belong to the order of Santalales which comprises five families of mistletoes – Misodendronaceae, Eremolepidaceae, Santalaceae, Loranthaceae and Viscaceae (Kuijt 1969; Restrepo et al. 2002; Nickrent 2011) – which developed independently five times (Nickrent 2002). With about 1000 and 550 species, respectively, the two latter families together comprise more than 96% of all mistletoe species (Nickrent 2011). The majority of the mistletoes are aerial stem parasites which require other woody plant species as hosts. As hemiparasites they are capable of performing photosynthesis, but require water, minerals and nutrients from the host plant (Kuijt 1969). This is realized via a root-like organ called haustorium which connects to the host both anchoring the mistletoe and tapping into the host's vascular system to absorb water, nutrients and minerals (Thoday 1951; Calder 1983). Therefor it is essential for the plant's successful dissemination that the seeds within mistletoe fruits are deposited on suitable hosts. While there are only a few reports of mammalian seed dispersal by marsupials (Amico and Aizen 2000) and bats (Allen 1962), the wind dispersed Misodendronaceae or the explosive seeds of the American dwarf mistletoe (*Arceuthobium americanum*) (Hinds et al. 1963), in most cases this is achieved by the help of birds (Reid 1991; Reid et al. 1995; Restrepo et al. 2002; Aukema 2003). In fact, many birds are highly specialized on the mistletoe diet (Reid 1991; Reid et al. 1995; Ladley and Kelly 1996; Martínez del Rio et al. 1996; Watson 2004) and there is evidence for a potential co-evolution between mistletoes and birds (Reid 1991). The birds are attracted by mistletoe fruits which offer water and nutrients as a reward for their logistic service. Additional to the avian transport the seeds need to be firmly fixed onto the potential host. To achieve this, most mistletoe species developed sticky seeds, typically covered by a mucilaginous tissue called viscin (Kuijt 1969; Reid 1991; Heide-Jorgensen 2008), which acts as an adhesive gluing the seed onto its new host after deposition. To activate the adhesive viscin properties the seed needs to be released from the surrounding fruit skin. As described above, this mainly happens by bill wiping, regurgitation or defecation (Reid 1991; Reid et al. 1995; Kuijt 1969; Snow and Snow 1984; Snow and Snow 1988). Once the seed becomes successfully attached to a potential host, the surrounding viscin tissue dries and firmly fixes the seed (Fig. 2-3A+B). While seeds of tropical mistletoe species often start to germinate shortly after host attachment (Lamont 1983), some species living in temperate zones including *Viscum album* L. can show a longer resting period of several weeks up to months before germination starts

(Heinricher 1912; Nierhaus-Wunderwald and Lawrenz 1997). During germination the hypocotyl typically elongates and grows towards the host (Fig. 2-3A). Upon contact a disc-like holdfast is formed, which firmly connects the hypocotyl to the host bark (Fig. 2-3B, Thoday 1951). Once the mistletoe has entered its host tissue, the development of the haustorium begins (Thoday 1951). For more detailed information on the typical lifestyle and lifecycle of mistletoes the reader is referred to the comprehensive works of Tubeuf (1923), Kuijt (1969) and Heide-Jorgensen (2008).

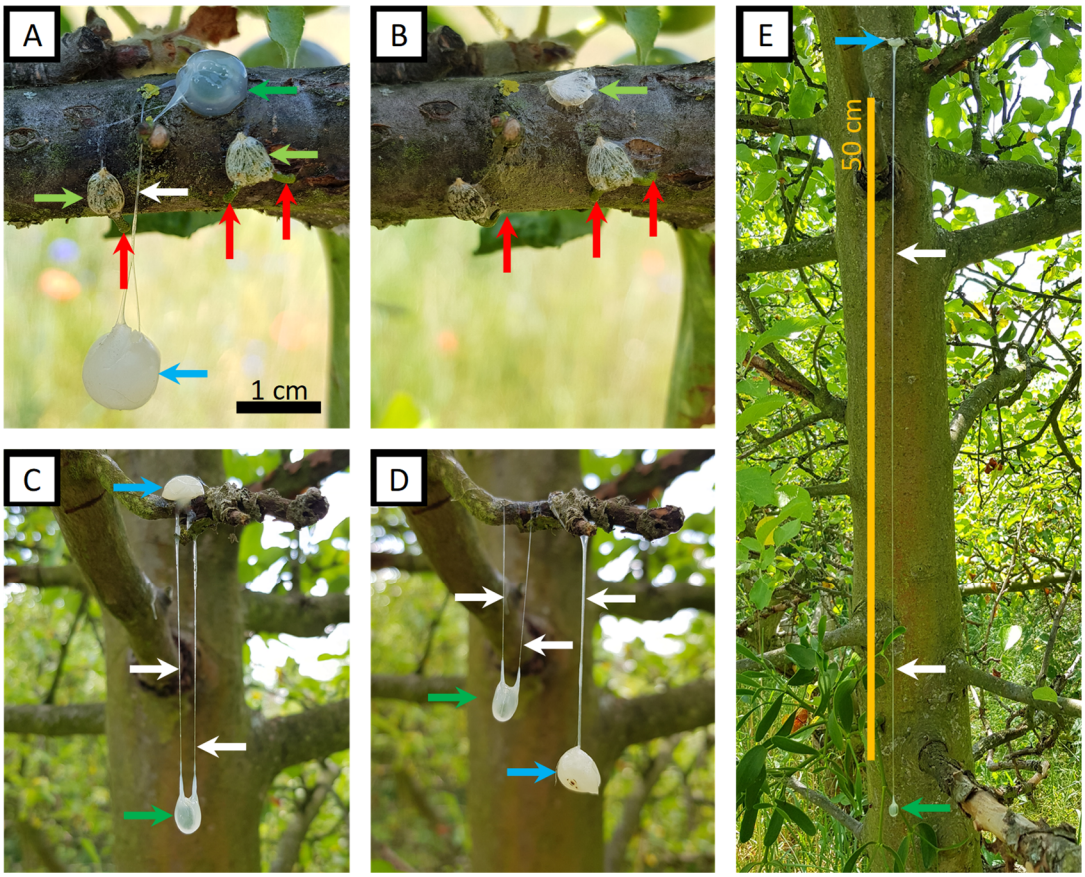

Figure 2-3: Mistletoe seed-host adhesion. A) *Viscum album* L. ssp. *album* seeds on an apple tree (*Malus domestica*) branch. A freshly isolated and manually deposited seed (dark green arrow) attaches via the surrounding viscin, a sticky translucent hydrated tissue from which emerges an adhesive fiber (white arrow) which connects the seed with the remaining skin of the berry (blue arrow). Previously attached and already dried seeds (light green arrows) show the presence of a white tissue covering the green seed. Hypocotyl (red arrows) start to grow from inside of the seed. Scale bar: 1 cm. B) The hydrated viscin layer from (A) dried out firmly fixing the seed onto the branch. The previously greenish seed is now also covered by a white tissue. The fiber and the remaining berry skin fell off. The hypocotyl radicals grew towards the bark of the branch leading to the formation of a disk-like holdfast fixing the hypocotyl radical and the seed onto the bark. C) Feshly deposited berry attached to the branch via the sticky viscin beneath the fruit skin (blue arrow). The hydrated seed (dark green arrow) is pulled out of the berry but is still connected with the remnants above via two characteristic individual fibers (white arrows). D) The adhesive fiber emerges from both ends the seed and the viscin beneath the fruit skin. E) A manually drawn mistletoe fiber connecting the berry skin and the sticky viscin layer surrounding the hydrated seed. Fibers can reach a length of >1 m. Scale bar: 50 cm.

2.2.2 The species *Viscum album* L.

Viscum album L., known commonly as the European mistletoe, belongs to the family of Viscaceae. As the common name suggests, the species is native to most of Europe, but has an even broader distribution range along North Africa, the Middle East, and Continental Asia all the way to East Asia where it occurs in Japan and Korea (Tubeuf 1923; Becker 1986; Zuber 2004; Maul et al. 2019). *V. album* L. is an evergreen shrub with thick leathery leaves. The young shoots of this perennial plant start to grow in fan-like manner initially, but after a few years the plant grows into its typical globular shape. Single individuals can reach maximum globe diameters of more than 2 m (Heide-Jorgensen 2008). *V. album* L. is a dioecious plant with either male or female reproductive organs on individual plants and both male and female flowers are rather inconspicuous. Only the female inflorescence which is typically pollinated by insects in late winter/spring develops into a berry (Nierhaus-Wunderwald and Lawrenz 1997). The development starts in spring/summer and the berries mature in late autumn/winter (Nierhaus-Wunderwald and Lawrenz 1997). Mistletoe berries are not true berries in a strict botanical sense as they do not develop from a true ovule and because axis tissue is also involved in the fruit development. That is why the term pseudoberry would be more technically accurate, but in the literature, the term berry is well accepted and shall be used in the present work. The seed is also not a true seed in a botanical sense since it does not possess true seed coat, which typically develops from the integuments of the ovule. Instead, the embryos are loosely embedded into a sac-like compartment which also develops from axis tissue of the inflorescence. However, like the berry this pseudoseed is also well accepted as a seed in the literature. The berries typically contain a single seed with one or two and in rare cases three embryos (Tubeuf 1923). For a more detailed background on the biology of *Viscum album* L., the reader is referred to Tubeuf's 'Monographie der Mistel' (1923) and the work of Zuber (2004).

Importantly, all mistletoes show a certain degree of host specificity (Norton and Carpenter 1998), which means that they can only grow on a limited number of host species. In the case of *V. album* L., the host specificity led to an early differentiation into subspecies based on specific cohorts of host species. In Europe four subspecies are currently known four *V. album* L.:

***V. album* subsp. *album* L. (*V. album*)** grows on a wide range of hardwood species preferably on apple trees (*Malus* ssp.), but also on birch, maple, poplar, robinia, widow, linden and many more. In fact, with more than 384 registered host taxa *V. album* is reported to have one of the biggest ranges of accepted host amongst all mistletoes (Barney et al. 1998). With a natural distribution from England to Japan the subspecies can be found in Europe, North Africa, along the Middle East up to East Asia. It has also the largest distribution range of all subspecies (Tubeuf 1923; Zuber 2004; Maul et al. 2019). Although not native, the species can also be found in Western North America, where it was successfully introduced by a German florist around 1900 presumably in order to harvest and sell the plant as a traditional Christmas decoration (Scharpf and Hawksworth 1976). Starting from a small area and only a few individuals, the species has successfully expanded across the western

coast of North America ranging from California to British Columbia (Hawksworth and Scharpf 1986).

***V. album* subsp. *abietis* (Wiesb.) Abromeit (*V. abietis*)** grows on firs (*Abies* ssp.) and its geographical distribution is mainly limited to Europe and the Middle East (Zuber 2004; Maul et al. 2019).

***V. album* subsp. *austriacum* (Wiesb.) Vollmann (*V. austriacum*)** grows on pine and larch (*Pinus* ssp. and *Larix* ssp.) and is native to Europe and the near East (Zuber 2004; Maul et al. 2019).

***V. album* subsp. *creticum* (*V. creticum*)**, which occurs on a sole pine host (*Pinus brutia*) on the isle of Crete (Böhling et al. 2002).

As a potential fifth subspecies ***Viscum album* var. *coloratum* (*V. coloratum*),** which grows on hardwoods similar to *V. album* is worth mentioning. However, this related species which is native to Continental and East Asia (Zuber 2004; Maul et al. 2019) is treated by some as its own species (Qiu and Gilbert 2003). On the one hand the status of true subspecies was supported by early cross infection experiments in which seeds of individual subspecies were artificially sown onto a wide range of host species (Heinricher 1911; Tubeuf 1923). The results supported the existing categorization as the seeds typically failed to grow into vial plants on hosts outside their known range with only a few exceptions, which were unknown in nature. On the other hand recent phylogenetic investigations showed that there are also distinct genetic differences, which are in good agreement with the early taxonomic categorization of *V. album* L. (Zuber and Widmer 2000; Zuber and Widmer 2009; Maul et al. 2019).

Amongst the abovementioned subspecies of *V. album* L. the berries can vary in size (5-12 mm) and color (white, yellow, pink, red) (Tubeuf 1923; Zuber 2004; Heide-Jorgensen 2008). Besides these external characteristics, the berries also possess important internal morphological differences, which have been attributed to the individual subspecies. Tubeuf (1923) was the first author who mentioned the ability of the viscin tissue from *V. album* berries to form adhesive fibers (Fig. 2-2) as a distinct morphological difference when compared to *V. austriacum* and *V. abietis*. Although earlier works focused on the chemical and structural characterization of *V. album* berries (Gjokic 1896; Tomann 1906), none of these works tried to compare the berries from coniferous hosts and deciduous hosts. Indeed, it seems they were not aware that there were any differences between them and so they did not mention the subspecies or the host. Later works also described the fiber forming ability of mistletoe viscin, but do not mention the subspecies or the host tree (Mangenot et al. 1948; Boespflug 1964). A subsequent comparative study on the morphology of more than 300.000 berries of the aforementioned *V. album* L. subspecies including *V. coloratum* confirmed that the fiber forming ability can be used a distinct morphological trait to discriminate between fiber forming subspecies (*V. album* and *V. coloratum*) and non-fiber forming subspecies (*V. abietis* and *V. austriacum*) (Grazi and Urech 1981). Although their study

briefly illustrates the morphological and functional differences after seed removal on the macroscopic level, the work does not include any mechanistic insights or investigations on possible microstructural differences linked to the fiber formation. Indeed, there are few reported insights into the anatomical and functional features of fiber formation across *V. album* L. subspecies, which is a point I will address in chapters 4 and 5 of this thesis.

2.2.3 The structural organization of *Viscum album* berries

Although the literature is scarce, the remaining part of the chapter will address what is known of the internal hierarchical structure of *V. album* berries with respect to the potential origin of adhesive viscin fibers. Figure 2-4 shows a diagram of the rough structural organization of the tissues within the berry. The green seed is located in the center of the berry. It contains one or more embryos which are embedded into the endosperm. The seed is surrounded by the pericarp (Sallé 1983; Azuma et al. 2000). The latter consists of three layers where the innermost layer is the endocarp, a thin cellular layer surrounding the seed endosperm. The outermost layer is the thick epicarp which shows characteristic dark brown floral traces of the four tepals surrounding the central stigma (Wangerin 1937). The floral traces are located on the opposite side of the peduncle, which carries the berry. The center layer is the mesocarp, which is the part of the tissue that is typically referred to as viscin. Based on early works around 1900, the viscin is a mucilaginous layer which consists of an inner indigestible pectosic slime and an outer digestible cellulosic slime (Gjokic 1896; Tomann 1906). The inner pectosic slime comprises radially oriented cells that are connected to the endocarp and surround the seed. Based on chemical staining, the cells were reported to have an inner cellulosic cylinder with spiral wall thickenings and an outer pectic cylinder (Gjokic 1896). The outer cellulosic slime was found to surround the inner pectosic slime and upon squashing the berries one part of the slime remained attached to the epicarp and the other part remained attached to the seed. Both authors described the presence of numerous elongated cells within both slime layers which could readily be stretched out into thin elongated cellulosic filaments. The cellulosic character was concluded from successful chemical staining with cellulose dyes (Gjokic 1896) and observations with polarized light microscopy due to an intense birefringent signal of the stretched filaments under crossed polars (Tomann 1906). The macroscopic viscin fibers were reported to consist of numerous of these microscopic filaments, each interpreted as a single stretched cell (Gjokic 1896). Apart from the chemical differentiation both works do not offer any further microscopic insights on potential structural differences of the two slime layers.

After this initial work, the understanding of viscin microstructure and chemical composition did not advance further for the better part of a century. In the early 1980s, Sallé (1983, Fig. 2-4A) was able to confirm the presence of elongated cells with spiral wall thickenings oriented radially around the seed. It was also confirmed that these cells comprise an inner cellulosic cylinder with a helicoidal structure and an outer pectic cylinder. Additionally, the author describes another cell type which is located mainly between the inner pectosic viscin layer and the epicarp, but also between the individual elongated cells. This cell type was

described as highly vacuolated cells with thin cell walls. All cell types are reported to be embedded into a polysaccharidic substance. Interestingly, the work does not mention any further viscin layers like the outer cellulosic slime found in earlier works. Although the author was well aware of the morphological differences described earlier (Grazi and Urech 1981), the work does not give reference to the host or subspecies and so it remains speculative whether this may underlie the different observations.

Finally, one of the most important works on the structural organization was performed by Azuma et al. (2000) on berries of *V. album* grown on apple trees. It contained important new insights into viscin structure across several hierarchical levels starting from the whole berry down to the micro- and nanostructure of the viscin. Beginning with a schematic organization of the entire berry (Fig. 2-4B) their description mainly follows the observations from previous studies regarding the external characteristics, seed structure, and the location of endocarp and epicarp. However, the morphological description of the mesocarp significantly went beyond previous studies. According to Azuma and co-workers the mesocarp comprises four different tissue types: 1) Radially oriented elongated cells, which were described as hairy cells, surround the seed; 2) The viscin tissue, a highly viscous substance which surrounds the seed and the layer of hairy cells, comprises clusters of elongated cells (viscin cells) with an individual length close to 1 mm and widths ranging from 10 to 50 µm. The cell clusters are reported to be attached to the mesocarp close to the peduncle and from there on, they arc around the layer of hairy cells as two mirroring domains, which are joined above the seed at the opposite side of the peduncle forming a continuous ring. As observed with PLM, these cells were highly birefringent and revealed a peculiar cellulose arrangement in which the cellulose fibrils were tightly coiled around the cell wall perpendicular to the cell long axis. A minor fraction of the viscin tissue was reported to extend as string-like cells into 3) a spherical gel layer which is located between the viscin tissue and the epicarp; 4) Vacuolated cells were located mainly around the outer surface of the viscin tissue.

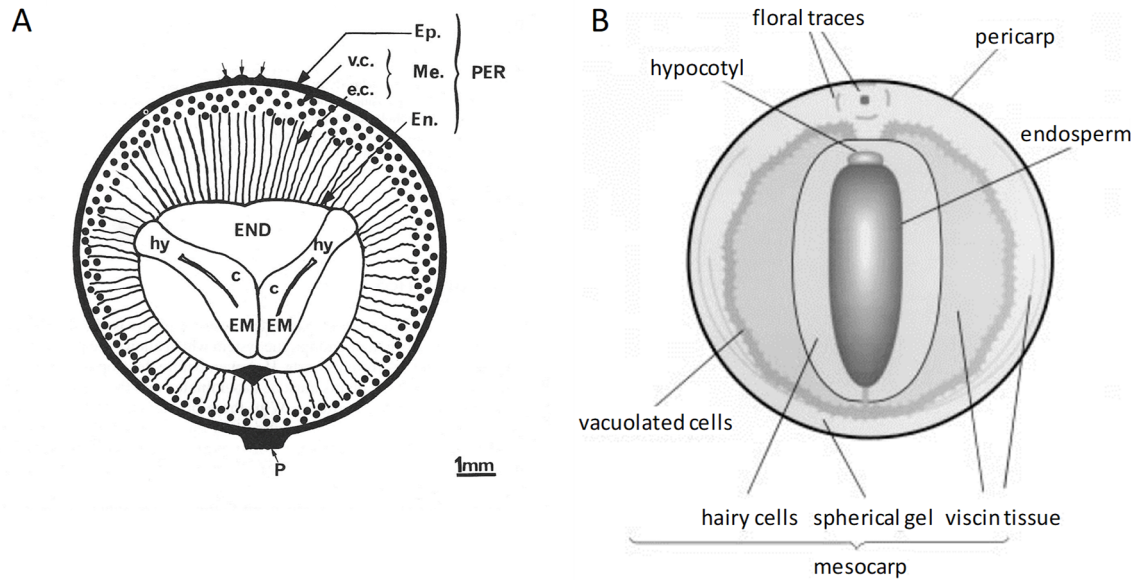

Figure 2-4: *Viscum album* L. berry organization. Longitudinal sections showing the schematic organization mature berries. A) The berry comprises the seed and the pericarp (PER). The seed comprises two embryos (EM) with the cotyledons (c) and the hypocotyls (hy) embedded into the endosperm (END). The pericarp consists of the endocarp (En.) surrounded by a layer of elongated cells (e.c.) arranged in a ray-like manner around the seed followed by a layer of vacuolated cells (v.c.). Together, h.c. and v.c. build the mesocarp (Me.). The berry is protected on the outside by the epicarp (Ep.). On the bottom the berry is connected to the peduncle (p). Arrows: traces of flowering structures, e.g. scars of the tepals and the stigma. Reprinted from Sallé (1983) with permission from Elsevier. B) The berry comprises the seed and the pericarp. In this schematic the mesocarp consists of 4 tissue types: hairy cells, the viscin tissue, vacuolated cells and a spherical gel. Reprinted from Azuma et al. (2000) with permission from Springer Nature.

2.2.4 The micro- and ultrastructure of viscin from *Viscum album*

Based on PLM images of carefully dissected viscin tissue and in agreement with previous studies (Gjokic 1896; Tomann 1906). Azuma et al. (2000) were able to demonstrate, that the viscin cells can be readily stretched into thin cellulosic filaments with a typical diameter of 1-3 µm (Fig. 2-5A). TEM studies on viscin cell cross-sections showed that viscin cells comprise massive cell walls with an irregular shape and small central lumen where the transverse cellulose arrangement was confirmed using electron diffraction (Fig. 2-5B). TEM images of stretched viscin cells showed that the individual filaments consist of bundles of slender long microfibrils with a width of ~3 nm. The microfibrils showed a very high degree of orientation parallel to the filament as confirmed with X-ray diffraction (XRD) and electron diffraction. Complementary XRD and nuclear magnetic resonance (NMR) investigations further revealed that the cellulose is of low crystallinity and belongs to cellulose I (IV). A follow-up study by one of the authors compared viscin of *V. album* to a closely related subspecies from *V. coloratum* and reports similar morphological characteristics for viscin cell clusters including the ability to form macroscopic adhesive fibers (Azuma and Sakamoto 2003).

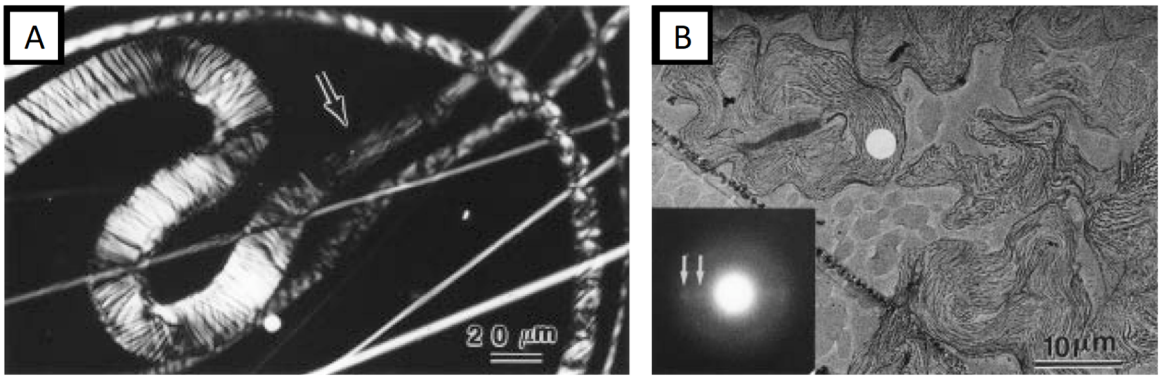

Figure 2-5: Viscin cell microstructure. A) PLM image of a viscin cell partly stretched into a filament. The arrow points towards the stretching zone. Reprinted from (Azuma et al. 2000) with permission from Springer Nature. B) TEM image of a viscin cell cross-section. Insert: electron diffraction pattern of the circled area. Reprinted from (Azuma et al. 2000) with permission from Springer Nature.

Interestingly, an earlier in-depth study of the development of viscin cells from *Phthirusa pyrifolia* (Loranthaceae), a species which is native to South and Central America, showed similar results regarding cell wall organization and functionality of viscin cells (Gedalovich and Kuijt 1987). Although there are distinct differences in the reported berry morphology, especially regarding location and distribution of viscin cells compared to *V. album,* PLM and TEM investigations also showed viscin cells with massive cell walls and a transverse cellulose orientation. The viscin cells of *P. pyrifolia* were reported to be somewhat smaller in width and length (Gedalovich and Kuijt 1987) compared to *V. album* (Azuma et al. 2000). However, similar to *V. album*, these cells could also be readily stretched into cellulosic filaments of similar size and a high degree of cellulose orientation on the nanoscale, which may aggregate to form macroscopic adhesive fibers.

2.2.5 Viscin biochemistry

Apart from the morphological characterization and the differentiation into a cellulosic slime fraction and a pectosic slime fraction around the beginning of the 20th century, a few studies presented further insights into the chemical composition of viscin from *V. album* and other mistletoe species. Early on, the viscin of *V. album* L. was generally characterized as cells embedded into a polysaccharidic substance (Sallé 1983). More specifically, for *V. album* (Azuma et al. 2000) and a closely related subspecies of *V. coloratum* (Azuma and Sakamoto 2003) it was found that the mechanically isolated and washed viscin comprises similar amounts of cellulose (~45% dry weight (d.wt.); 47% d.wt., respectively), hemicelluloses (~53% d.wt.; 53% d.wt.), pectins (~2% d.wt.; 2% d.wt., estimated from uronic acid content) and was essentially free from proteins. Due to the polysaccharidic nature, the extracted biopolymer was named ‘viscan’. It remains unknown how the washing procedure might have affected the chemical composition as it was also reported that the viscin tissue lost its adhesive properties after washing (Azuma et al. 2000) and therefore an important property of the suggested natural function. This clearly indicates that some viscin components might have been washed off and were missing in the subsequent chemical analysis. Due to the

absence of lignin in combination with the small lateral size of the cellulose fibrils as deduced from XRD, AFM and NMR results (Azuma et al. 2000; Azuma and Sakamoto 2003) the viscin cell walls were classified as belonging to the primary cell walls

Further examples of a chemical characterization of viscin from other mistletoe species can be found in a comparative study between three American mistletoe species *Arceuthobium americanum* (Viscaceae), *Phorandendron californicum* (Viscaceae) and *Phthirusa pyrifolia* (Loranthaceae) (Gedalovich-Shedletzky et al. 1989). The study confirms that the major part of all viscin mucilage is made of a mixture of polysaccharides. Neutral sugars were found to make the major contribution with 10-55% d.wt. accompanied by a minor percentage of uronic acids (3-30% d.wt.). Furthermore, all species showed substantial amounts of proteins (5-44% d.wt.) and minor amounts of phenolic compounds (2-7% d.wt.). The work precisely reports how the viscin extraction and the chemical analysis were performed based on an earlier study of *P. californicum* (Gedalovich et al. 1988). However, the morphology of the compared viscin tissues differs substantially (Gedalovich and Kuijt 1987; Gedalovich et al. 1988; Ross 2006). For example, only *P. pyrifolia* exhibits a similar ability to form adhesive fibers (Gedalovich and Kuijt 1987) like *V. album* (Azuma et al. 2000), while the two Viscacean species examined do not. Thus, despite the overall similarities in the basic chemical composition of the viscin tissues, it remains unknown how the individual components are distributed within the complex berry architecture and how they contribute to the different proposed functionalities of mistletoe berries such as seed adhesion (Tubeuf 1923), mechanical protection of the seed (Kuijt 1969) or the offer of nutrients to attract the vector (Snow and Snow 1988).

In summary, the sparse literature dealing with the viscin of *V. album* and the diverse viscin tissues from only a few other mistletoe species reveals just how little is known about both the morphology and chemistry of this highly interesting biological adhesive material. It will require further systematic investigations coupling multiscale structural analysis to chemical analysis to elucidate its complex structure-function relationships.

3 Experimental

3.1 Materials

Whole *V. album* L. ssp. *album* plants with mature berries were collected from apple trees (*Malus domestica*) near Golm, Germany in winter 2015/16, 2016/17, 2017/18 and 2018/19. Whole plants with mature berries from *V. album* ssp. *austriacum* were collected from pine trees (*Pinus sylvestris*) in Berlin Adlershof. To investigate the development of the berries single berries were collected from both species from spring to autumn in 2017. All berries were cut from the mistletoe branches in groups with intact peduncles to maintain the structural integrity of the individual berries. Berries were either used immediately for experiments or were flash frozen by collecting berries in 50 ml falcon tubes sealed with parafilm and submerged into liquid nitrogen for 5 minutes. Falcon tubes were stored at -20 °C and single berries were thawed for later use. The freeze-thaw process did not result in noticeable differences of the fiber or film forming ability which was checked by thawing numerous berries directly after flash-freezing. However, berries were never used for more than one year after harvest as some berries showed distinct changes in the viscosity of the viscin tissue which became less viscous. This way it was intended to reduce possible tissue alterations due to an aging of the berries during storage in the freezer.

3.2 Methods

3.2.1 Sectioning

Frozen berries were taken out of the freezer (-20 °C) and immediately sectioned by hand with a chilled razor blade. It was taken care to act as fast as possible to keep the berries from early thawing, which makes a proper sectioning impossible due to its viscous properties. Berry sections along specific anatomical planes were performed with the guidance of external characteristics as described in chapter 4. Fresh sections were immediately immersed in distilled water on glass slides with an included deepening and covered by a cover slip for a later microscopic examination. The deepening and the sample thickness were chosen such that sections did not experience any compressive or shear stresses from the cover slip.

A Zeiss rotary microtome RM2255 was used to trim dried samples mounted on glass slides to obtain a homogeneous sample thickness.

3.2.2 Light microscopy and polarized light microscopy

Berry hand sections were imaged with a Basler acA1920-40uc USB camera mounted on a Leica MZ7-5 stereomicroscope in transmission mode. The same sections were investigated directly afterwards with a digital microscope (Keyence VHX-S550E) equipped with a universal objective (VH-Z100UR) operated in transmission mode for conventional light microscopy (LM) or under crossed polarizers with optional use of a red full-wave retardation

plate for polarized light microscopy (PLM) exploiting the natural birefringence of crystalline cellulose. The entire sections were imaged with the help of an automated stitching routine provided by the Keyence control software at 100x magnification.

Freshly drawn fibers were either directly glued to glass slides exploiting the natural adhesiveness. Alternatively fibers were dried under ambient conditions and then mounted on a glass slide for LM/PLM imaging. For investigation of the fiber formation, seeds were extracted from the berry as described in chapter 5 and viscin cell bundles (VCBs) were excised near the seed interface. The emerging fiber was cut a few mm from the tip of the VCB. The obtained samples were carefully translocated onto a glass slide with the help of fine tweezers. The samples were investigated with a digital microscope (see above) for LM and PLM imaging. Since the sample thickness in the native unstretched VCB dramatically differed from the much thinner resulting fibers, air dried samples were further trimmed with a rotational microtome (Leica RM2255) to obtain a homogeneous sample thickness. Thus, a qualitative evaluation of the resulting polarization colors with respect to the cellulose orientation was possible.

3.2.3 Environmental scanning electron microscopy

Mistletoe samples were investigated with a Quanta FEI FEG 600 environmental scanning electron microscope (ESEM) in low vacuum mode (0.75 torr). Images were obtained with a secondary electrons detector at an acceleration voltage of 4-5 kV. The sample stage allowed vertical tilting to obtain oblique views.

3.2.4 Confocal fluorescence microscopy

Freshly isolated viscin tissue was stained with 1 mg ml^{-1} Direct Yellow 96 (Sigma Aldrich) solubilized in a water-ethanol mixture (25%/75% v/v). The samples were stained in 5 ml vials overnight and then thoroughly washed in a pure water-ethanol mixture (25%/75% v/v). Stained samples were mounted between a glass slide and a coverslip, immersed in a water-ethanol mixture (25%/75% v/v) and sealed with nail polish. Images were acquired using a Leica SP8 confocal scanning fluorescence microscope equipped with a 63x (NA=1.2) water immersion objective. The samples were excited at a wavelength of 458 nm and the fluorescence signal was collected with a HyD detector with a bandpass filter of 468-518 nm.

In a second set of experiments dried viscin fibers were stained with 2 mg ml^{-1} Direct Red 23 (Sigma Aldrich) solubilized in either ethanol or water. One set of fibers was fixed on a glass slide, stained for 30 min in S4B diluted in ethanol, then thoroughly rinsed with ethanol before they were mounted between the slide and a coverslip with antifade AF1 (Electron Microscopy Sciences). The prepared slides were sealed with nail polish. A second set of fibers was mounted on a glass slide, treated with pectinase (from *Aspergillus aculeatus*, Sigma Aldrich, 3800 µg ml^{-1}) solubilized in water for 1h and then thoroughly rinsed with water. Afterwards fibers were stained for 30 minutes in S4B diluted in water, thoroughly

rinsed with water before they mounted between the slide and a coverslip as described above. A control group was only stained in S4B diluted in water without pectinase treatment and further prepared for imaging as described above. Images were obtained with a Zeiss Axio Observer Z1 /7 equipped with an oil immersed 63x/Alpha Plan Apo (NA=1.46). Fluorescence was excited at a laser wavelength of 561 nm and the fluorescence signal was detected with a bandpass filter of 598-660 nm. Image stacks were processed with Fiji 1.51 and single representative z-slices were exported as images.

3.2.5 Second-harmonic generation microscopy

Cellulose fibrils were imaged by second-harmonic generation using a customized multiphoton microscope (FV1200 MPE, Olympus Canada Inc., ON, Canada). Samples were excited with 780 nm, 200 fs pulses from an ultrafast Ti:Sapphire laser (Mira 900F, Coherent, CA, USA) pumped by a 532 nm laser (Verdi V18, Coherent, CA, USA). Laser excitation power was computer-controlled with a custom variable attenuator consisting of a half-wave rhomb retarder (FR600HM, Thorlabs, NJ, USA) mounted on a rotational stage (PRM1Z8, Thorlabs, NJ, USA) driven by a custom LabVIEW VI (National Instruments, TX, USA), and a linear Glan-Laser polarizer (GL10, Thorlabs, NJ, USA). Excitation light was focused on mistletoe tissue with a 25x (NA=1.05) water immersion objective (XLPL25XWMP(F)), Olympus Canada Inc, ON, Canada). Emitted light was collected in a forward configuration using a 0.9 NA dry top condenser lens, split by a 425 nm long pass dichroic mirror (T425LPXR, Chroma Technology, VT, USA) and detected by two photomultipliers. Second harmonic generation light emitted by the sample was filtered by a 400 nm filter (ET400/40X, Chroma Technology, VT, USA) just prior to detection.

3.2.6 Manual fiber drawing

Mistletoe fibers were manually drawn following a newly developed protocol described in detail at the beginning of chapter 5. Freshly drawn adhesive fibers were attached to a laboratory stand and allowed to dry at ambient conditions under the weight of the attached seed.

3.2.7 Semi-automated fiber drawing coupled with polarized light microscopy

A custom built mistletoe fiber drawing device (Fig. 3-1) was developed for PLM video imaging with in situ fiber drawing. Seeds of *V. album* were isolated and spiked on a sample holder connected to a high precision load (Honeywell 31E) cell with a maximum capacity of 0.5 N to measure the drawing forces. The initial short and sticky viscin fibers resulting from the manual seed isolation were attached to a spinning wheel (using the natural adhesive properties) connected to a LEGO® Technic™ step motor with a tunable rotation speed ranging from ~30 µm s^{-1} to ~6 mm s^{-1} placed under a digital microscope (Keyence VHX-S550E) with crossed polarizers in transmission mode. The drawing direction was set to an angle of 45° relative to the polarizers via a rotational stage and a video was recorded of the

drawing process with a frame rate of 15 Hz and a single frame resolution of 1600 x 1200 pixels.

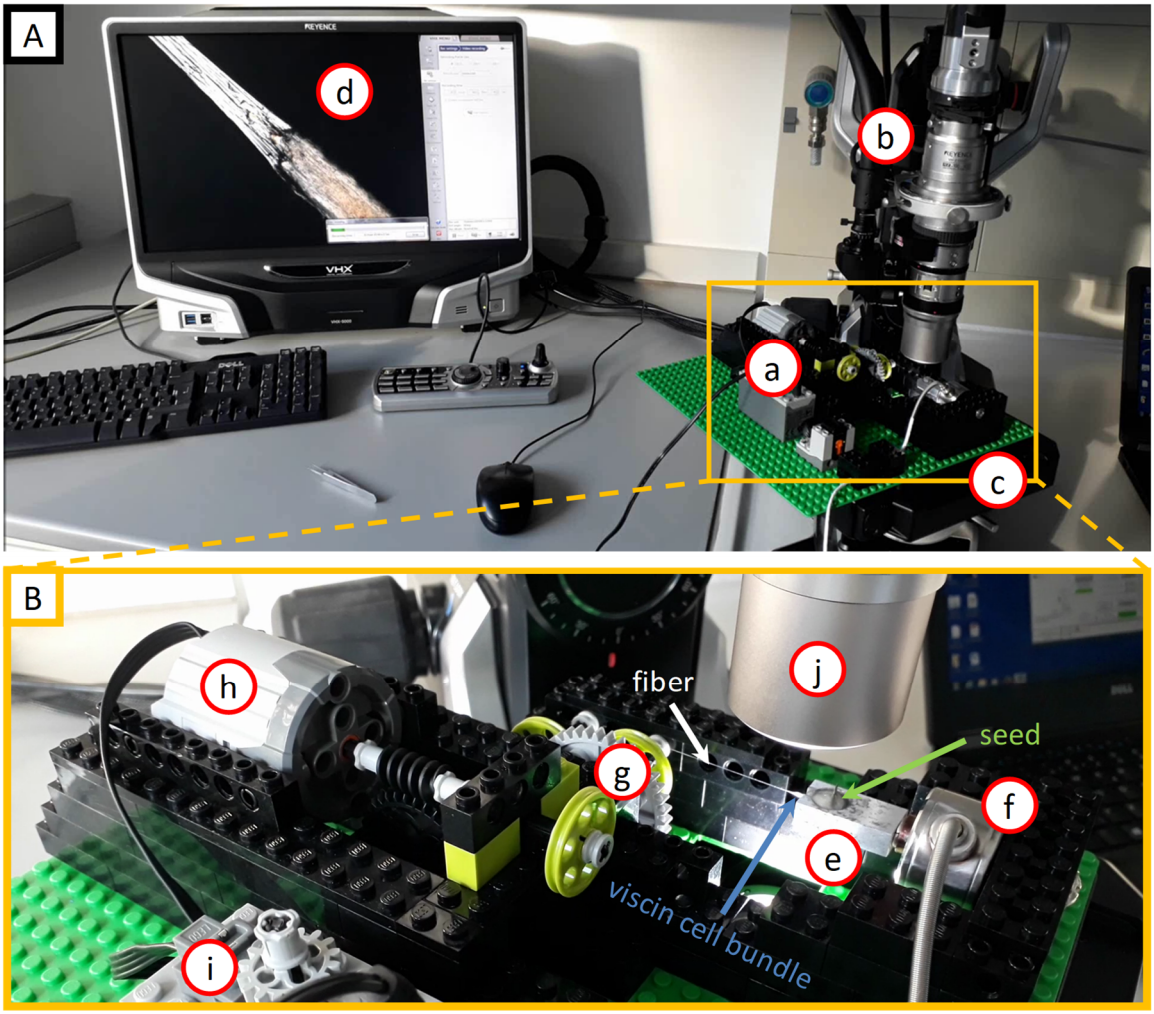

Figure 3-1: PLM video imaging with in situ fiber drawing. A) Custom-built Lego® Technic™ fiber drawing device (a) mounted under a digital microscope (Keyence VHX-S550E) (b) on an integrated motorized xy-stage (c). The automated fiber formation process was tracked with an integrated camera displayed on a monitor of the digital microscope (d). B) Close-up of (a) showing the mistletoe seed (green arrow) spiked on a sample holder (e) connected to a load cell (f). The emerging fiber (white arrow) was attached to a spinning wheel (g) which was driven by a Lego motor (h) powered by a battery (i). The device was placed under the objective (j) focusing on the viscin cell bundle (blue arrow) in the center.

Additionally, a commercially available universal table-top testing machine (Zwick Zwickiline; 10 N load cell) was utilized, which allowed higher drawing speeds up to 1.66 cm s^{-1} with a maximum linear travel distance of ~65 cm. Seeds were isolated from the berry as described in chapter 5 and clamped on the bottom of the device while the remaining part of the berry including fruit skin was clamped on the crosshead side without cutting the fiber or the tissue.

3.2.8 Micro-tensile tests under controlled climatic conditions

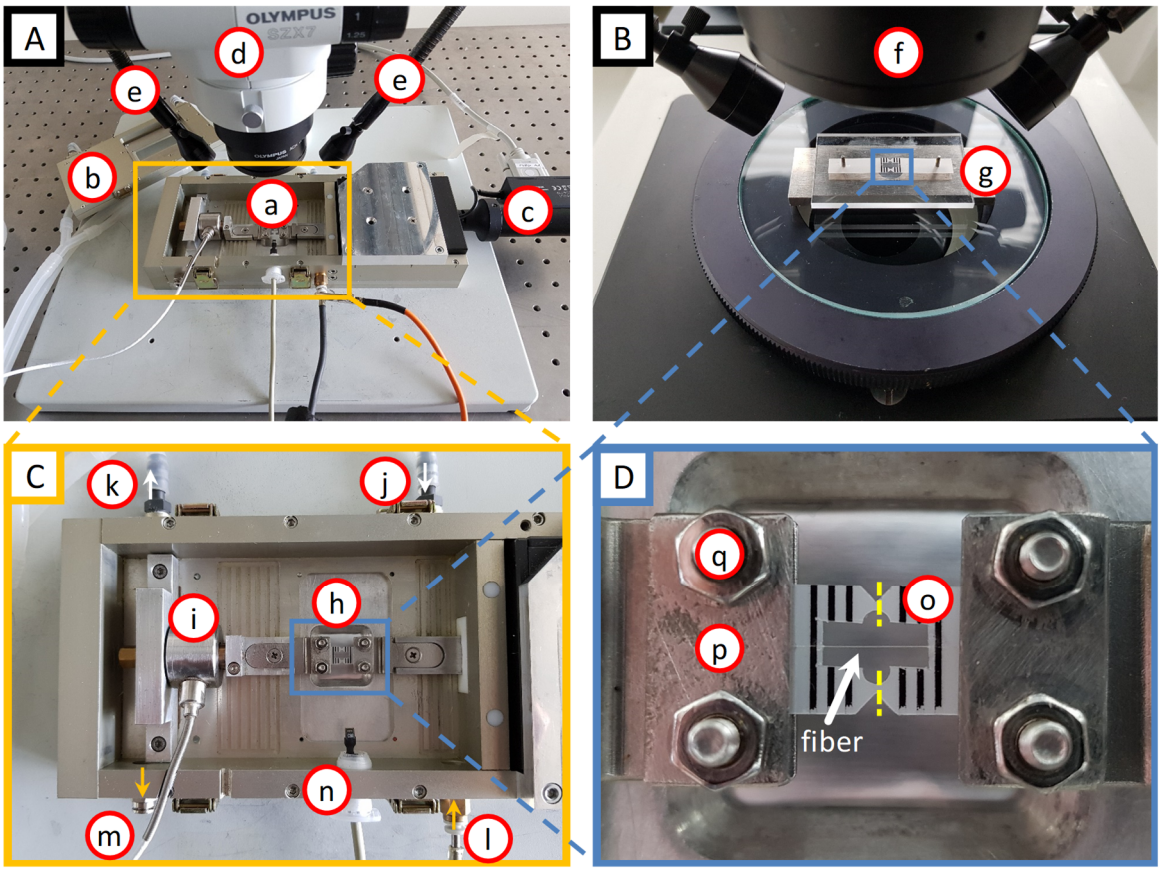

Figure 3-2: Micro-tensile testing under controlled environmental conditions. A) The device comprises a sample chamber (a) with a removable cover (b) and a precision linear stage (c). The device is placed under a stereomicroscope (d) equipped with a digital camera for video extensometry. An external cold light source (e) lightens the sample. B) For mechanical testing mistletoe fibers were glued onto foliar frames under a stereomicroscope (f) and a gluing frame (g) which facilitates centering and aligning the fibers along the later drawing direction. C) Close-up of (a) showing the sample holder (h) connected to the load cell (i) and the linear stage. The body of the device is thermally controlled via a heat circulation thermostat connected via an inlet (j) and an outlet (k) for the circulating fluid. Air temperature (T) and relative humidity (RH) inside the chamber are controlled with a humidity generator connected via a heated transfer line to the gas inlet (l). Air circulation is ensured via an air outlet (m). Air T and RH inside the chamber were recorded with a Sensirion SHT75 sensor (n). D) Close-up of (h) showing the foliar frame (o) carrying the fiber (white arrow), clamped by two metal plates (p) tightened via screws (q). After clamping the sample, the supporting bridges of the foliar frame are cut with a cautery pen along the dashed yellow lines.

For mechanical testing, fibers were drawn manually and dried under the seed's own weight at ambient conditions overnight. Small homogenous segments from individual fibers were glued onto a foliar frame using cyanoacrylate superglue (Loctite 454) and cured overnight. The initial free fiber length was determined by taking micrographs with a digital microscope (Keyence VHX-S550E) and further analyzed with Fiji 1.51n resulting in a fiber length of ~5.4 mm. Mechanical experiments were conducted using a custom-built tensile tester operated with custom built software (1D force table by K. Bienert), which allowed for the control of the RH and the T inside the testing chamber. With the help of a custom-

built humidity generator (HumiGen, Dr. Wernecke Feuchtemesstechnik, Potsdam, Germany) RH and T of the air was regulated during the experiment and the tensile tester T was kept constant at ~20 °C via a thermostat (Huber Ministat 125cc). Samples were loaded in foliar frames and fixed between two clamps on the tensile tester. Frames were cut on both sides flanking the fiber so only the fiber was connecting both ends of the tensile apparatus. Force was measured in a sealed chamber with a load cell (Honeywell 31E) with a maximum capacity of 0.5 N at a testing speed of 5 µm s^{-1}, while deformation was recorded using a digital camera (Basler acA1920-40um) mounted on a stereo microscope (Olympus SZX7). All samples were stored in a sealed box with silica gel before testing. Each fiber was equilibrated for at least 3 h at 0% RH and 20 °C before it was successively tested at the following RH levels: 20/30/45/60/75/90% with an equilibration time of 30 min after each successive change of the RH. Each test consisted of three cycles with a motor travel distance of 25 µm (0% to 45% RH) or 75 µm (60% to 90% RH). Stress was calculated on the basis of the fiber diameter at each RH level assuming a cylindrical cross section as confirmed with ESEM. Diameter was determined at each RH level by calculating the mean of 10 measurement points per sample with a digital microscope (see LM section above). Tensile stiffness was determined as the mean value of the slope of the initial linear region of the stress-strain curves of three subsequent cycles. Five fibers from five different berries were tested successfully.

3.2.9 Thermogravimetric analysis

The moisture content (MC) as a function of relative humidity was measured with a thermogravimetric analysis (TGA) system (Sensys Evo TG-DSC, Setaram, France), connected to a custom-built humidity generator (HumiGen, Dr. Wernecke Feuchtemesstechnik). The water sorption–desorption isotherms of ~17 mg of mistletoe fibers (dry weight, d.wt.) were measured at 29 °C by applying a step-by-step humidity program with 10% RH steps and equilibration time of 4-5 h. The MC was calculated using Equation 1:

$$= \frac{\cdot \quad -\bar{A} \quad)}{} \times 100\% \qquad \text{(Equation 1)}$$

Where MC is the moisture content in %, m_{wet} is the varying mass in mg of the sample during adsorption/desorption, m_{dry} is the mass in mg of the dry sample measured after equilibration at 0% relative humidity.

3.2.10 X-ray diffraction

3.2.10.1 Small angle X-ray scattering

Synchrotron based small angle X-ray scattering (SAXS) experiments were conducted at the mySpot beamline (Paris et al. 2007) at the BESSY II synchrotron radiation facility (Helmholtz-Zentrum Berlin, Adlershof). Fibers were prepared as described for mechanical testing and mounted vertically and perpendicular to the incident X-ray beam in a custom built

tensile tester replacing glass windows with Kapton foils. The fiber was pre-stretched at low forces at ambient conditions to ensure a straight vertical alignment. During the entire measurement the force was kept constant. A humidity generator (Wetsys, Setaram, France) was connected to the tensile testing chamber applying a step-by-step humidity program with 10% RH steps equilibration time of 1.5 h. Continuous line scan across the fiber were performed to measure changes during hydration/dehydration with 5 adjacent measuring points with a beam size of 50 µm and a measurement time of 120 s per scan point were performed. To avoid beam damage each successive line scan was shifted vertically by 100 µm along the fiber. The wavelength of the incident beam was 0.082656 nm. SAXS patterns were collected with a 2D CCD detector (Rayonix MAR Mosaic225, USA) with total area of 3072 x 3072 pixels and a pixel size of 73.2 µm x 73.2 µm at a sample-to-detector distance of ~85 cm.

3.2.10.2 Wide angle X-ray scattering

Wide angle X-ray scattering (WAXS) experiments were performed at the same beam line as described above. WAXS patterns were collected at a sample-to-detector distance of ~30 cm. Samples from the transition zone between VCB and fiber were mounted vertically and perpendicular to the incident X-ray beam. Mesh scans were performed with a 2 x 2 detector binning and a measurement time of 45 s per point. Two mesh scans with a grid of 25 x 9 and 10 x 5 scan points with a beam diameter and step size of 50 µm resulted in two adjacent scanned total areas of 1.25 mm x 0.45 mm for the VCB and 0.5 mm x 0.25 mm for the fiber, respectively. Line scans were performed on viscin films scanning across the films with a 50 µm step size and a measurement time of 60 s per point. Cellulose crystallite dimensions were determined using a Si 111 DC monochromator to reduce signal broadening due to the experimental setup of the beam line. Three spots were measured on each of two fibers harvested in two different seasons in winter 2016 and 2017. The measurement time was 120 s. The beam diameter was 50 µm. The 2D scattering patterns were further processed and analyzed with dpdak v.1.3, an open source XRD analysis tool (Benecke et al. 2014). The fundamental principles underlying XRD can be found in Spieß et al. (2009). XRD on cellulose crystallites is based on Bragg's law (equation 2),

$$2 \sin = \qquad \text{(Equation 2)}$$

which describes the general conditions for constructive interference for radiation scattered on a three-dimensional crystal lattice, where d is the distance between two parallel lattice planes, Θ is the Bragg angle, n is a positive integer and λ is the wavelength of the incident X-ray beam. The radial scattering intensity profiles in this work are presented as a function of the scattering vector q according to Equation 3:

$$= 4 \frac{\sin}{} \qquad \text{(Equation 3)}$$

Where q is the scattering vector in nm^{-1}, λ is the wavelength of the incident X-ray beam (0.082656 nm) and Θ is the Bragg angle. The q-values from reciprocal space were transformed into real space using Equation 4:

$$= \frac{2\bar{A}}{} \qquad \text{(Equation 4)}$$

Cellulose crystallite dimensions in the direction normal to the lattice planes responsible for the Bragg reflection were calculated using the Scherrer equation (Equation 5):

$$= \frac{}{\bar{A}\cos} \qquad \text{(Equation 5)}$$

Where L is the mean crystal size normal to the lattice plane, K is a dimensionless shape factor close to unity (0.9), λ is the wavelength of the incident X-ray beam (0.082656 nm), B is the analyzed full width at half maximum (FWHM) of the indexed reflection in rad after subtracting the instrumental line broadening and Θ is the Bragg angle in rad.

3.2.11 Fiber welding

Method 1: Viscin fibers were drawn manually as described above. The fibers were glued onto a cardboard frame spanning a squared window of ~2 cm x 2 cm as follows: One end of the freshly drawn fiber was attached to an arbitrary point of the cardboard, exploiting the natural adhesive character of the fiber which instantly adheres firmly to the cardboard. The loose end of the fiber is drawn over the cardboard window towards an arbitrary edge where the fiber is laid down which again instantly adheres the drawn fiber along the small segment which is contact with the cardboard. The loose end of the fiber is again drawn over the cardboard window towards an arbitrary edge of the cardboard where the fiber is laid down. Repeating this procedure quickly allows to generate a fiber network of any desired pattern. When the fiber comes in contact with previously laid down segments the crossed fiber segments instantly attach and fuse. The fiber network quickly dries under ambient conditions after which it was cut free along the edges of the cardboard frame with scissors or a razor blade. The squared fiber networks could be handled with tweezers. Six networks were arranged as a cube where a large number of free fiber ends along the edges of the individual networks was used to create a temporary interlocking. The cube was exposed to a stream of saturated water vapor for 60 seconds generated by a humidifier which leads to a permanent fusion of the numerous crossed fiber segments along the edges of the cube.

Method 2: A viscin fiber was drawn manually as described above. The fiber was attached to a laboratory stand and dried under the load of the seed's own weight. The dried fiber was cut into short segments of ~2 cm. The fiber segments were glued onto a foliar frame with super glue, leading to a free fiber length of ~5 mm. The glued fiber and the foliar frame were cut in the center with a razor blade. The two loose fiber ends were moved together again so that they aligned parallel with an overlap of ~1 mm. Then the cut fiber was exposed to a stream of saturated water vapor for 90 seconds generated by a humidifier which leads to a permanent fusion of the loose fibers ends. The fusing process was observed with PLM

video imaging using a digital microscope as described above. The fused fiber segment was cut with a razor blade perpendicular to the long axis and imaged with ESEM.

Method 3: Viscin fibers were drawn manually and dried as described above and cut into short segments of ~2 cm. The fibers were glued onto a cardboard frame spanning a circular window with a diameter of 16 mm as follows: A first layer of parallel fibers was glued onto the cardboard in a horizontal string pattern. Each fiber was placed in position with the loose ends on the cardboard. The tip of the index-finger was moistened and gently pressed onto one loose fiber end for a ~2 seconds. Afterwards the fingertip is moistened again and pressed on the other fiber end. This was repeated for all horizontal fibers. Analogously a second layer of fibers was deposited in a vertical string pattern. In the same way multiple further layers can be added. The crossed fibers were investigated with PLM and ESEM. Then the structure was exposed to a stream of saturated water vapor for 90 seconds generated by a humidifier which leads to a permanent fusion of all crossed fibers. After drying under ambient conditions for 5 minutes the fused fibers were investigated with PLM and ESEM.

3.2.12 Viscin multimaterial adhesion tests

Viscin was isolated from single berries as described for the making of viscin films above where the seed and the fruit skin were cut off at both ends of the isolated viscin. The viscin of a single berry was deposited on the top surface of an erected cylinder and drawn into a fiber which was attached to a horizontal steel bar of a laboratory stand placed above the cylinder. This way 10 viscin fibers were made connecting the metal bar with a 10 lined up cylinders each consisting of a different material: brass, aluminum, stainless steel, quartz glass, polytetrafluoroethylene (PTFE), high density poly ethylene (HDPE), polycarbonate (PC), polyamide (PA), polypropylene (PP) and Beech wood. Each cylinder had a diameter of 10 mm and a weight of ~10 g. The viscin was allowed to dry for 2 h until the metal bar was lifted by 10 cm so the dried viscin fibers were carrying the load of the free hanging cylinders.

To test the adhesive properties of viscin in combination with cartilage a pork knee joint was used from a fresh pork leg, bought from Fleischerei Domke, Berlin. The cartilage from the knee joint was isolated from the surrounding tissue. Viscin and seed were extracted as described for the making of viscin films and attached to the freshly exposed cartilage tissue.

3.2.13 Making films from mistletoe viscin

The viscin inside berries of *V. album* can be used to make adhesive films. Berries were either used freshly after harvest or flash frozen berries were thawed before usage. Initially the simplest way to make a viscin film shall be described: first the peduncle of the berry has to be pulled off. By gently compressing the berry between two fingertips the seed is pushed out of the bottom opening of the berry skin. Then the remaining berry is grabbed with two fingers of both hands each and a firm pressure is applied on the berry until it bursts

(Fig. 3-3A). The mucilaginous remaining viscin within the berry is released which will instantly adhere to the fingertips. Now both hands and both fingertips can be moved apart by a few centimeters inducing the formation of a semitransparent 2-dimensional film which is firmly connected to the fingertips and the seed (Fig. 3-3B). The freshly formed film area can be instantly decreased again by simply moving the fingertips and/or hands closer to each other and can be increased again the other way around. Not only the size but also the film shape can be dynamically changed by independently moving the fingers or even rotating the hands. A freshly formed adhesive viscin film can be applied onto a wide range of material surface and readily adapts to various surface shapes and surface topographies, e.g. curved or flat, rough or smooth surfaces.

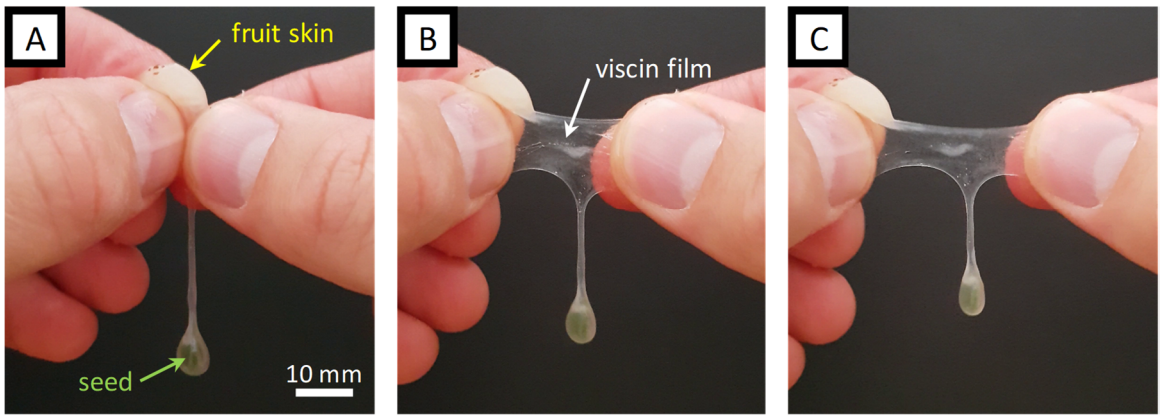

Figure 3-3: Viscin film formation. A) After the peduncle is removed and the seed is released from the berry, the remaining berry is compressed between the fingertips. Scale bar: 10 mm. B) With the viscin firmly adhering to the skin the viscin can be stretched into a semitransparent film by moving both hands apart. C) The film readily extends upon further stretching.

Drawing dimensionally stable free standing 2D films: Single berries were given into a small glass Petri dish with a diameter of 5 cm. A large incision was made on the top of the berry with a razor blade. Through this opening in the fruit skin und the fleshy layer underneath the seed was carefully taken out of the berry with fine tweezers and put aside in the Petri dish close to the remaining berry (Fig. 3-4A). Then the viscin was carefully isolated by hand using tweezers with a broad tip in a stepwise procedure as follows: The tweezers were used to grab the viscin cell clusters, located on the inside of the fruit flesh, and pull it out of the berry with a short and slow movement to reduce the mechanically induced formation of fibers as best as possible. The viscin was deposited on the bottom of the Petri dish next to the seed. The last two steps were repeated until the viscin inside the berry was depleted (Fig. 3-4B). The remains of the fruit skin were grabbed with tweezers and glued to the edge of the Petri dish exploiting the natural adhesive properties of the viscin. Then the seed was glued to the opposite side of the Petri dish and the isolated viscin was carefully lifted off of the bottom, which leads to the formation of a thick viscin strand between the seed and the fruit skin (Fig. 3-4C). To form a triangular shaped film one can grab the strand at any location and pull it towards an arbitrary edge of the Petri dish where it can be fixed by pressing the newly formed pointed end of the film onto the glass for ~30 s (Fig. 3-4D+E). While

pressing the film has to be gently kept under tension to maintain the film shape because otherwise the hydrated viscin film promptly collapses into three thick strands. To form a quadrangular shape one can grab another film edge and pull it towards any edge of the Petri dish and fix it (Fig. 3-4E+F). A quick repetition of this procedure allows to form various 2-dimensional polygons as long as the viscin is hydrated. In order to achieve more complex 3-dimensional film geometries one can select different height levels for the exterior connection points. The resulting film spans the area between the connecting points like a stretched tarpaulin. The viscin films quickly dry under ambient conditions. The thinner center area of the films dries faster than the thicker edges. After drying the dimensionally stable films can be manipulated with tweezers and cut into any shape with tools such as razor blades, knifes or scissors. Tapered ends can also be simply sheared off with a blunt tool.

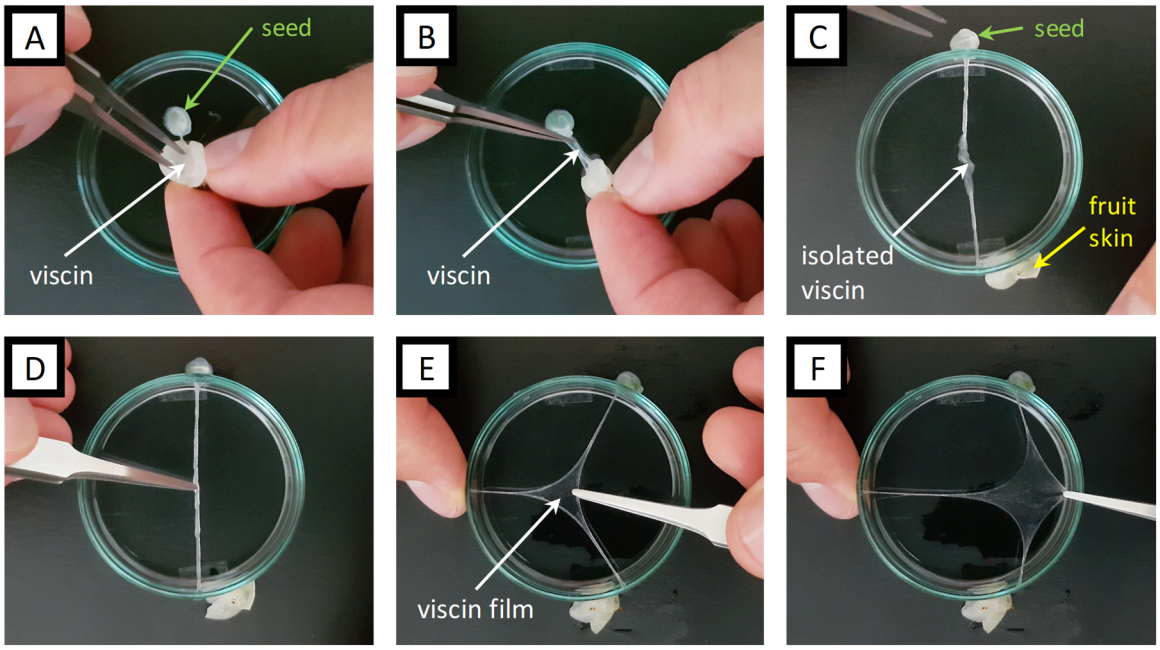

Figure 3-4: The making of free standing viscin films in a Petri dish. A) After making an incision on top of the berry skin, the seed is removed from the berry and put closely aside. B) Using broad tipped tweezers the viscin is carefully pulled out of the berry with slow and short strokes. The viscin is deposited in the center of the Petri dish bottom. C) Exploiting the natural adhesive properties the seed is attached to one edge of the Petri dish, the remaining fruit skin to an opposite edge. Both seed and fruit skin are connected via a thick strand of the isolated viscin. D) The viscin strand is gently grabbed with tweezers and pulled towards the left edge of the Petri dish. E) The viscin was attached to a third connection point which leads to the formation a triangular shaped viscin film. The edge of the freshly formed film is grabbed again and pulled towards an edge on the right. E) A quadrangular viscin film is being formed.

3.2.14 Preparing wound sealings and skin coatings from viscin

The viscin of multiple individual berries can be mixed. Therefore, the viscin can be isolated and collected in a Petri dish as described in the previous section after which the isolated material can be cut free from the seed on one end and from the fruit flesh and skin on the

other end using a razor blade or scissors. The viscin of a second berry can simply be added to the existing viscin. The two viscin units instantly adhere and can only be separated again within the first minute after initial contact. Afterwards they permanently fuse into a sticky mass. By adding viscin of more berries the total mass of viscin can be increased at will. The mixing can be enhanced by slowly stirring the viscin mass with a spatula. The sticky coherent mass can be picked up from the Petri dish either by hand or with tools like tweezers or spatulas. The bulk viscin can then be deposited onto the skin region it is supposed to seal. Starting from the initially covered region the viscin can be readily distributed by shearing the material along its edges where it instantly adheres to the newly covered area. Within several minutes the viscin dries into a transparent film. If the viscin mass is not sufficient enough to cover the desired surface, the remaining area can simply be covered by adding isolated viscin from more berries. This can be done with freshly applied viscin but also when the viscin sealing already partly or even completely dried. Alternatively, the freshly mixed viscin can be manually drawn into films as described above for single berries which can then directly be applied onto the skin. Dried films can readily be peeled or rubbed off of the skin again, leaving no visible traces.

Following remarks about ancient recipes for the use of viscin for making birdlime and skin coatings, viscin was isolated and mixed as described above and then submerged in commercially available olive oil (de Cecco, Italy) or walnut oil (Kunella Feinkost, Germany) for 5 minutes including gentle stirring with a spatula. Afterwards the coherent viscin mass was removed from the oil bath and the oil covered viscin is kneaded by hand for one minute. The resulting viscin-oil mixture was applied to human skin analog to the oil free viscin as described above. The applied viscin was allowed to dry into a transparent film within a few minutes. After testing the film can readily be removed off the skin by pealing or rubbing.

Within this work the author used his own hands to test the viscin adhesive properties in combination with live skin tissue. However, tests for the potential use as a wound sealant were performed on porcine skin from a pork leg. A fresh pork leg was purchased from Fleischerei Domke in Berlin and used the same day. Six parallel incisions were made with a razor blade. The incisions were ~20 mm long and ~5 mm deep with a gab of ~10 mm to the neighboring incision. In an alternating sequence three incisions were treated with viscin and the remaining three incisions were taken as a reference. Fresh viscin was isolated from one single berry for each incision and distributed as a thin layer onto the porcine skin. The viscin was allowed to dry for 1 h until the incisions were mechanically loaded by stretching the skin perpendicular to the long axis of the incisions.

4 Exploring the hierarchical structure of mistletoe viscin: A comparative study

4.1 Introduction

The ability of seeds from the mistletoe species *Viscum album* L. to adhere securely to the branches and trunks of host trees with a sticky substance, known as viscin, is a crucial aspect driving the propagation of this parasitic plant and consequently, in the adaptive success of the species (Kuijt 1969; Heide-Jorgensen 2008). The term viscin is used for a variety of plant tissues within different families of mistletoe and in general, describes the soft mucilaginous tissue that surrounds the mistletoe seed. It was reported previously that certain structures within the viscin tissue of *V. album* are able to form long cellulosic fibers, which have been implicated as a key part of the adhesion mechanism (Grazi and Urech 1981; Azuma et al. 2000); however, fiber formation is not universal to all *V. album* L. subspecies. Indeed, while berries from *Viscum album* L. ssp. *album* (*V. album*) exhibit fiber-forming ability, those of a closely related subspecies *Viscum album* ssp. *austriacum* (*V. austriacum*) do not. Furthermore, it should be noted that these two subspecies are found growing on very different host species with *V. album* found on hardwood trees and *V. austriacum* found typically on pine and larch trees, suggesting perhaps that specific aspects of their adhesive mechanism, including fiber formation, are adapted for colonizing specific host species (Grazi and Urech 1981). While this remains an untested hypothesis, I explore here whether particular structural features of the berry structure may help explain the functional differences between the two subspecies, with a focus on the fiber forming capacity of the viscin tissue and its adhesive properties. Specifically, this chapter investigates the structural organization of berries of *V. album*, growing on apple trees (*Malus domestica*) and *V. austriacum* growing on Scots pines (*Pinus sylvestris*). The main objective of this comparative study is the identification and characterization of structural features involved in the seed-host adhesion and the observed formation of adhesive fibers. As mentioned, *V. austriacum* was chosen as a closely related reference model since it is reported to lack the ability of fiber formation (although it is not clear why), but still manages to adhere successfully to its potential host tree. (Tubeuf 1923; Grazi and Urech 1981).

To gain a deeper insight into the anatomical and subcellular origins of fiber formation and the adhesive mechanisms inherent in these two subspecies, I performed here an in-depth histological analysis of the viscin tissue structure from *V. album* and *V. austriacum* across multiple length scales. The work of Chanzy and co-workers (Azuma et al. 2000) has come the furthest in understanding the complexities of this adhesive tissue. However, two shortcomings of earlier studies were 1) a lack of understanding of the localization of these tissues within the three-dimensional structure of the viscin, leading to potential confusion concerning the functional roles of specific cell types and 2) a lack of full characterization of the subcellular/nanoscale structure of these tissues and their role in adhesion and fiber formation. Moreover, the structural differences between *V. album* and *V. austriacum* viscin have never been clearly delineated with respect to their functional differences.

4.2 Results

4.2.1 *V. album* and *V. austriacum*

The mature berries of *V. album* and *V. austriacum* share some characteristics (Fig. 4-1). Both have a spherical shape and grow on short peduncles. On the opposite side of the peduncle of both berries one can find floral traces in the form of scars deriving from the four tepals and the stigma of the female inflorescence. *V. album* produces berries with typical size of 8-11 mm and often appear silverfish white. Berries of *V. austriacum* are a bit smaller with 7-9 mm and often yellowish white. A clear optical differentiation between collected samples of both species within this work was not possible based on two factors: There was 1) some overlap of characteristics between both species and 2) high biological variation regarding the color and the size within the species as well as within individual plants. However, consistent with the previous work (Tubeuf 1923; Grazi and Urech 1981), it could be confirmed based on examination of several thousand berries that there is one reliable functional characteristic to differentiate the two subspecies – mechanical removal of the seed from the berry of *V. album* invariably leads to the formation of adhesive fibers, while not a single berry of *V. austriacum* exhibited fiber formation.

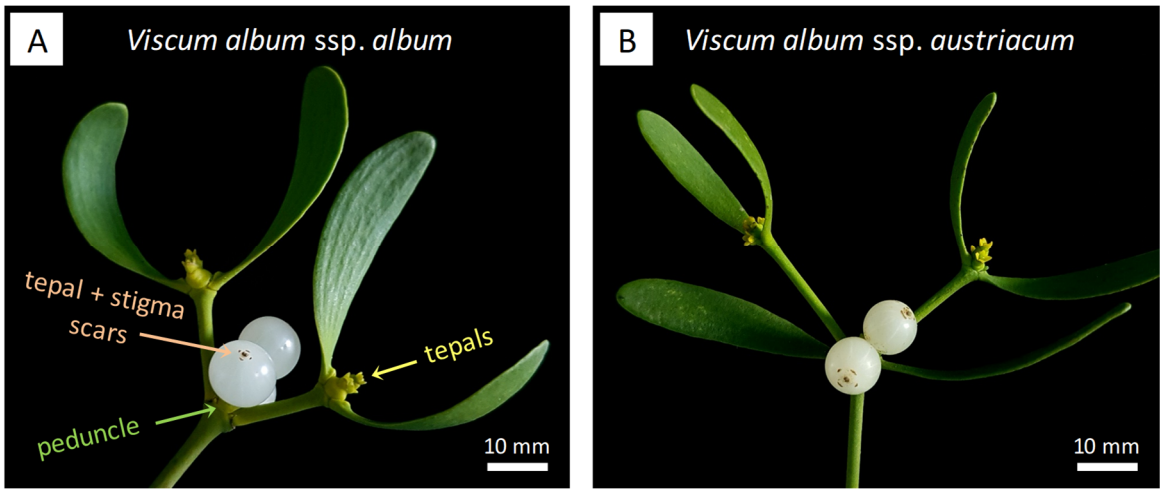

Figure 4-1: Leafed mistletoe branches with (pseudo-)berries of two subspecies of *V. album* L. A) *Viscum album* ssp. *album*: Whitish berries are carried by a peduncle (green arrow). The top of the berry is marked by dark brown scars of the tepals and the stigma (brown arrow). Younger terminal branches show the tepals (yellow arrow) of the female inflorescence of the next growth period. B) *Viscum album* ssp. *austriacum*: Berries of *V. austriacum* are typically smaller than *V. album* and show a yellowish white color. Scale bars: 10 mm.

4.2.2 The mistletoe berry

To understand the reason for the functional differences between subspecies, I first focused on a deep structural characterization of the viscin of *V. album*. Mistletoe berries of *V. album* were collected during various stages of their development cycle. At early stages in the beginning of European summer (June) the green berries were ~3-5 mm in diameter and match the color of the mistletoe leaves, while the whole mistletoe shrub itself is well hidden in the

canopy of the fully leaved apple tree. As shown in Figure 4-2A the berry color gradually changes from a darker green via a lighter green towards the characteristic silvery-white appearance in late autumn and winter while simultaneously growing in size until they reach their final size of ~8-11 mm in diameter. It is conceivable that the color change serves a functional role helping birds recognize the potential food source from a distance against the evergreen leaves of the mistletoe only once the berries are ripe (Kronfeld 1888). Starting even from the earliest developmental stages the ability to form adhesive fibers was observed to be an intrinsic property of berries of *V. album* (Fig. 4-2B). In contrast, berries of *V. austriacum* did not exhibit fiber formation capacity, regardless of developmental stage.

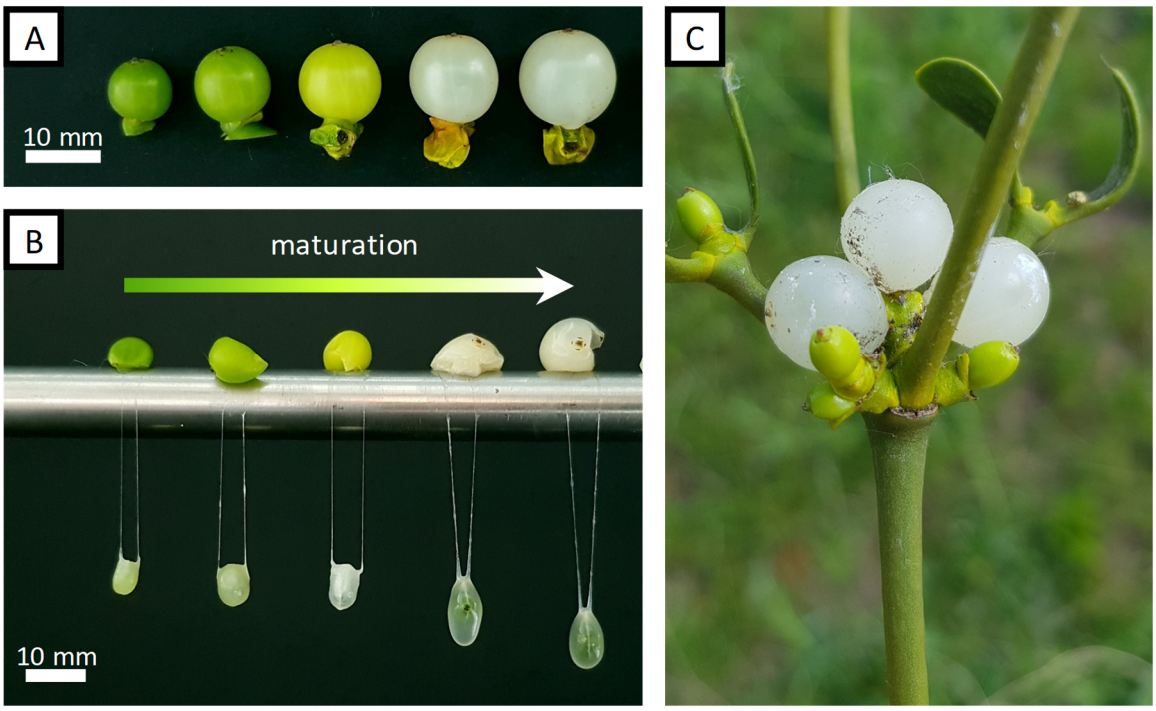

Figure 4-2: Mistletoe fiber formation as an intrinsic property of berries of *V. album*. A) From left to right: With increasing age the berries grow in size and gradually change their color from a dark green in early summer to its characteristic silverish white of the mature berries in late autumn/winter. B) Adhesive mistletoe fibers glued to a laboratory stand. From very early developmental stages to post-maturation a formation of adhesive fibers could be observed. C) Mature white berries next to early development green berries of the next growth period on the same branch. Picture was taken in June. Scale bars: 10 mm.

Assuming such functional differences between the subspecies arise from differences between the adhesive viscin tissue of the berries, histological analysis was performed to identify variations of the inner berry structure between the subspecies using a variety of microscopy methods including conventional light microscopy (LM), polarized light microscopy (PLM), confocal fluorescence microscopy (CFM) and second-harmonic generation microscopy (SHGM). Histological analysis required development of microtomy methods that preserved the microstructure of the berry tissue, which was performed initially on *V. album* to establish a consistent sample preparation methodology and morphological baseline. Initial efforts to hand section fresh mature berries of *V. album* with a scalpel or razor blade were

unsuccessful as the soft mucilaginous viscin layer surrounding the seeds instantly adheres to any blade used for sectioning and was accompanied by an instant adhesive fiber or film formation. While these observations further support the functional role of the inner tissue as an effective adhesive, this approach was not useful for sectioning.

To preserve the berry tissue as close as possible to its native condition during the histological analysis cryo-sectioning was applied. Hand sections of berries of *V. album* under frozen conditions dramatically improved the quality and the dimensional stability of the acquired sections significantly. An important observation of numerous hand sections was that the internal tissue arrangement of the spherical berries is highly anisotropic. This was primarily indicated by the high variation of the seed cross section shapes from a high number of individual berries sliced in half at randomly chosen cutting angles.

Therefore, it was necessary to identify and further define anatomical planes of the mistletoe berry in order to reproduce desired sections. A major drawback of cryo-sectioning was that the frozen berry becomes shiny white after freezing and loses its translucent character as observed in the unfrozen state. Thus, it was difficult to define any anatomical planes based on the physical appearance besides the transverse plane. The latter can be defined by its normal which is formed by the imaginary axis between the peduncle on the bottom, and on the top by the center of 4 typical tepal scars with a pointed stigma scar in the center.

Fortunately, the berries of *V. album* growing on apple trees frequently grow as triplets (Fig. 4-3A). Within a triplet, all berries are connected by the peduncle, which itself is connected to the mistletoe branch. The front, top and side view of such a triplet (Fig. 4-3C, E, F) reveal, that the three berries form a common geometrical plane in which the center berry is typically oriented parallel to the long axis of the peduncle as seen in the front view. With respect to the center berry its two neighbors are tilted by an angle φ (Fig. 4-3C), approximately close to 90° and -90°, respectively. The top view of a triplet reveals that the dark brown scars left by the tepals are shaped like a hair cross (Fig. 4-3E, inset) with a dotted scar from the stigma in the center surrounded by 4 lined scars. These lined scars are located symmetrically around the central scar at angles of 0°/180° (left/right in Fig. 4-3E) and 90°/270°, respectively (top/bottom in Fig. 4-3E). Indeed, their arrangement forms a reliable coordinate system, which allows the definition of the frontal plane of the center berry with its normal defined by the connecting line between the top and bottom scar (Fig. 4-3E, dotted purple line) and the median plane, respectively with its normal defined by the connecting line between the right and left scar (Fig. 4-3E, dotted yellow line).

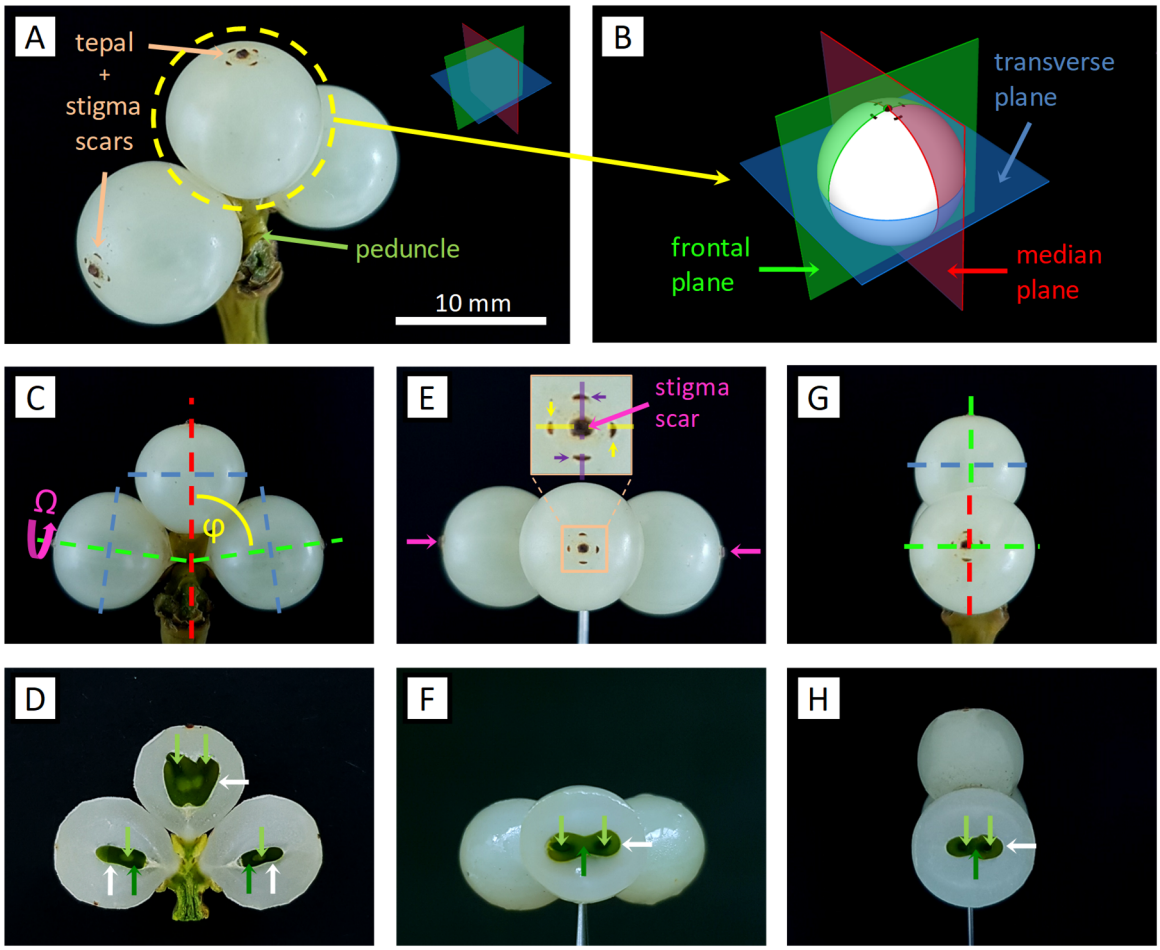

Figure 4-3: Anatomical planes and sections of berries of *V. album*. A) Oblique view of a triplet of berries connected by the peduncle (green arrow) at the bottom and typical tepal and stigma scars (brown arrow) on top of each berry. B) Schematic of the center berry of (A) and its defined anatomical planes. C) Front view of a triplet. Dotted blue line: transverse plane of the central berry and the neighboring berries. For the latter the transverse plane is tilted by the angle φ (close to 90°/-90°). With respect to the median plane of the center berry (dotted red line). Dotted green line: frontal plane of the neighboring berries which is tilted by an angle Ω (~90°) with respect to the frontal plane of the central berry which lies in plane of this front view. D) Hand section of a triplet along the frontal plane of the central berry showing the heart-shaped seed cross section with two light green embryos (light green arrows) embedded in the green endosperm (dark green arrows), surrounded by the endocarp (white arrows). E) Top view of a triplet. The inset highlights the tepal scar arrangement which serves as a coordinate system with its origin in the stigma scar (pink arrow). Dotted connection lines between the mirroring scars mark the normal of the frontal plane (purple) and the normal of the median plane (yellow) of the central berry. Pink arrows: stigma scars. F) Transverse section of the center berry. G) Side view of a triplet. Dotted red line: median plane of the center berry. Dotted blue line: transverse plane of the center berry. Dotted green line: frontal plane of a neighboring berry. H) Transverse section of a neighboring berry.

When these triplets are harvested, frozen and sectioned as a whole it is possible to define anatomical planes with regard to the three-dimensional orientation of the seed within the berry. When sectioning a triplet along the frontal plane of the central berry as defined above the section (Fig. 4-3D) reveals the heart-like shape of the seed of the central berry with its two embryos embedded into the endosperm. In contrast, the sections of the neighboring

berries show an oval seed shape where only one of the two embryos can be seen. Additional sections along the median plane of the central berry on similar triplets show that the median cross section of the center berry equals the cross section of the neighboring berries as observed from the section in Figure 4-3C. Numerous sections along all three anatomical planes as illustrated in Figure 4-3B led to the observation, that the anatomical plane assignment as described above is indeed only valid for the central berry. However, it could be concluded that the transverse plane of the neighboring berries is tilted by the angle φ and additionally the median and frontal planes are rotated by an angle Ω of ~90° around the berry long axis. As a result, the described sectioning of a triplet along the frontal plane of the central berry actually leads to a median section of the neighboring berries with respect to the orientation of the seed within each berry. This is illustrated by sections along the individual transverse planes as indicated by the dotted blue lines in Figure 4-3C where the shape of the seed transverse section of the center berry (Fig. 4-3F) resembles the shape of the seed transverse section of the neighboring berry (Fig. 4-3H). This description applies to heart-shaped seed typically carrying two embryos as shown here, but also to the rather elliptic-shaped seeds which carry only one embryo.

With respect to these observations, the shape and the orientation of the seed can be used to describe the relative location of the remaining tissue structures within the berry. However, the halved surfaces of the described sections in Figure 4-3 hardly reveal any details of the surrounding tissue due to the rather homogenous whitish appearance and insufficient optical contrast. Therefore, ~1 mm thick slices were manually cut with a razor blade along the three different anatomical planes defined in Figure 4-3B. The transmission LM image of a median section (Fig. 4-4A, left) enables visualization of the outlines of a multilayered tissue organization within the mistletoe berry. Despite the overall grayish-white appearance in the LM image, there are moderate differences in the optical density which allow for tissue discrimination. As a complementary technique, transmission PLM was used to image the same section (Fig. 4-4A, right), providing further contrast. The outer skin or epicarp appears darker in the LM image and consists of several layers of densely packed cells. Beneath the epicarp lies a fleshy layer which appears brighter in transmission and was earlier described as an outer part of the mesocarp, which spherically covers the entire inner surface of the epicarp (Azuma et al. 2000). Below the fleshy layer, the actual viscin tissue is located. As observed in the median section, it comprises two mirrored bundles of densely packed elongated cells which are connected to the seed endocarp at the bottom of the seed. Due to their distinct organization into bundles, they are named viscin cell bundles (VCB) within the present work. The tissue exhibits a higher degree of birefringence with PLM than the surrounding tissue (Fig. 4-4A) and is assumed to be a part of the outer cellulosic viscin slime as it was described in the earlier literature (Gjokic 1896; Tomann 1906). As illustrated in Figure 4-4A (dotted lines) these VCBs are ~1 mm wide and arc around the seed in the center towards the top of the berry, which is similar to the description of Azuma et al. (2000).

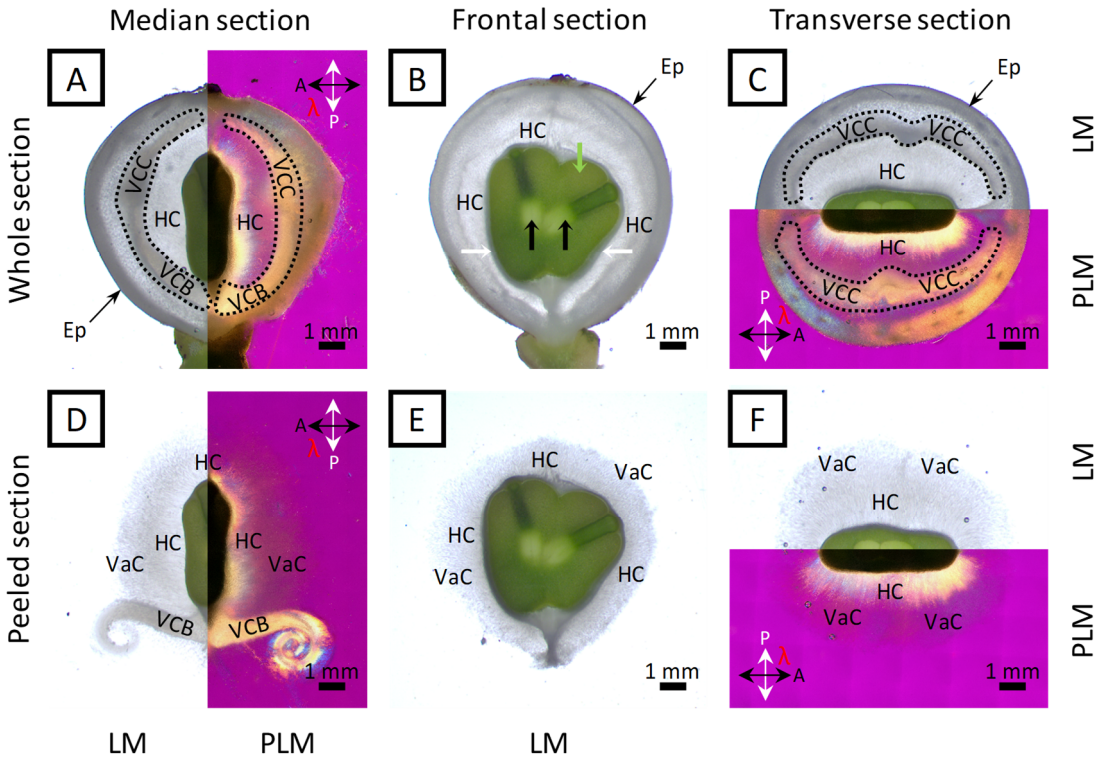

Figure 4-4: Hand sections of *V. album* berries under hydrated conditions. A) median section observed with LM (left) and PLM (right) with highlighted outlines (dotted line) of viscin cell bundles (VCB) and viscin cell clusters (VCC). Radially oriented hairy cells (HC) surround the green seed in the center. B) Frontal section observed with LM. VCB and VCC are not able to be observed in this cutting plane. The embryos (black arrow), endosperm (green arrow) and endocarp (white arrow) and the epicarp (Ep, black arrow) are indicated. C) Transverse section observed with LM (top) and PLM (bottom). The outlines of the VCC are highlighted (dotted line). D) Section from (A) with peeled off epicarp, fleshy layer and VCC. Two short initial fibers each emerging from a region between VCB and VCC were cut so the seed and the attached VCB could be isolated from the surrounding tissue. E) Peeled section from (B). Vacuolated cells (VaC) are mingled between and around the HC. F) Peeled section from (C). Scale: 1 mm.

The viscin cells are embedded in a more transparent sticky mucilaginous substance (Fig. 4-4A). While the individual viscin cells within the VCB in the lower half of the section are oriented along the long axis of the VCB in a rigorously parallel arrangement, there is a change in the cell orientation in the upper half towards the top of the berry (Fig. 4-5A). Here, the individual cells are oriented radially towards the fleshy layer to which they are connected via thin strings that reach out into the fleshy layer. The viscin cells in the upper half are also less condensed than in the VCB, which results in a higher degree of mobility of the individual cells within the surrounding mucilage. Due to the differences in orientation and packing evident from the higher magnification PLM measurements (Fig. 4-5B), they will be referred to as the viscin cell clusters (VCCs) to discriminate them from the tightly packed VCB. This terminology follows the work of Azuma et al. (2000) which described the entirety of viscin cells in the outer viscin layer (presumably both VCB and VCC) also as clusters. Despite these differences in the overall organization VCB and VCC

appear to be a continuous tissue as observed with LM and PLM and a clear separation was not possible. Interestingly, both VCB and VCC are absent in the frontal section of the berry (Fig. 4-4B), whereas the transverse section (Fig. 4-4C) reveals that the VCCs bend around the seed in a sickle-like shape on both sides of the seed. Furthermore, although the two individual VCB/VCC strands on both sides of the median section bend towards each other above the seed or towards the center in the transverse section, they are not connected to each other. This agrees with observations of the frontal section in which neither the VCB nor the VCC can be seen, and contradicts conclusions of previous investigations which describes the tissue to form a continuous ring around the seed (Azuma et al. 2000).

Aside from the fleshy layer and the VCB/VCC, a third layer can be found within the mesocarp. This layer is located between the VCB/VCC and the seed and surrounds the entire seed. It comprises elongated cells which are connected directly to the endocarp that have been described in the literature as so-called hairy cells (HCs) (Azuma et al. 2000). They are accompanied by highly vacuolated cells (VaCs), which are mainly located between the HC and the VCB/VCC, but also between the individual hairy cells and between VCB/VCC and the fleshy layer. While transmission LM reveals hardly any details of the HCs and VaCs, PLM, in contrast, clearly differentiates the two cell types based on differences in birefringence (Fig. 4-4D-F) and illustrates the ray-like orientation of the HCs around the seed and the dimensions of the cells (Fig. 4-5B, center). Indeed, the HCs have a high aspect ratio tapered shape with a length of ~1-2 mm and a cell diameter that varies from a maximum of up to ~50 µm at the base close to the seed where they exhibit highest birefringence to a minimum of only a few µm at their pointy ends. PLM further reveals helical cell wall thickenings with a helical angle of ~65-75° with respect to the cell long axis, which are characteristic for this cell type (Fig. 4-5B, right). Although this cannot be confirmed for all HCs many of these cells exhibit a wavy serpentine shape when viewed with PLM. It can be assumed that together the HCs and VaCs are identical to what was described in the earlier literature as the inner pectosic viscin slime (Gjokic 1896; Tomann 1906) where the hairy cells were found to be comprising of an outer pectic cylinder and an inner cellulosic cylinder.

During the microscopic examination, the different tissues were also probed with regard to their potential individual functionality. With the help of fine tweezers, the different tissues were poked, stretched and placed under shear stress. The HCs showed a high flexibility in bending and a high mobility of the individual cells when they were gently poked. Grabbing several HCs at their pointy ends they showed a generally elastic response by gentle mechanical loading and unloading. But when they were exposed to intense stretching, the individual cells could be irreversibly drawn into thin filaments of a few mm in length, which revealed an intense birefringence under crossed polarizers. In comparison, when probing the VCC with tweezers, the slightest touch of the tissue leads to an instant adhesion of the tweezer tip to the VCC. Furthermore, gently shaking the adhered tissue reveals that the VCC is extremely flexible and mobile. Many cells which extend into the HC/VaC layer with their loose pointy ends are seen to perform wavy movements within the surrounding

mucilage. When the tweezers were then retracted, adhesive fibers were formed from within the VCC, which could easily be extended to a length of ~20-30 cm, which showed intense birefringence in PLM.

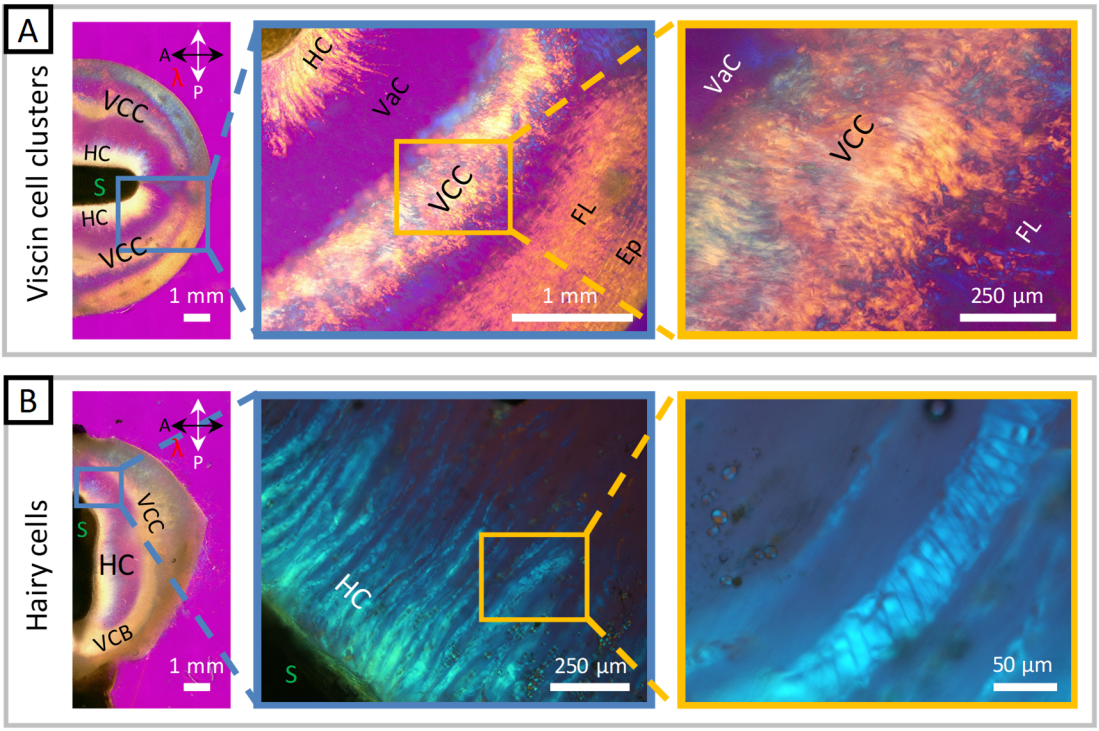

Figure 4-5: PLM images using a red full-wave retardation plate highlighting selected tissue types within the mesocarp of berries of *V. album*. A) Left: half transverse section. Scale bar: 1 mm. Center: selected region from the blue inset (A, left) showing the layered tissue arrangement of the mesocarp. The birefringent HC are directly connected to the seed (S), followed by the non-birefringent layer of VaC. The VaCs are surrounded by the viscin cell cluster (VCC) which exhibits a strong birefringence. The VCC is surrounded by the outer layer of the mesocarp, the fleshy layer (FL). The epicarp (Ep) is the outermost layer of the berry. Scale bar: 1 mm. Right: detail of the VCC which reveals that this layer has a radial thickness of ~ 1 mm and comprises of highly birefringent elongated cells with a preferred radial orientation which partly reach out into the FL. The FL exhibits only weak birefringence close to the VCC. Scale bar: 250 µm. B) Left: half median section. Scale bar: 1 mm. Center: selected region from the blue inset (B, left) showing so called hairy cells (HC) which are connected to the endocarp surrounding the seed (S). The birefringent HCs are oriented in a ray-like fashion towards the epicarp. Scale bar: 250 µm. Right: detail of a HC which reveals spiral cell wall thickenings. Scale bar: 50 µm.

By gently poking the VCB in the lower half of the median section, it was observed that the whole cell bundle is very flexible and readily bends in all direction as a whole without undergoing any noticeable damage. Apart from the firm connection to the bottom of the seed, the VCB showed no visible connection to the surrounding HC/VaC layer on the inner side or the fleshy layer towards the outside. A gentle tugging at the bottom of the seed leads to an observed elastic response of the VCB, which readily stretches under small loads and contracts immediately after unloading. However, under larger pulling forces, the following characteristic macroscopic observations were made: 1) The HC/VaC layer stays firmly connected to the seed, while it detaches from the VCC. 2) The VCBs stay firmly connected to

the seed, while they detach from the HC/VaC layer on the inside and the fleshy layer on the outside. 3) A further continuous pulling at the seed leads to the formation of two adhesive fibers emerging from a transition zone between the VCB and the VCC along both sides of the seed. 4) The VCC and VCB are still connected via the fibers. 5) The VCC stays connected to the fleshy layer and the VCB with the epicarp. As a result, it is possible to peel sections as shown in Figure 4-4D-F in which the epicarp, the fleshy layer and VCC were removed mechanically. A peeling of the median section leads to the characteristic fiber formation between the VCB and VCC when the seed is pulled out (Fig. 4-2B). The emerging fiber was cut with surgical scissors close to the zone which can be described as the tip of the VCB (i.e. the region at which fiber formation is initiated under large forces) to stop the mechanically induced fiber formation. This way further changes of the native tissue arrangement could be reduced, enabling a more detailed investigation of the tissue. As VCB and VCC are absent in the frontal section the seed can easily be pulled out from the surrounding tissue without any observation of a fiber formation. In the transverse section, the VCC seems to have no direct connection to the inner layers and so it readily detaches from the HC/VaC layer that is connected to the seed while no fiber formation is observed when the seed is pulled out.

4.2.3 Comparative structural analysis of berries from *V. album* vs. *V. austriacum*

After the basic anatomical features of the subspecies *V. album* were clearly identified above, and the fiber-forming capacity was clearly associated with the VCB/VCC, I performed a careful structural comparison with berries from the subspecies *V. austriacum*, which, as already stated, are incapable of forming adhesive fibers. Anatomical comparison between berry sections of *V. album* and *V. austriacum* (Fig. 4-6) revealed major differences in the internal tissue organization of the two subspecies. In the median section of *V. austriacum* the VCB and VCC – the presumed origin of the viscin fibers in *V. album* – are completely absent, providing a clear structural correlate to the observed functional differences between the subspecies. While the outer cellulosic viscin layer is apparently missing there is an inner pectosic viscin layer which shows very similar characteristics compared to *V. album*. The seed is also surrounded by a layer of radially oriented hairy cells which are accompanied by vacuolated cells. Compared to *V. album* there is also only a small fleshy layer surrounding the HC/VaC layer, which is enclosed by the epicarp. The fleshy layer readily detaches from the epicarp and the HC/VaC layer. The general lack of VCBs and VCCs and the similar organization of the HC/VaC could also be confirmed for frontal and transverse sections of *V. austriacum* (not shown).

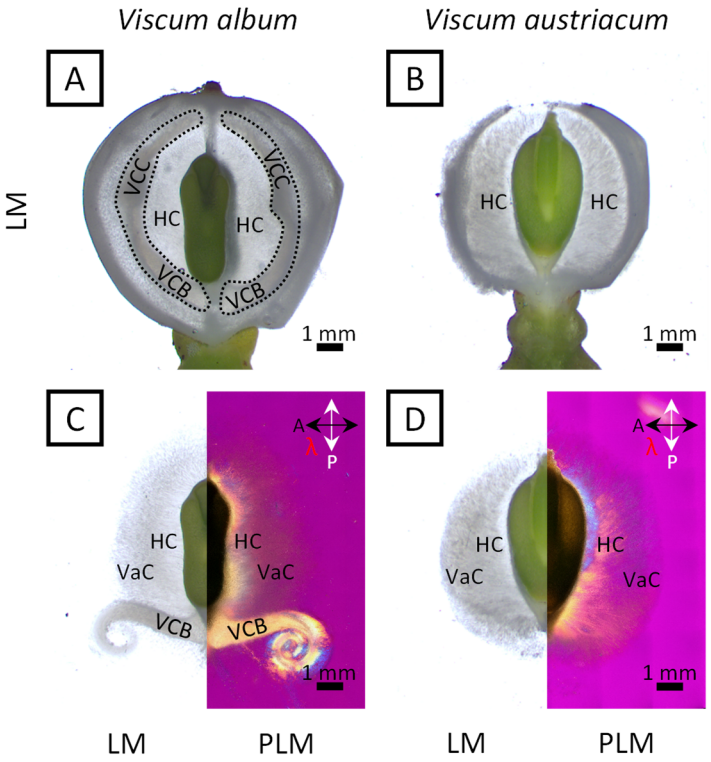

Figure 4-6: Comparative median berry sections of *V. album* and *V. austriacum* under hydrated conditions. A) LM image of *V. album* with highlighted viscin cell bundle (VCB), viscin cell clusters VCB and hairy cells (HC). B) LM image of *V. austriacum*. VCB or VCC are absent. C) peeled section of (A) observed with LM (left) and PLM (right). D) Peeled section of (B). Scale bar: 1 mm.

4.2.4 Detailed structure of the VCB from *V. album*

Based on the complete absence of VCB in *V. austriacum*, coupled with the observation that the VCB/VCC in *V. album* readily forms long fibers, while the other tissue structures do not, I examined the hierarchical organization and fiber-forming capacity of the VCB tissue from *V. album* in greater detail. To achieve this, the seed and the attached VCB were mechanically isolated from the whole berry by making a small incision in the epicarp on the bottom of the berry to create an opening. With the help of fine tweezers, one can grab the seed through this opening and pull it slowly out of the berry. The entire seed is surrounded by the HC/VaC layer, which appears as a spherical translucent shell around the exposed seed. On the bottom of the seed, the two mirroring VCBs can be observed. Pulling the seed further away from the berry leads to an intense stretching of the VCBs, which initiates the formation of fibers that could easily reach a final length of more than 1 m. Similar to the peeling of the sections as described above, it was intended to preserve the natural condition of the tissue as best as possible and so the initial very short fiber between VCC and VCB was cut right after the seed was pulled outside the berry and after the VCBs detached from the HC/VaC layer.

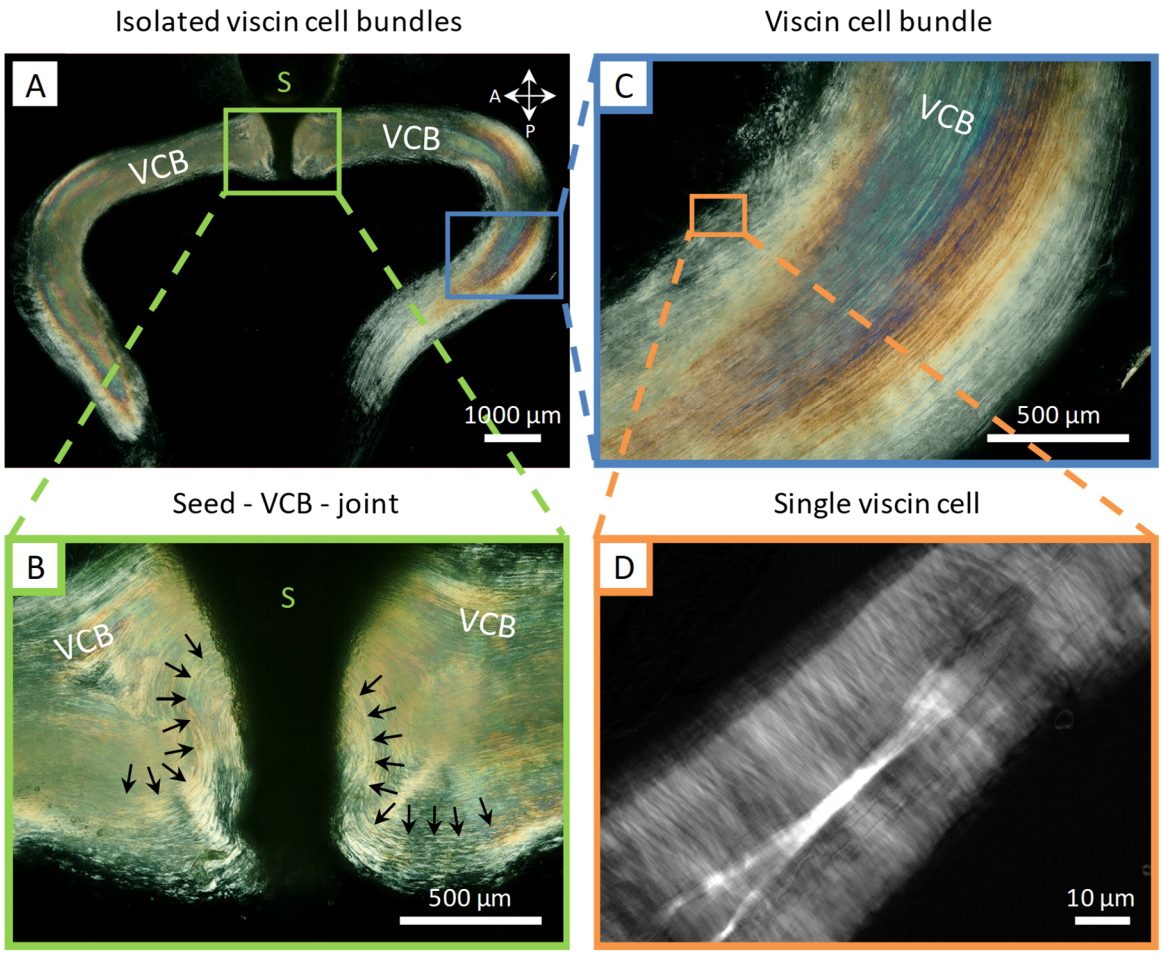

Figure 4-7: Mechanically isolated viscin cell bundles (VCBs) imaged with PLM. A) The two mirroring VCBs are imaged directly after isolation under still hydrated conditions. The VCBs are firmly connected to the bottom of the seed (S), which appears dark as it is only weakly birefringent. To demonstrate their flexibility, the VCBs were mechanically bent downwards (opposite direction compared to the native orientation within the berry) which does not inflict noticeable damage to the cell bundle. Scale bar: 1000 µm. B) Detail of (A, green box): even moderate bending of the entire VCB may cause extreme local bending at the base of the VCB close to the seed. Arrows: exemplary bending line with extreme bending in opposite directions on a small local scale. Scale bar: 500 µm. C) Detail of (A, blue box): VCB consists of densely packed elongated cells which exhibit strong birefringence. Changing polarization colors indicate a gradient in the bundle thickness. The thickness increases towards the center and shows an arched cross-sectional shape. The thickness also decreases from the base to the tip. Scale bar: 500 µm. D) Detail of (C, orange box): The individual cells show the presence of submicron sized cellulosic filaments with a perpendicular orientation with respect to the cell long axis. Scale bar: 10 µm.

Figure 4-7 shows PLM images of freshly isolated VCBs still attached to the seed. The two bundles are ~1 mm wide and consist of densely packed elongated cells as revealed by the intense birefringence under crossed polarizers. The length of isolated VCBs varied within a range of 5-10 mm (Fig. 4-7A). The individual viscin cells showed the presence of submicron sized cellulosic fibrils oriented perpendicular to the cell long axis with a mean microfibril angle of ~90° (Fig. 4-7D), which can also be confirmed for the cells in the VCC. This peculiar structural organization agrees with earlier studies reporting the presence of viscin

cells with a similar arrangement for *V. album* L. (Azuma et al. 2000) and *Phthirusa pyrifolia* (Gedalovich and Kuijt 1987). The submicron sized fibrils appear to be homogeneously distributed in size and evenly spaced within the cell wall (Fig. 4-7D). Figures 4-7A-C demonstrate the flexibility of the entire VCB under hydrated conditions. The native VCB inside the berry bends upwards around the seed as shown in the previous sections. Here, it can be shown that the bundle can be manually flipped in the opposite direction without inflicting noticeable damage. Indeed, at the base of the VCBs near the bottom of the seed, the individual viscin cells within the bundle demonstrate a high compliance when exposed to extreme bending in opposite directions on a small local scale (Fig. 4-7B). It has to be noted that the different tissue types within the viscin, e.g. VCB, VCC and HC only remain flexible as long as they are hydrated. Either they were kept hydrated in water or they were examined directly after mechanical isolation by acting quickly. The air exposed samples quickly dried, which led to excessive shrinking and to a gradual loss of flexibility up to a point where the viscin becomes completely brittle during mechanical stimulation.

4.2.5 The transition from cell tissue to fibers

While the previous sections gave important insights on the pristine viscin tissues within the berry the following sections will examine the phenomenon of the fiber formation process in more detail. VCBs were isolated as described above without restricting the fiber formation process this time. Freshly isolated samples including the seed, VCB and the emerging fiber were mounted on glass slides. An investigation with PLM revealed that the stretched VCB exhibits a strong necking behavior in the transition zone where the VCB transitions into a fiber (Fig. 4-8). Numerous micron sized filaments emerge apparently from individual cells within the VCB, which co-align in a parallel fashion along the fiber long axis; however, PLM does not provide sufficient lateral or depth resolution in order to visualize changes at the level of the cell wall and beyond.

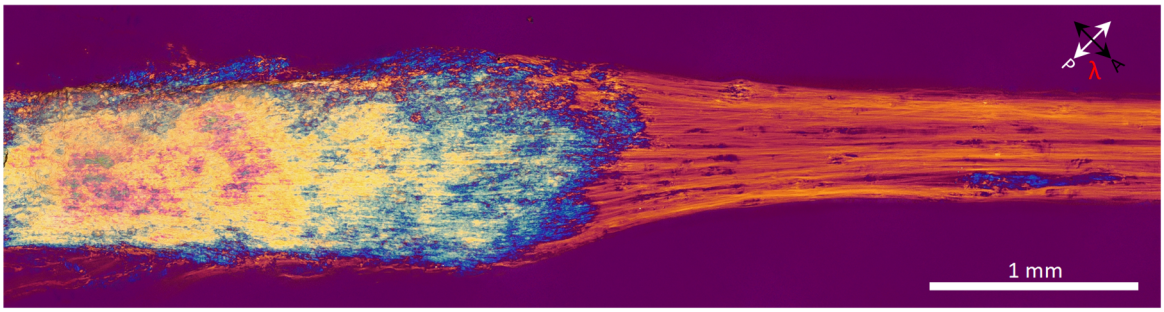

Figure 4-8: PLM image of a mechanically isolated (left) and stretched (right) viscin cell bundle. Scale bar: 1 mm.

In order to determine what occurs within the viscin cell wall of individual cells during fiber formation, I employed confocal fluorescence microscopy (CFM) and second-harmonic generation microscopy (SHGM). Representative CFM images from selected volume scans of the VCB-fiber transition zone, the emerging fiber and the fiber stained with fluorescent

cellulose dyes (Direct Yellow 96, Direct Red 23) are shown in Figure 4-9 with a view at the top of the VCB and at a central plane within the bundle and fiber, respectively.

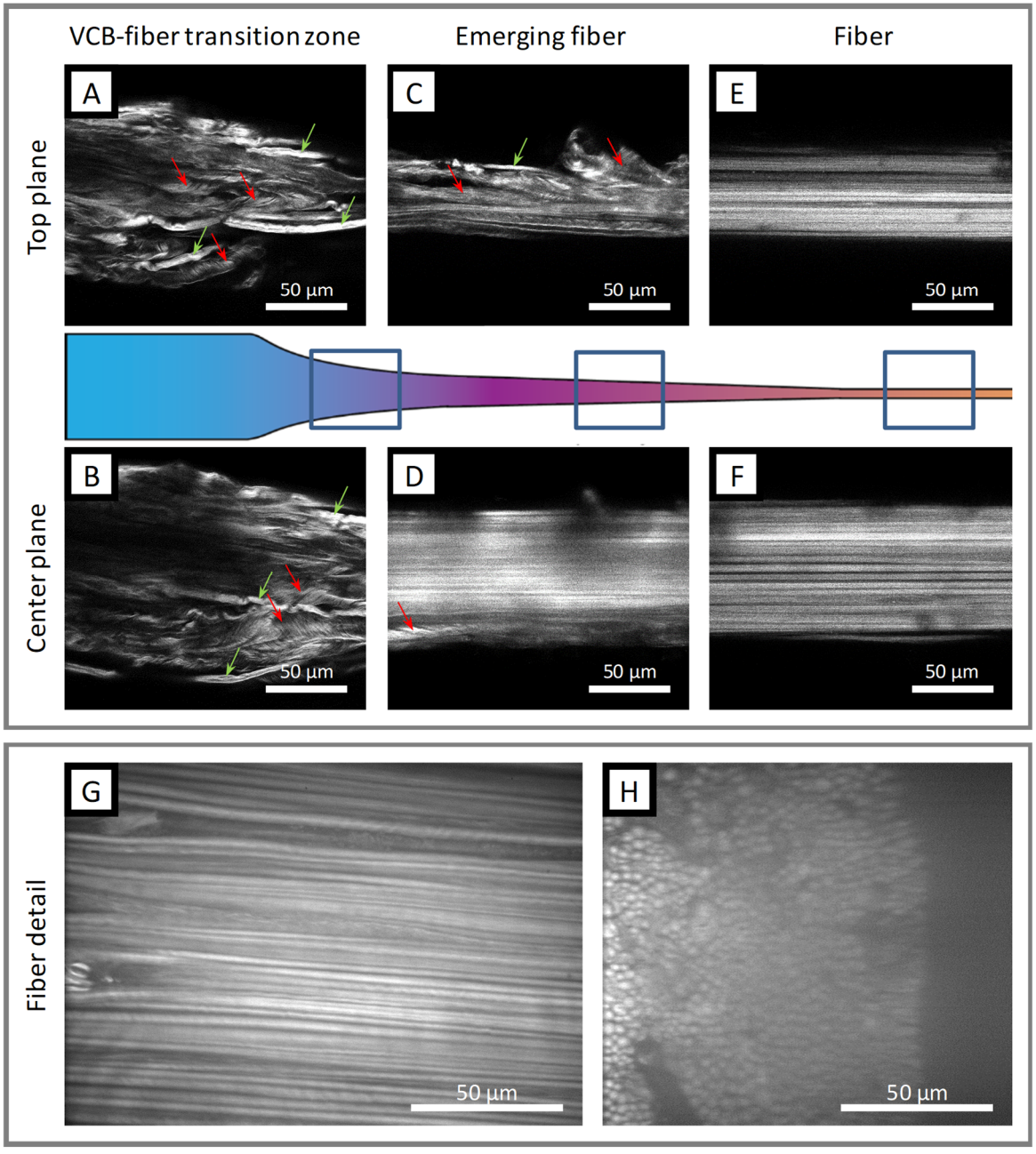

Figure 4-9: Representative CFM images from selected regions along the transition from the VCB to the emerging viscin fiber, stained with Direct Yellow 96 (A-F) and Direct Red 23 (G+H). A,C,E: images from a top plane of a CFM image stack. B,D,E: images from a center plane. A) Stretched (green arrows) and pristine viscin cells (red arrows) in the VCB-fiber transition zone. B) As in (A) taken from a center plane. C) On the top of the emerging fiber pristine cells and stretched cells are still intermixed. D) In the center plane of the emerging fiber most filaments are already highly aligned along the fiber long axis. E+F) Further along the fiber the entire cross-section consists of highly aligned filaments. G) Top view. Fiber detail, revealing the size and the straight parallel filament alignment. B) Virtual fiber cross section. Scale bars: 50 µm.

Figure 4-10 shows SHGM images of the unstretched VCB cells, as well as stretched VCB fibers in the natural unstained state, taking advantage of the inherent strong SHG signal of cellulose (Cox et al. 2005). Both imaging methods reveal the presence of submicron sized cellulose fibrils wrapped around the VCB cell walls oriented essentially perpendicular to the cell long axis, consistent with the observations with PLM (Fig. 4-7D). Images of the fibers similarly show the presence of thin cellulose filaments, but in the fibers, they are highly aligned along the fiber axis and appear to be larger than the pristine transverse fibrils with a typical diameter between 2-3 µm (Fig. 4-9 G+H; Fig. 4-10B). Notably, in CFM images of fiber cross-sections (Fig. 4-9H), the filaments appear evenly spaced by a non-staining material, which is likely comprised of the previously postulated matrix component that enables sliding and alignment of the microfibrils in the wet state, but binds the microfibrils like a cement in the dry state (Horbelt et al. 2019). Closer examination of the VCB in the transition zone where the tissue is in the process of fiber formation reveals a disorganized arrangement of cells some of which are partially uncoiled, mixed among cells that are pristine and unstretched (Fig. 4-9A+B). One can deduce from these imaging studies that individual cells rupture separately from other cells, providing a potential "reserve" of hidden length.

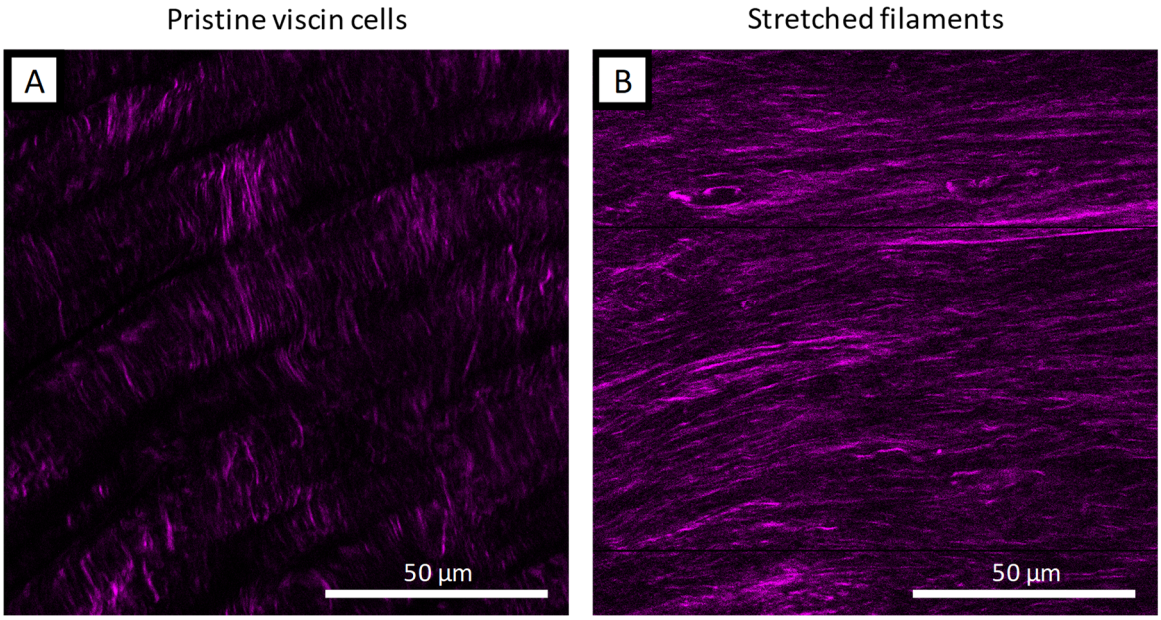

Figure 4-10: Second-harmonic generation microscopy images from selected regions of the pristine viscin bundle cells and the drawn fiber. A) Top view of pristine cells within the VCB showing the typical perpendicular cellulose fibril arrangement. B) Top view of the fiber region showing numerous filaments with a parallel orientations. Scale bars: 50 µm.

It was previously proposed that the matrix between the cellulosic components of *V. album* L. is comprised of hemicelluloses and possibly pectins (Azuma et al. 2000; Azuma and Sakamoto 2003). Similar results were reported within a comparative study of viscin tissue of *P. pyrifolia*, *P. californicum* and *A. americanum* (Gedalovich-Shedletzky et al. 1989) also providing evidence for pectins. This is consistent with observation of a non-staining

or non-SHG active material observed between cellulose filaments in VCB cell walls and fibers. To test the possible role of pectins as a functional matrix component important for fibers formation, fibers were treated with pectinase, an enzyme that breaks down pectin. Interestingly, this resulted in an increase in the disorder of the fiber, as well as the breakdown of the micron scale filaments into smaller nanofibrils on the scale of 250 nm (Fig. 4-11B). This indicates yet another hierarchical length scale at which this material is structured, and may help explain the ability of the cellulosic fibers to slide and align upon an applied force. However, in order to draw precise conclusions, the chemical composition of this matrix material must be further characterized in the future.

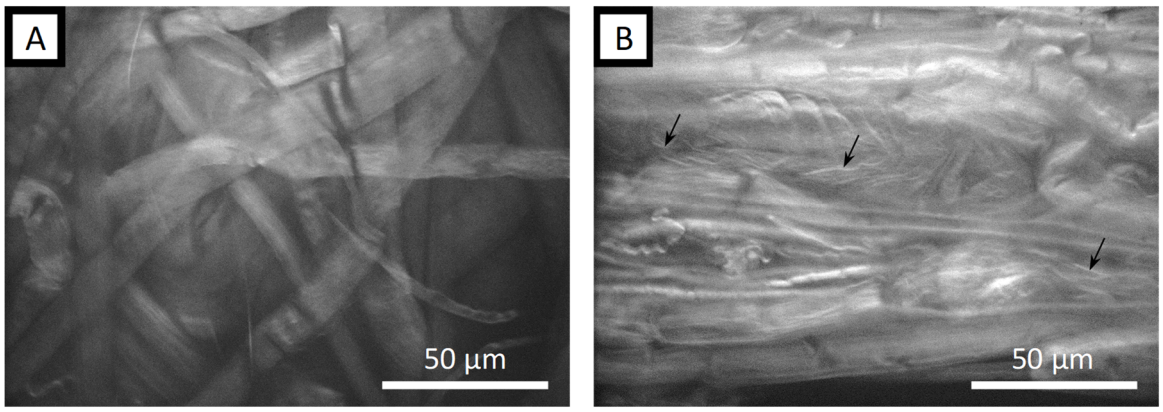

Figure 4-11: CFM images of viscin fibers stained with Direct Red 23 (S4B), immersed in water. A) Top view. Water based staining after pectinase pretreatment showing a disordered filament arrangement with some filaments revealing the presence of smaller cellulosic fibrils (black arrows). B) Top view. Control sample without pectinase treatment. Water-immersed filaments lost their preferred parallel orientation as a result of the staining procedure. They also change their shape from a circular cross-section towards a flat broad band but individual filaments are still discernable. Scale bars: 50 µm.

4.2.6 The impact of drying and rehydration of viscin on adhesion

The previous sections have clearly indicated that only *V. album* is able to form fibers, and this is due to the presence of the VCB tissue and its hierarchical organization of cellulose filaments and an uncharacterized matrix material that facilitates fibril sliding and reorientation. Fiber formation has been implicated as an adaptation toward increasing likelihood of seed propagation (Kuijt 1969; Grazi and Urech 1981). However, *V. austriacum* is still able to colonize host branches and trunks without fiber formation, owing to the adhesive properties of the viscin tissue. In this section, I explore the nature and process of the adhesive interactions of viscin and the role of hydration in this process for the two subspecies.

Literature concerning the seed attachment of *V. album* L. provides contradicting statements concerning the drying and rehydration of seeds and their implications for adhesion. Several references describe the natural attachment of the hydrated seed to its potential host and the subsequent drying as an irreversible hardening of the viscin layer (Heide-Jorgensen 2008). In contrast, other studies report isolating and drying mature seeds in winter, which could

be stored for later use (Ramm et al. 2000). For sowing in spring, it was suggested to rehydrate the seeds by submerging them in water before manual deposition on a selected host tree branch. Through my own experience of dealing with thousands of mistletoes berries used for the structural characterization, the viscin tissue adhered strongly to all kinds of surfaces – lab glass, plastic dishes, metal bars, clothes, human skin and hair – just to name a few. Attempts to remove the dried samples mechanically either required excessive forces, which would often damage the labware or could lead to a rather painful experience with regard to human beard hair, for instance. Even after successful removal of most of the viscin tissue, there were always remnants left adhering firmly to the surface. It was much simpler to remove dried samples when they were allowed to soak in water for some time before removal. Based on these experiences, the reports of an irreversible hardening of the viscin seem doubtful, leading to the question: How does the rehydration affect the adhesive properties of the viscin tissue and is it (fully) reversible?

Mistletoe seeds of *V. album* were mechanically isolated as described above. The isolation of *V. austriacum* was performed in a similar fashion; however, due to the inability to form fibers, the seed can either be pulled out with tweezers or alternatively, the berry can be compressed between two fingertips until the epicarp bursts after which the seed readily slips out of the berry. Notably, the exposed seeds of *V. austriacum* are more slippery compared to the rather tacky seeds of *V. album* and can easily be separated from the loosely attached fleshy layer which remains partly on the inner surface of the epicarp and partly on the viscin layer surrounding the seed. For each subspecies, one group of seeds was attached to a syringe needle to image the drying process. The seeds were imaged immediately after isolation as well as after 2, 4, 6 and 8 h of subsequent drying (Fig. 4-12A). Under fresh and thus naturally hydrated conditions the green seeds of both species are covered by a jelly-like, milky, translucent shell formed by the hydrated viscin layer. In the front view of seeds of *V. album*, the cut VCB can be seen, which is missing for *V. austriacum*. After 4 h of drying under ambient conditions (23 °C and 50% RH), the volume of the mucilaginous shell has already dramatically decreased and the clear outlines of the seeds of both species become visible. This is accompanied by observation of a white weave that covers the green endocarp, that is slower to emerge in in *V. austriacum* and cannot be seen yet after 4 h, but initiates after 6 h (not shown). After 8 h of drying the seeds of both species are entirely covered by the white weave.

Only minor further volume changes could be observed after 8 h of drying. Aside from the white weave, the dried viscin of both species becomes completely transparent with a waxy texture and a weak tack reminiscent of the initial stickiness of *V. album* seeds. After the initial drying phase, the seeds were rehydrated for 1 h by submerging them in Petri dishes filled with distilled water. During rehydration of the *V. album* seeds parts of the viscin layer came off of the bulk layer and sank to the bottom of the Petri dish. After rehydration the viscin layer was swollen again for both species, as observed from the reemergence of the translucent shell and disappearance of the white weave structure (Fig. 4-12B). The volume of this gelatinous shell is smaller for all specimens of both species compared to the initial

volume. However, after 6 h of subsequent re-drying, the weave reforms and becomes even more intense as the network of white strands appears to become denser. The final volume of the re-dried seeds themselves of both species appears slightly smaller than after the initial drying phase. Additionally, the seed surface turned solid and the viscin coating loses its waxy and adhesive character. The samples were rehydrated a second time which again resulted in the reswelling of the viscin layer accompanied by the disappearing of the white weave (Fig. 4-12C). After the second rehydration cycle, the procedure could be repeated at least ten times observing a constant swelling and shrinking of the viscin layer and the formation and disappearance of the white weave (not shown), indicating this is indeed a reversible process.

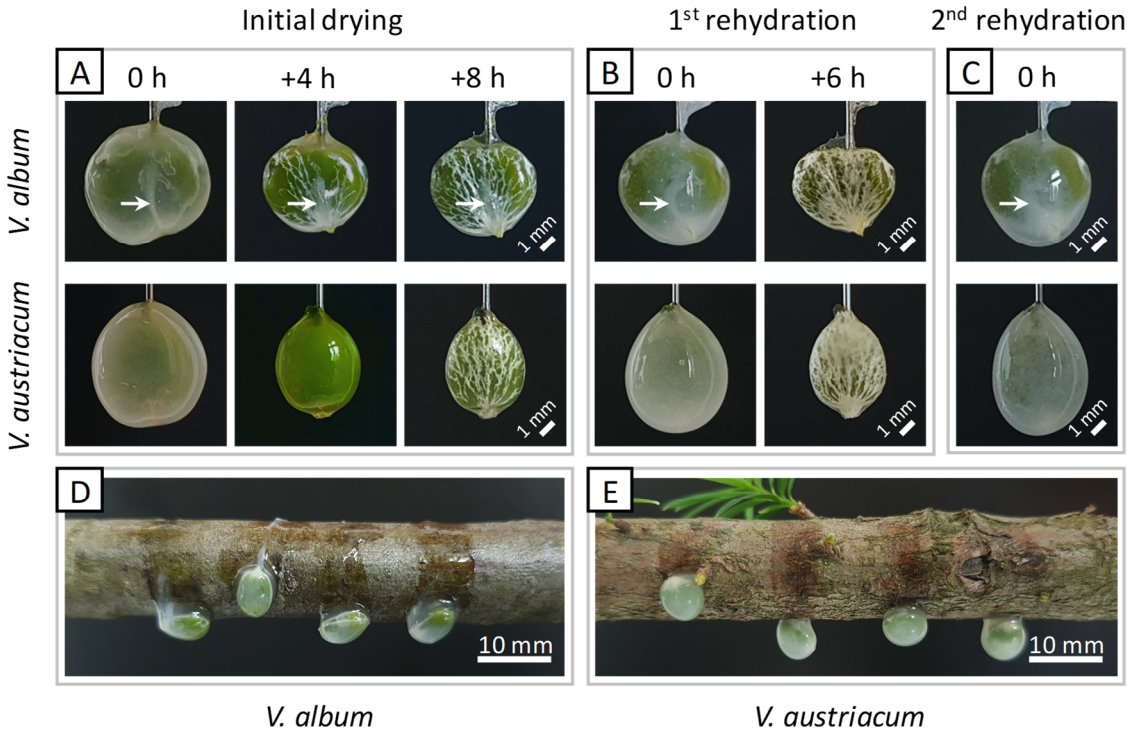

Figure 4-12: Time series images of mistletoe seeds during drying and rehydration. A) Front view of seeds of *V. album* (top row) and *V. austriacum* (bottom row) during initial drying after exposure to air. Images were taken immediately after mechanical isolation (0 h), after 4 h and 8 h. B) Seeds imaged after the 1st rehydration step in a water bath for 1 h and after 6 h of subsequent drying. C) Seeds imaged after the 2nd rehydration step. Scale bar in A-C: 1 mm. D) Rehydrated seeds of *V. album* after manual deposition on top of an apple tree branch. Within seconds the seeds start to slide down to the lower side of the branch which leaves visible slime traces. E) Rehydrated seeds of *V. austriacum* after manual deposition on a pine tree branch. As in (D) they slid downwards leaving behind watery traces. Scale bar in E+D: 10 mm.

In order to investigate the role of the dehydration process in the adhesive behavior of the extracted seeds, two groups of seeds from both subspecies were placed on 1) the flat bottom of glass Petri dishes and 2) on the curved bark of ~13 mm thick branches of their specific host trees, namely apple tree and Scots pine to examine the initial seed adhesion and be-

havior following subsequent drying cycles. The seeds of both groups could easily be removed from the glass surface shortly after being placed on the surface (i.e. before drying) without any effort by lifting them with tweezers. Interestingly, the Petri dishes of the *V. album* seeds group could be turned by 90° into a vertical position, where the seeds demonstrated a strong initial tack indicating that they were held in position by the soft adhesive viscin layer that clings to the flat glass surface. On the contrary, all seeds of the *V. austriacum* control group immediately began to slide down even though they also clung firmly to the flat surface. When turning the Petri dishes upside down the seeds of *V. album* did not move, nor did any seed fall off, and although the seeds of *V. austriacum* slightly moved during 180° flipping, none of the seeds fell off.

In the second set of experiments, seeds of both subspecies were deposited at arbitrary positions along a horizontal branch of their typical host species. All the seeds from *V. album* remained where they were initially placed with only a few seeds showing an initial vertical movement in the order of ~1-2 mm, while the *V. austriacum* seeds immediately slid down to the bottom of the branch leaving a watery trace along their path. Remarkably, the seeds of *V. album* even stayed in position after arbitrary vigorous rotation of the branch along all axes, indicating a strong adhesive behavior. On the contrary, after arbitrary rotation most seeds of *V. austriacum* promptly slid or even tumbled downwards following gravity: e.g. across the branch for a horizontal branch alignment or along the branch for a vertical branch alignment. This sliding behavior stopped after the seeds covered a distance of a few cm or hit an obstacle on their path like a knot or a side branch. Afterwards further movement of the branch only led to further sliding in very rare cases. After only a few minutes following deposition, no *V. austriacum* seed showed any noticeable dislocation after further branch moving similar to the initial behavior of *V. album* seeds.

After 2 h of drying, all seeds of experimental groups 1 and 2 could still be removed easily by lifting them off of the Petri dish or branch, respectively and could promptly be reattached afterwards. Notably, at this time point in the drying process, the seeds of *V. austriacum* developed a modest tack which prevented the seeds from further slipping along the surface during/after subsequent rotation. After 4 h, all seeds of both experimental groups revealed a dramatic volume reduction of the viscin layer as seen in Figure 4-12A. Most of the *V. album* seeds of experimental group 1 (glass) and all of experimental group 2 (branch) exhibited the formation of the white weave which was accompanied by a weakly noticeable pulling resistance against seed removal. While some *V. austriacum* seeds of experimental group 2 already showed the formation of the weave, none of the seeds of experimental group 1 showed weave formation. All *V. austriacum* could still be removed easily. After 6 h all *V. album* seeds were covered by the weave and the required pulling forces for seed removal increased further. At this time point, all *V. austriacum* seeds of experimental group 2 and most of experimental group 1 were now covered by the weave accompanied by a noticeable resistance against manual seed removal. After 8 h, all seeds of both experimental groups were largely covered by the weave and required moderate forces to pull the seeds

off of the glass surface and slightly higher forces for the branches. After 10 h considerable forces were needed to pull off the seeds of all groups indicating a strong surface adhesion.

A third experimental group of seeds of both species were placed into Petri dishes similar to experimental group 1, but in this case the dishes were not turned to mechanically probe the adhesion. After 10 h of drying, the Petri dishes were filled with distilled water and the seeds were soaked in water for 1 h. After 10 min, the viscin layer around the seeds of both species was slightly swollen again. After 30 min, it was intensely swollen and the weave began to disappear again. The seeds were still firmly attached when attempting to lift them off. It took another 30 min (total 1 hour submersion) until the seeds could be readily lifted off of the glass. At this point, the weave was no longer visible and the green endocarp of the seeds became visible again shining through the milky translucent viscin layer. The slippery seeds were taken out of the Petri dish and placed into a dry Petri dish which removed excess water surrounding the swollen viscin. Following this step, the rehydrated seeds of both species were manually deposited on top of a branch of their specific host tree. All seeds of both species immediately slid down to the bottom of the branch (Fig. 4-12D+E). While the seeds of *V. album* left a slimy trace, the seeds of *V. austriacum* left a watery trace on their path down to the bottom. This behavior agrees with the behavior of freshly isolated seeds of *V. austriacum,* but differs to the behavior of freshly isolated seeds of *V. album* which could be placed on any position of the branch without sliding off due their strong initial tack. It is consistent with reports on the loss of viscin adhesive properties after washing isolated viscin (Azuma et al. 2000). However, after artificial rehydration most seeds of both species still manage to successfully attach to their potential host where they subsequently dry and firmly adhere. It shall be emphasized at this point that the mentioned forces are based on the author's subjective sensation and shall be understood as a means of comparative description.

4.3 Discussion

By closely examining and comparing the adhesive properties and hierarchical structural organization of the viscin tissues from closely related subspecies that possess (*V. album*) and lack (*V. austriacum*) the capacity to form adhesive attachment fibers, I gained novel insights into the function of these tissues that were unclear based on previous studies. Below, I discuss the implications of the findings from these comparative histological studies in terms of the anatomical origin of fiber formation in *V. album* and the adhesive function of viscin from the two subspecies, and will then attempt to put these differences in terms of the possible evolved adaptive response towards a structure-function understanding.

Comparative viscin anatomy and fiber formation

Combining light microscopy and polarized light microscopy of thinly sectioned frozen berries, it was possible to discern several distinctive cell and tissue types within the viscin tissue including the hairy cells (HCs), vacuolated cells (VaC), viscin cell bundle/cluster (VCB/VCC). These structures had largely been identified by Chanzy and co-workers

(Azuma et al. 2000), but their higher order organization within the tissue was not described. Here, I was able to clearly localize these different tissue types within the three-dimensional structure of the berry by developing a set of orientational axes defined by several defining morphological features of the berry.

In light of these extensive anatomical studies examining several thousands of berries, the most notable difference between the viscin tissue of *V. album* compared with *V. austriacum* is the VCC/VCB tissue consisting of elongated and very flexible cells, which is present in the former and completely absent in the latter (Fig. 4-6). Functional studies of the VCC/VCB tissue of *V. album* clearly identified this tissue as the source of fiber formation, but also identified loosely defined boundary between the VCB and VCC acting as a breaking point delineating the point at which fiber formation is initiated when the seed is separated from the berry. However, the lack of VCB/VCC tissue in *V. austriacum* berries should not be misconstrued as the absence of viscin tissue – indeed, the HCs and VaCs together build an inner pectosic viscin layer which provides a modified adhesive function in the absence of fibers as discussed in more detail below. As suggested previously (Azuma et al. 2000), the VCB/VCC tissue is distinct structurally and functionally from the hairy cells directly surrounding the seed, although they share several common characteristics at the microscopic level (e.g. individual hairy can be stretched into filaments (albeit much shorter than VCB cells) and both cell types are birefringent due to cellulosic fibrils wound around the cell. Indeed, these superficial similarities may have led to misconceptions by earlier authors that the hairy cells were responsible for the fiber formation (Gjokic 1896; Heide-Jorgensen 2008 p. 114 f.; Heide-Jorgensen 2015).

The viscin cell bundles (VCB) are organized as two flexible, mirrored tissue structures, which originate from the bottom of the berry close to the peduncle where they are firmly connected to the endocarp of the seed. From there, the VCBs extend along the flat surfaces of the seed, and consist of a great number of elongated and very flexible cells which were named “viscin cells” in the present work. Histological analysis with PLM, CFM and SHGM investigations reveal that the pristine cell walls of the viscin cells exhibit a peculiar arrangement of submicron-scale cellulose filaments, which are coiled perpendicular to the long axis of the cell, which is good agreement with earlier PLM and TEM studies of the viscin of *V. album* (Azuma et al. 2000), *V. coloratum* (Azuma and Sakamoto 2003) and similar to PLM and TEM studies of the viscin cells of *Phthirusa pyrifolia* from the family of Loranthaceae (Gedalovich and Kuijt 1987). CFM and SHGM were specifically harnessed to visualize the cellulose filaments during the transition of viscin cells into fibers in fixed and unfixed VCB tissue respectively since the transition occurs at a distinct localized region within the VCB under tensile load, and not throughout the entire VCB simultaneously. Notably, the transition region consists of intact viscin cells, partially unraveled viscin cells, and fully extended viscin cells in the form of filaments, while the fiber predominantly consists entirely of extended filaments, suggesting that the dominant mechanism of fiber formation is the uncoiling of the submicron sized cellulose microfilaments in the cell wall along the axis of applied load assembling into micron sized larger filaments, consistent with

previous conjectures (Gjokic 1896; Tomann 1906; Mangenot et al. 1948; Gedalovich and Kuijt 1987; Azuma et al. 2000; Azuma and Sakamoto 2003). Moreover, numerous such filaments originating from single viscin cells further assemble into meter long fibers, apparently glued together by a mucilaginous matrix, which likely contains pectin. In summary, the work in this chapter coupled macroscopic observations on the hierarchical level of the whole berry to in-depth microscopic investigations to provide a much broader understanding of the role and structure of the VCB tissue. The fiber formation process and nanoscale mechanisms underlying it will be addressed in more detail in the following chapter.

Comparative adhesive function

In addition to the anatomical differences discovered between the two subspecies, I was also able to demonstrate a clear functional difference in the adhesive properties of their viscin in the hydrated and dehydrated states. *V. austriacum* adhered to branches and glass surfaces in the wet state, but tended to slide along such surfaces under the force of gravity. In contrast, the viscin of *V. album* did not slide under gravity, but rather exhibited strong initial adhesion. However, viscin of *V. album* lost this tackiness when rehydrated suggesting that this is the default performance of the viscin tissue and that the initial adhesive response of *V. album* viscin arises from a water soluble, loosely bound glue component.

When fully dried, the viscin of both subspecies adhered quite strongly to surfaces tested. Although the physical and chemical interactions mediating this are unclear, I conclude here that they must be water-sensitive and non-covalent, as soaking the adhesive in water for extended periods leads to the easy removal from the surface. Importantly, this reversible adhesive response can be repeated over numerous cycles which is in agreement with observations from reversible rehydration of seeds from the American dwarf mistletoe (*A. americanum,* Viscaceae) (Paquet et al. 1986). The chemical composition of the viscin likely holds the key in understanding this behavior; yet, there has only been relatively limited investigation, and they have been inconsistent in terms of which part of the viscin tissue were examined. Nevertheless, chemical analysis of viscin from *V. album* and other related mistletoe species from the Viscaceae family reveal the presence of hemicelluloses and pectins, which were previously speculated to mediate adhesion (Heide-Jorgensen 2008 p. 115). Additionally, several mistletoe species show an elevated presence of proteins enriched in glycine and histidine up to 40 % by dry weight (although only ~2% in *V. album*), as well as the reported presence of catechols (Gedalovich-Shedletzky et al. 1989), which have been implicated in the adhesive mechanisms of many marine organisms including mussels (Waite 2017). Presently, it is impossible to say what chemical feature might initiate adhesion, or how this might vary between species and subspecies; however, this will be a very exciting area of research in the future that will be discussed further in chapter 6.

Functional adaption of the viscin tissue in European mistletoe subspecies

In light of the clear morphological and functional differences in the subspecies examined, it is tempting to speculate upon the possible adaptive benefits of these differences with respect to the host species. To reiterate, *V. album* viscin, which produces fibers and exhibits stronger initial adhesion colonizes deciduous hardwood tree species, while *V. austriacum* viscin, which lacks fiber forming capacity and exhibits a tendency to slip along surfaces, colonizes coniferous hosts. Indeed, aside from these subspecies, fiber formation was previously observed to be linked to mistletoe species infecting deciduous hosts, while species with non-fiber forming viscin often grow on coniferous hosts leading some to suggest that this may represent a host-specific adaptation (Grazi and Urech 1981). Stated succinctly, this hypothesis posits that if seeds of mistletoes of a coniferous host are released onto the potential host, e.g. from the droppings of birds, they most probably attach to the evergreen needles, which constitute a large degree of the surface area, rather than the host branches. Since the seed hypocotyl radicle is only able to elongate to a final maximum length of a few mm to create a holdfast, this would prevent colonization if the seed became trapped in the needles. However, when swollen the seeds of *V. austriacum* are slippery and will slide down the needles toward the branch where they get trapped, and following drying firmly attach to the host, where they can successfully germinate (Grazi and Urech 1981). A similar behavior is observed for seeds of *A. americanum*, which also colonizes exclusively coniferous species (Hawksworth and Wiens 1996).

In contrast, the seeds of *V. album* are typically released onto a leafless deciduous host in winter or early spring, and thus, their only chance of germinating is by creating secure attachment to the bare host branch. As examined, *V. album* viscin sticks firmly in the wet state to various surface including host branches. From this perspective, the adhesive fibers, which are formed automatically as the seeds pass through the digestive tract of birds, can be interpreted as an additional strategy to successfully attach to a host. Typically, the seeds are excreted by birds perched on a branch as a long chain of several attached seeds connected by sticky viscin fibers – like pearls on a string – increasing the likelihood of attaching to a host branch simply by enlarging the area or rather the length of the string (Kuijt 1969; Heide-Jorgensen 2008; Heide-Jorgensen 2015). If one seed directly hits the branch the rest of the string is saved from hitting the ground and may eventually find its way to a lower hanging branch by shaking in the wind. Alternatively, it is conceivable that during subsequent water uptake (e.g. during precipitation), the weight of the attached seeds may induce further stretching of the softened fiber, leading to a successful attachment on the host.

In both subspecies, the rather loose embedding of seeds enables the seeds to easily slip out of the berry during mechanical isolation. This was observed in the lab, but also seems to be the case for birds feeding on the berries. The seed needs to get out of the surrounding tissue, since the hypocotyls of the seed embryo may not actively penetrate the thick epicarp when

they start to grow during germination (in late spring many seeds are observed to start germinating within the berry. The hypocotyl radicle grows towards the epicarp but is not able to penetrate and gets stuck.). They require the help of birds. Therefore, an easy slipping mechanism seems favorable. In the case that a bird does not swallow the entire berry, but pecks the berry open to feed from the fruit flesh only, the arrangement of the VCB/VCC in *V. album* most likely ensures that the beak gets immediately stuck to the viscin and thus, pulls out the seed almost no matter where the beak penetrates the epicarp and the fruit flesh. As deduced from my structural investigation, the VCC is spherically covering most of the upper half and part of the lower half of the berry. Due to the continuity of the VCC and VCB the seed is pulled out (this can be demonstrated by picking into the berry with a point tool and have the tool pull out an adhesive fiber). With regard to the natural dissemination it has been reported that birds tend to dislodge the seed stuck to their beak by wiping it off on the branch (Snow and Snow 1988; Reid et al. 1995), which would likely result in successful germination of the seed.

5 Unraveling the rapid self-assembly of adhesive fibers from mistletoe viscin

5.1 Introduction

One of the key findings of the previous chapter was the clear observation that fiber-forming capacity observed in the mistletoe subspecies *Viscum album* spp. *album* can be traced to a specific structural feature of the viscin tissue known as the viscin cell bundle (VCB) and viscin cell clusters (VCC) (Fig. 5-1). It was posited that the adhesive viscin fibers formed in nature provide an adaptive advantage for seed germination on deciduous hosts in winter months following the consumption and subsequent defecation of swallowed mistletoe berries by birds. Using confocal microscopy methods including fluorescence and second-harmonic generation microscopy, I was able to assign the fiber formation process to the uncoiling, alignment, sliding and gluing of cellulose microfilaments following the mechanical disruption of the cell walls of viscin well within the VCB. Yet, these methods do not provide insights into the nature of the dynamic fiber formation process at the nanoscale to molecular level. Moreover, there is a complete lack of understanding in the current literature about the parameters controlling fiber formation including hydration and the mechanical forces necessary. Indeed, freshly exposed VCB tissue is hydrated and soft with the consistency of a hydrogel, while drawn fibers dry rapidly under ambient conditions and appear to be quite stiff.

The main aim of this chapter is the unraveling of this highly dynamic process based on the study of manually or automatized drawn fibers under controlled lab conditions. To achieve this goal, I performed in-depth mechanical analysis, thermogravimetric analysis and X-ray diffraction of VCB, fibers and transition region. The findings of these studies provide a nanoscale view of the dynamic response of cellulose nanofilaments to both hydration and mechanical tensile forces, and highlight the key role of a swellable adhesive matrix material in the dynamic fiber formation process. These insights are relevant to ongoing efforts to produce novel composite materials from biorenewable nanocellulose extracted from a variety of sources (Eichhorn et al. 2010; Moon et al. 2010; Klemm et al. 2011; Jonoobi et al. 2015; Jarvis 2018). This chapter is reproduced in part with permission from [Horbelt et al. 2019]. Copyright [2019] American Chemical Society.

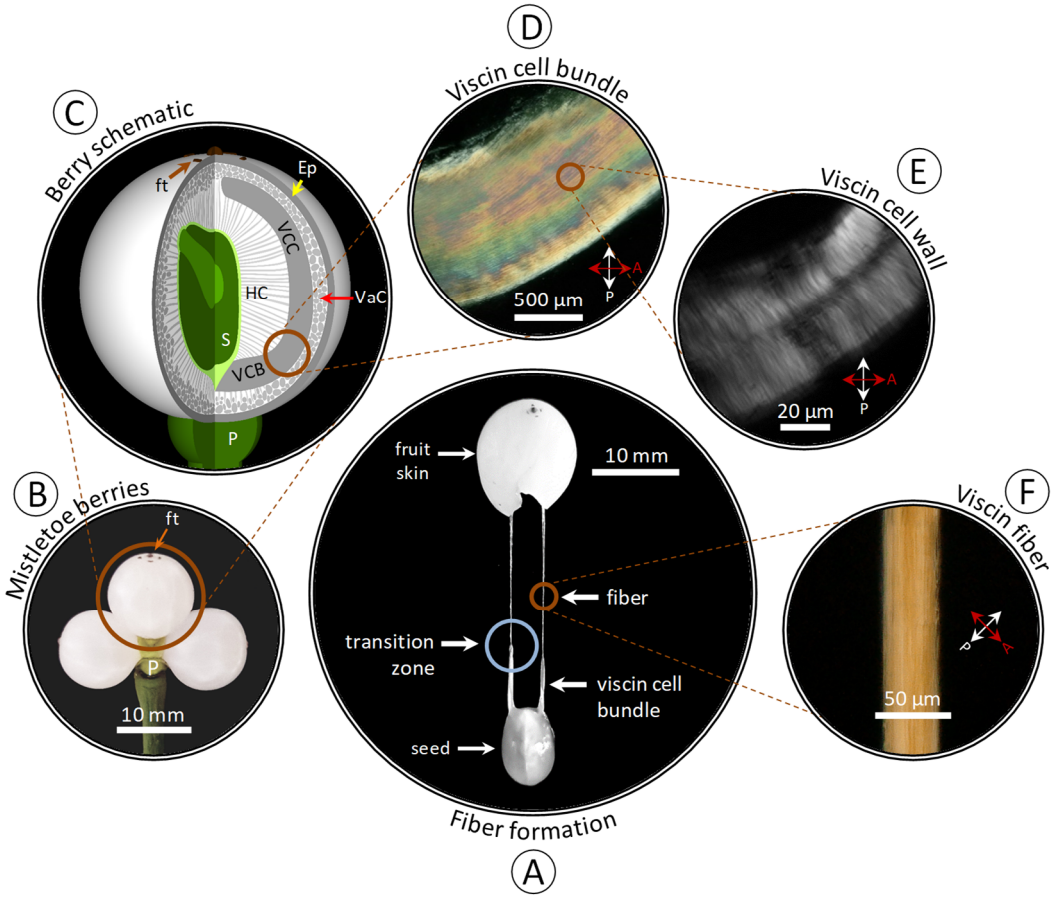

Figure 5-1: Hierarchical structural organization of *V. album* berries. (A) Photograph showing the typical formation of adhesive viscin fibers connecting the seed with the fruit skin. (B) White berries with small floral traces (ft) on the top collected in groups of three including the peduncle (P). (C) Schematic section of a mistletoe berry showing the inner organization with the green seed (S) in the center, surrounded by radially oriented hairy cells (HCs). Viscin cell bundles (VCBs) and Viscin cell clusters (VCCs) are connected to the bottom of the seed arcing toward the top of the berry which are covered by vacuolated cells (VaC) toward the epicarp (Ep). (D) Polarized light microscopy (PLM) image of a manually isolated and hydrated VCB viewed under crossed polarizers. (E) PLM image of a single viscin cell showing the perpendicular arrangement of cellulosic filaments. (F) PLM image of a typical mistletoe viscin fiber.

5.2 Results

5.2.1 Manual fiber drawing from mistletoe viscin

Mistletoe berries were harvested with the berries still attached to the peduncle to maintain the structural integrity of the berries (Fig. 5-1B). As described in a time series of images in Figure 5-2, holding the peduncle in one hand and pulling the berry with the other hand, the berry can be removed from the peduncle. This leads to a small opening at the former connection point. By mimicking the behavior of some mistletoe feeding birds, it is possible to squeeze the seed out of the berry by applying a gentle pressure onto the berry with one's fingertips (as some birds would do skillfully using their beak). The seed slips through the

opening which is widened as the seed passes the opening (Fig. 5-2B). Thereby the seed turns by 180° (Fig. 5-2C). By grabbing the sticky seed with tweezers it can be further pulled out of the remaining berry which results in the formation of two individual viscin fibers each emerging from the two mirroring VCB, connecting the seed with the remains of the berry (Fig. 5-4D). Initially these fibers were only a few mm to cm long, extremely sticky and highly extensible. Upon further drawing, they readily extend into thin fibers (diameter 20 - 100 µm) with a final length of more than 1 m each – a more than 100-fold increase in length. If the two individual fibers come into contact during the drawing process, they adhere and macroscopically fuse into a single fiber.

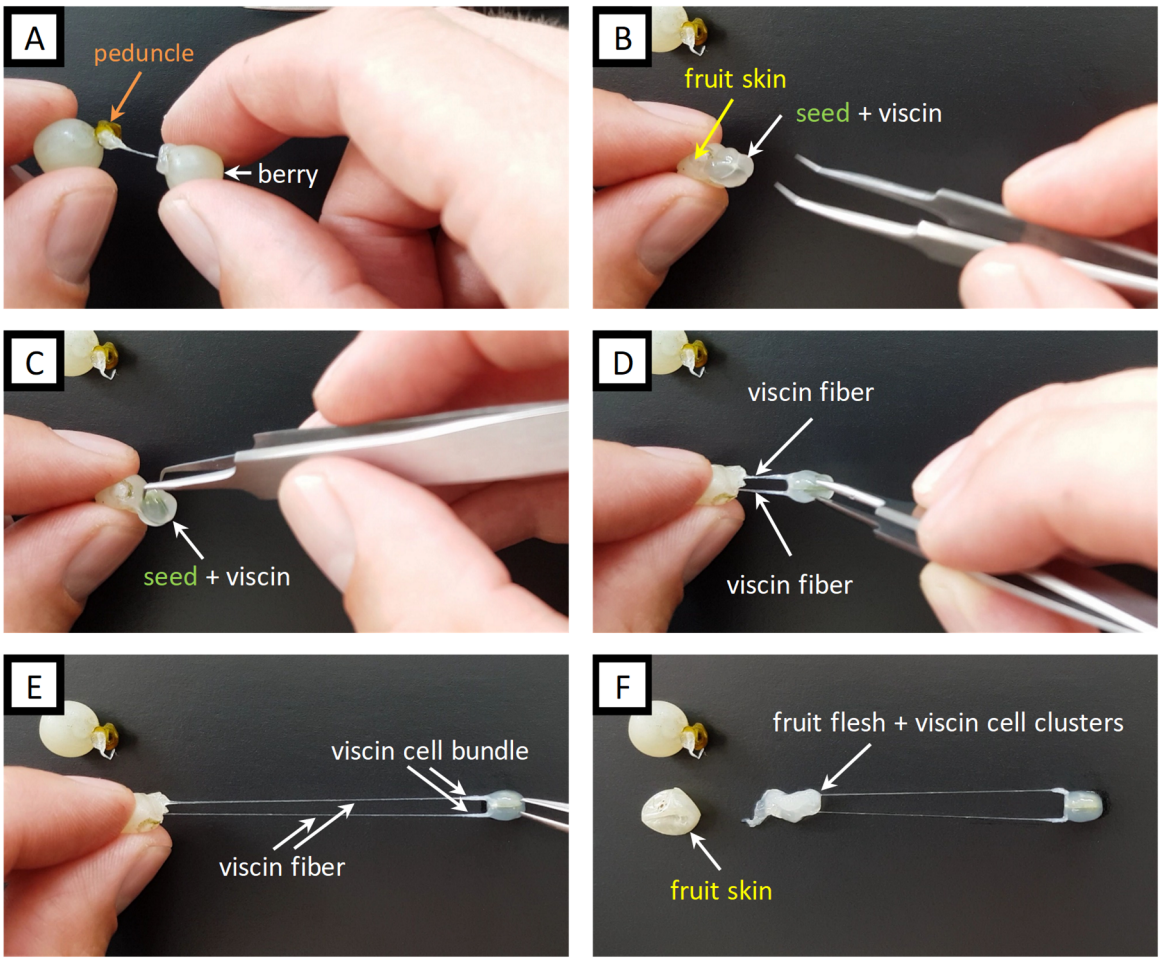

Figure 5-2: Time series images of the manual drawing of mistletoe viscin fibers. A) Removing the berry from the peduncle. B) Compressing the berry will press the seed out of the surrounding berry pericarp near the former peduncle. C) The exposed sticky seed can be grabbed with tweezers. D) Pulling the seed away from the berry leads to the initial formation of two viscin fibers. E) Pulling the seed further away leads to an elongation of the fibers. On one side the fibers emerge from two viscin cell bundles connected to the seed. F) On the other side they emerge from the viscin cell clusters which are still connected to the surrounding fruit flesh. The fruit skin can often be readily removed from the flesh.

5.2.2 From ultrasoft cells to stiff fibers

While the gelatinous viscin layer surrounding the seed remains rather sticky for several hours, the fibers and the VCB lose their viscous, adhesive character after only a few minutes of drying under ambient conditions and become quite stiff, but the fibers remain flexible in bending and twisting. In order to characterize this rapid and dramatic change in material properties, micro-tensile tests were performed using small segments of fibers. When tested under dry ambient conditions (23 °C; 20% RH), fibers exhibited a linear elastic behavior with no observed yield point, followed by brittle failure at ~1-2% maximum strain. Notably, fibers possessed an average tensile stiffness of more than 10 GPa, which is comparable to that of dragline spider silk (Vehoff et al. 2007) or wood cell wall (Burgert et al. 2005).

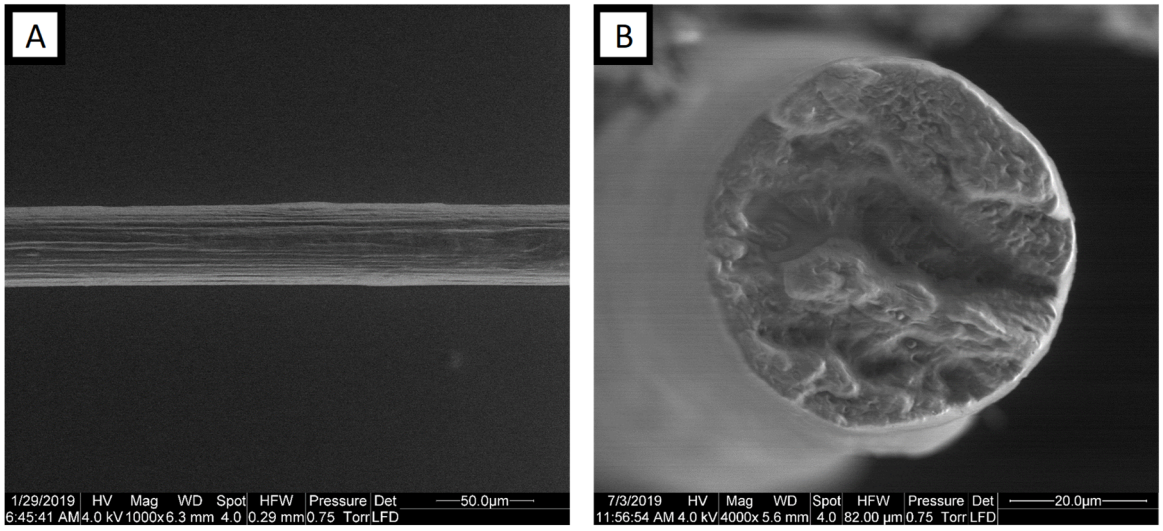

Figure 5-3: Mistletoe viscin fiber morphology observed with environmental scanning electron microscopy (ESEM). A) Side view of a viscin fiber. B) A fiber cross section reveals the circular shape of hand drawn fibers.

To further investigate the contribution of hydration to the formation and mechanical performance of viscin fibers, micro-tensile tests were performed under controlled RH and T conditions. Mechanical properties were calculated based on the assumption of a circular fiber cross section as confirmed by environmental scanning electron microscopy (ESEM) (Fig. 5-3B). The stress was calculated based on the initial cross section area. Potential changes of the fiber cross section area during tensile stretching as they are typical for polymeric materials were not determined. Therefore the true stress could not be determined and the calculated stress has to be understood as the engineering stress. The fiber material stiffness is highly dependent on humidity as illustrated by the extremely different stress-strain curves observed going from 0% to 90% RH, which resulted in a 35-fold drop in stiffness from ~14 GPa down to ~0.4 GPa (Fig. 5-4A+B). Examining the stiffness of fibers equilibrated over a range of different RH conditions reveals that stiffness plummets between 30% and 60% RH, clearly indicating that dehydration plays a key role in mediating the transition from viscous hydrogel to stiff fiber.

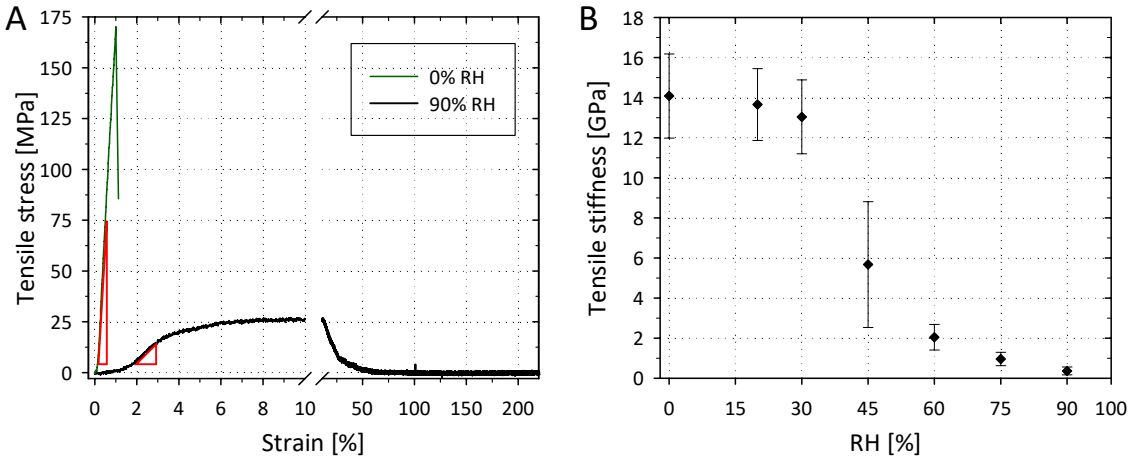

Figure 5-4: Mechanical properties of mistletoe viscin fibers. A) Exemplar stress-strain curves from mistletoe fibers measured at 0% and 90% relative humidity (RH). Red triangles: slope of the curve used for the determination of the stiffness. B) Tensile stiffness of mistletoe fibers as a function of RH.

5.2.3 Macroscopic swelling and fiber moisture content

A subsequent macroscopic analysis of the fiber swelling as a function of the RH showed almost no change of the volume from 0% RH up until 45% RH, followed by a sudden increase from 45% to 90% RH to a maximum volume swelling of ~23% (Fig. 5-5A). Here, the mean fiber diameter changed from 36 µm ± 4 µm at 0% RH to 40 µm ± 4 µm at 90% RH. A water sorption isotherm (Fig. 5-6B) obtained from thermogravimetric analysis (TGA) shows a similar behavior in which there is almost no water uptake from 0% to 30% RH, followed by a sudden increase in the moisture content (MC) up to ~34% MC at 95% RH, which is a highly unusual behavior compared with that of other natural cellulosic fiber materials (Xie et al. 2011). The desorption isotherm indicates that this process is fully reversible with almost no hysteresis observed.

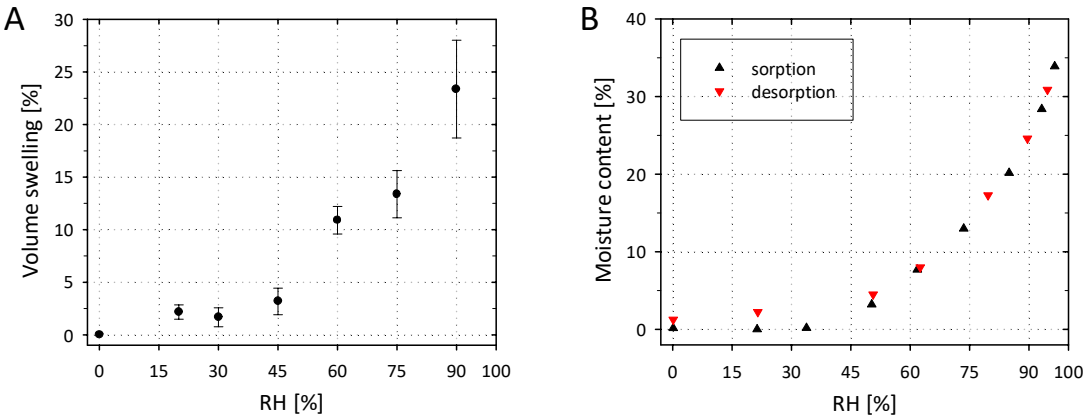

Figure 5-5: Viscin fiber-water relations. A) Macroscopic swelling calculated from changes of fiber diameter as a function of the relative humidity (RH). B) Sorption isotherm of mistletoe fibers based on differential scanning calorimetry coupled with thermogravimetric analysis (DSC-TGA) at 29°C.

5.2.4 PLM and XRD reveal the rapid change of cellulose orientation

To better understand this dramatic transition, we performed a multiscale structural analysis on the VCB with a specific focus on the transition zone where the VCB transforms into a thin fiber. After carefully dissecting VCBs from the seed, they were first examined using conventional light microscopy. The tissue was almost transparent, showing little contrast and revealing few details on its structure. On the other hand, polarized light microscopy (PLM) provided improved contrast due to the natural birefringence of the VCB arising from the anisotropic arrangement of cellulose. As previously reported (Gedalovich and Kuijt 1987; Azuma et al. 2000), PLM reveals that the VCB tissue consists of aligned and densely packed viscin cells with an elongated shape and a typical diameter between ~20-40 µm. The individual cells possess massive cell walls with irregular cross sections and a small lumen. Towards the edges of the VCB, the cells showed a more relaxed order with some viscin cells sticking out sideways, revealing their slender tipped ends. Also in agreement with earlier studies (Gedalovich and Kuijt 1987; Azuma et al. 2000) and confirmed with CFM in chapter 4, each cell showed the presence of submicron sized filaments oriented perpendicular to the long axis of the cell (Fig. 5-1E). In the hydrated state, the bundle as well as the individual cells were highly flexible while upon drying they lose their flexibility and finally become brittle.

While the bulk of the VCB is relatively uniform, an abrupt structural change was observed near the tip where fiber formation is initiated – numerous long filaments of ~2-3 µm in diameter were observed to extend from the VCB. These filaments were highly aligned along the fiber direction and glued together by a non-birefringent matrix material to form the macroscopic viscin fiber. The specific orientation of the cellulose within the VCB, transition zone and emergent fibers was investigated using a PLM equipped with a full-wave plate, which exhibits a change in the polarization color depending on molecular orientation. As shown in Figure 5-8A, within the transition zone, the cellulosic filaments abruptly change from a perpendicular arrangement in the VCB to a highly aligned parallel orientation in the resulting fiber with respect to the long axis, as revealed by the sharp transition of the polarization color from blue to yellow.

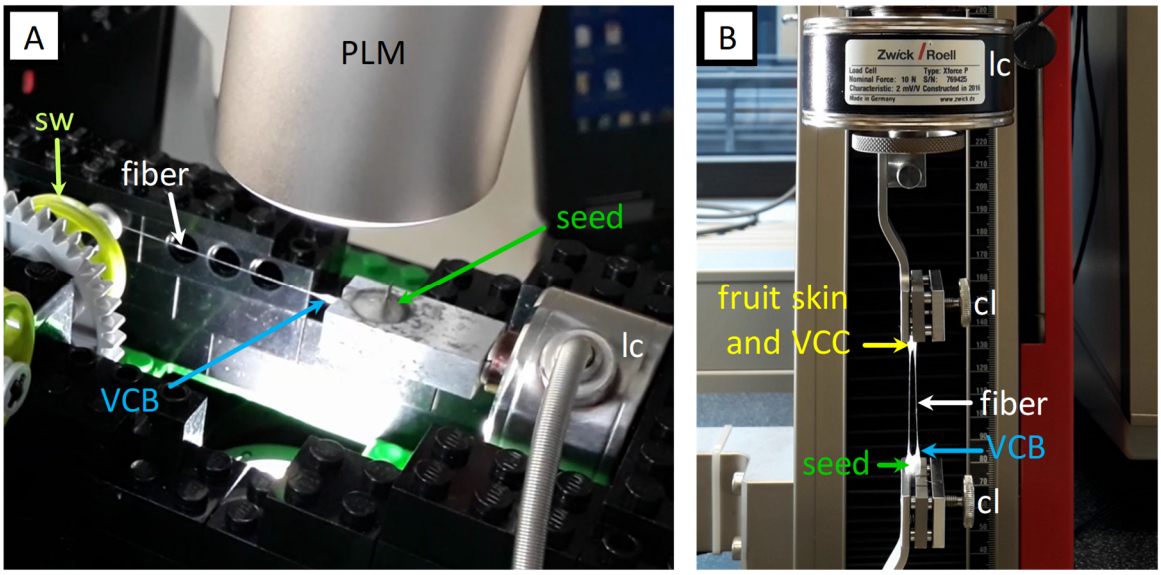

Figure 5-6: Semi-automated viscin fiber drawing devices. A) Detail of a custom-built horizontal fiber drawing device based on Lego® Technic™. The fiber drawing is initiated by hand as described as shown in Fig. 5-2. The seed is spiked on a sample holder which is connected to a load cell (lc). The fiber is glued to a motor driven spinning wheel (sw). The whole device fits under a PLM for video recording of the drawing process at the transition between VCB and fiber. B) An adapted tensile test setup from a vertical Zwick universal testing machine. The fiber drawing is again initiated by hand. Then the seed is fixed on the bottom clamp (cl) and the remaining berry skin including the VCC are clamped on top. The top clamp is connected to the motor side and the load cell (lc).

To gain further insights into the dynamic nature of the dramatic structural changes occurring at the transition zone, a custom-built fiber drawing device was developed to follow the transformation in situ during PLM measurements (Fig. 5-6A, for a more detailed description see chapter 3, Fig. 3-1). With the seed fixed on spikes and a short initial fiber from the VCB attached to a spinning wheel from the drawing device, the VCB was initially stretched at low drawing speed of ~30 µm s^{-1} until a steady state was achieved, after which continuous drawing resulted in fiber formation almost exclusively at the tip of the VCB, while the bulk VCB remains mostly unchanged (Fig. 5-7A-E). Although the bulk VCB shows only diffuse birefringence throughout the whole drawing process, the drawn fiber exhibited much stronger birefringence shortly after emerging from the bulk VCB. The extremely high degree of cellulose alignment in the fibers was further emphasized by the nearly total extinction of the birefringence upon aligning the fiber axis parallel to the polarizer (Fig. 5-7E), a characteristic reminiscent of hemp bast fibers in which cellulose orientation is nearly parallel to the cell long axis (Thygesen and Hoffmeyer 2005).

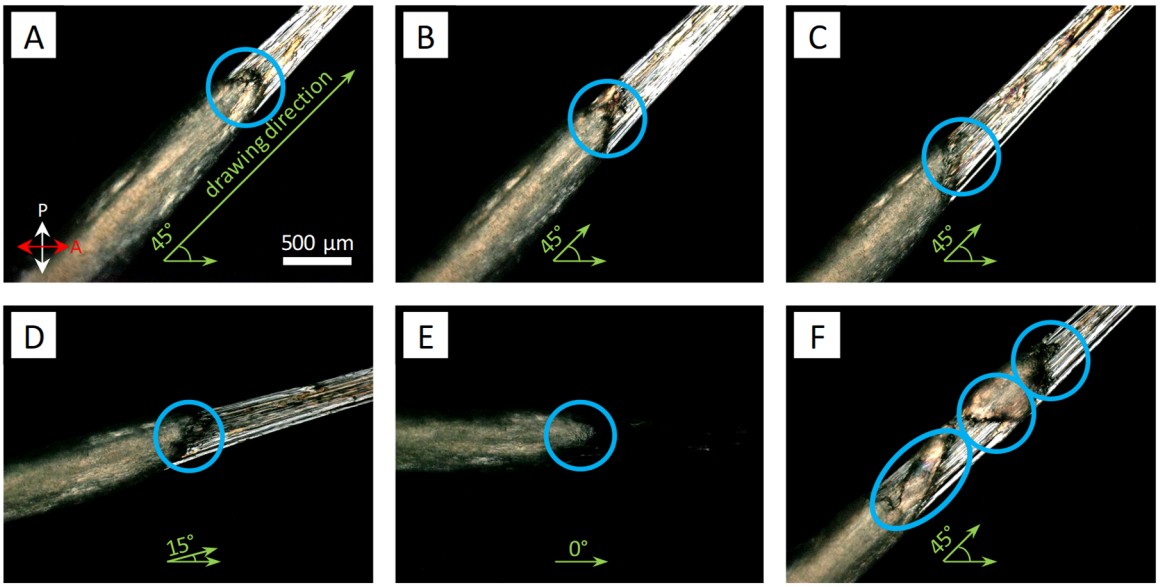

Figure 5-7: Time series PLM images of the fiber formation process. A) The fiber drawing device with the fixed sample is aligned along the drawing direction at an angle of 45° with respect to the analyzer. The fiber formation process is initiated at the tip of the VCB where numerous micron sized filaments emerge from the VCB (blue circled region). Scale bar: 500 µm. Continuous drawing (B+C) leads to a propagation of this fiber formation front along the VCB. D) When rotating the sample towards a parallel arrangement to the analyzer the birefringence in the fiber becomes weaker until it is mostly extinguished at 0° (drawing direction parallel to analyzer). F) With increased drawing time, the VCB integrity fails at multiple locations. While the tissue quickly starts to dry, fiber formation can be observed simultaneously at several "breaking points" with some parts of the VCB staying "intact".

Increasing the drawing speed stepwise up to a maximum of ~0.6 cm s^{-1} did not affect the fiber formation process. Higher automated drawing speeds (up to 1.66 cm s^{-1}) achieved using a commercial Zwick tensile tester also revealed a similar fiber formation mechanism localized at the VCB transition zone and showed that the fiber formation process can initiate from both ends of the VCB and the VCC connected to the berry skin (Fig. 5-6B). At maximum drawing speed, several samples broke before the maximum travel distance of ~65 cm was reached, which limited the maximum fiber length achieved by automated drawing. Remarkably, however, manually drawing fibers with tweezers (drawing speeds in the range of m s^{-1}), frequently resulted in the formation of fibers from a single berry longer than 2 m. With both tensile test devices, throughout a range of pulling speeds, we measured constant drawing forces in the order of ~20 mN during the simultaneous drawing process of two fibers emerging from a single berry, respectively ~10 mN for a single fiber.

Dynamic PLM studies revealed that nanoscale structural reorganization within the VCB localized at the transition zone plays a critical role during fiber formation. In order to investigate this hierarchical length scale and the potential role of cellulose orientation, we employed synchrotron WAXS, which is a well-established technique for investigating structural organization of cellulosic materials. Manually drawn and dried fibers were mounted in an X-ray beam (50 µm spot size) and scattering patterns were collected in a

mesh over the transition zone going from bulk VCB to fiber. An image of the sample grid can be seen in Figure 5-8B where each pixel equals one 2D scattering pattern of the scanned volume.

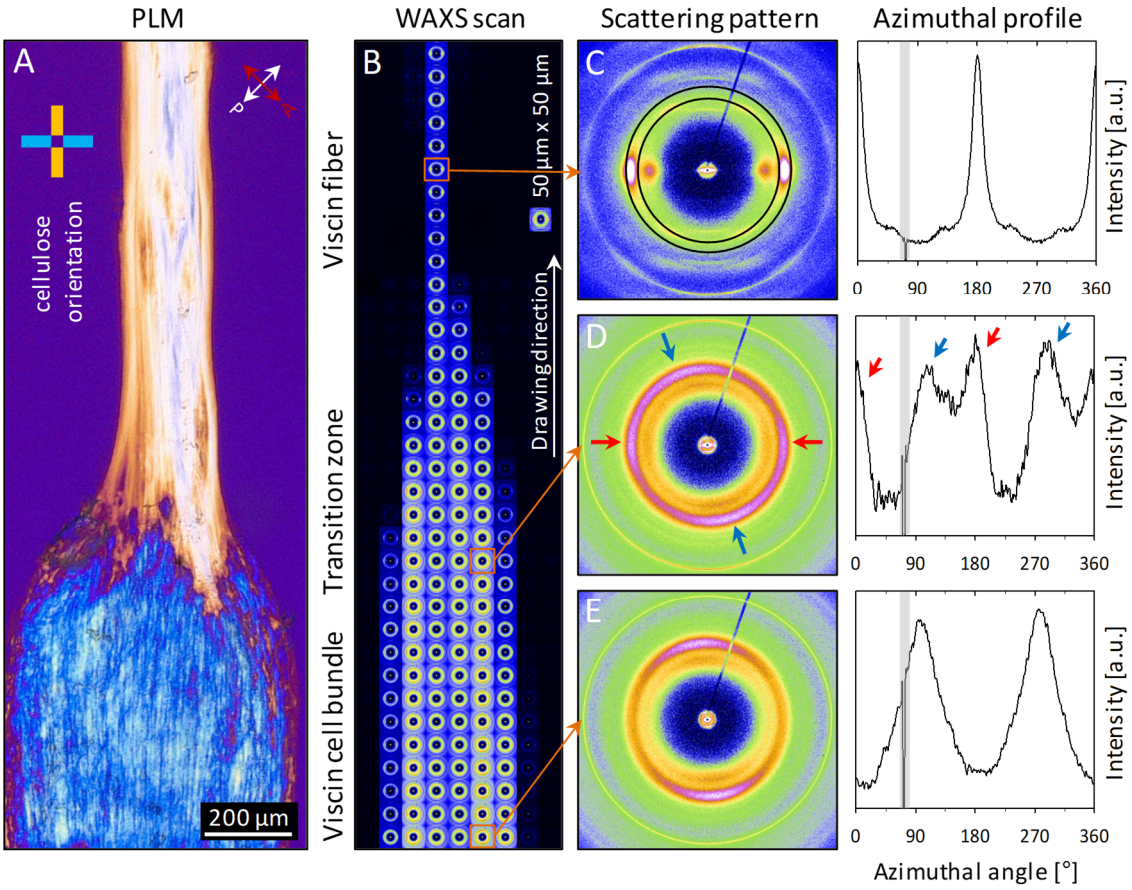

Figure 5-8: WAXS and PLM investigation of cellulose orientation across the VCB transition zone. A) PLM image of a VCB with an emerging fiber viewed under crossed polarizers and a quarter-wave plate. Changing polarization colors from blue (VCB) to yellow (fiber) indicate the sudden change of the cellulose orientation. B) Image of a mesh scan over the VCB transition zone where each 'pixel' represents a scattering pattern of the scanned volume with a beam diameter of 50 µm. C-E) Selected scattering patterns from the fiber (C), the transition zone (D) and the bulk VCB (E) and the corresponding azimuthal intensity profiles of the (200) cellulose reflection. The integration range is indicated by the black circles in (C). Data regions which are influenced by the glass capillary holding the beam are marked in gray.

Three selected scattering patterns (Fig. 5-8C-E) were chosen from the bulk VCB, the transition zone and the fiber in order to illustrate the large nano-structural changes occurring during transformation process. Azimuthal intensity profiles obtained from the most intense cellulose reflection (200) – notation for cellulose 1β (Sugiyama et al. 1991) – were used for a qualitative analysis of the cellulose orientation. Within the VCB, we deduce a preferred, but loosely organized cellulose orientation perpendicular to the drawing direction (i.e. perpendicular to the long axis of the VCB), based on the azimuthal profile (Fig. 5-8E), which shows two corresponding maxima with broad distributions centered around 100° and 280°.

The shift of ~10° from expected peak centers at 90° and 270° arises from a slightly tilted arrangement of the individual cells along the length axis of the VCB. In stark contrast, within the drawn fiber, cellulose is highly aligned along the fiber axis based on the two narrow peaks in the azimuthal intensity plot at 0° and 180° (Fig. 5-8C). The transition zone shows evidence for cellulose oriented both perpendicular and parallel to the fiber drawing axis (Fig. 5-8D) based on two pairs of maxima observed at 0°/180° and at 100°/280°. This is consistent with the observation using PLM that the transition zone is the site where the cellulose within the viscin cells flows and reorients to form the emerging fiber.

5.2.5 Synchrotron based WAXS and SAXS studies revealing the viscin cellulose dimensions and moisture dependent arrangement of secondary structures

In addition to the broad intense (200) reflection in the radial scattering profile, viscin fiber scattering patterns (Fig. 5-9A) showed the presence of an extremely sharp (004) cellulose reflection, which originates from the regular stacking of crystal unit cells along the crystal length axis (Sugiyama et al. 1991). Radial intensity profiles of small azimuthal sections along the meridian (004) and the equator (200) are shown in Figure 5-9D where a strong amorphous background arising from the matrix has been subtracted. Typical peak broadening due to a small crystallite width is evident in the equatorial profile based on the overlapping (1-10)/(110) reflections and broad (200) reflection (Kennedy et al. 2007). In contrast, the crystalline domains appear to be quite long based on the extremely sharp (004) reflection in the meridional profile. The (200) and (004) peak widths were further analyzed by Lorentz peak fitting allowing extraction of the full width at half maximum (FWHM) which was used to calculate the dimensions of the crystalline domains with the help of the Scherrer equation (Equation 5). Apparent mean width and length of L_{200} ~2.5 nm and L_{004} ~67 nm, respectively, were calculated leading to a quite high aspect ratio of ~27. While the obtained width is comparable to findings from other primary cell wall systems (Newman 2008; Newman et al. 2013), the apparent length is extraordinarily high compared to literature values based on WAXS analysis reported from spruce wood (Jakob et al. 1995; Andersson et al. 2003), sugarcane (Driemeier et al. 2012) and bamboo (Wang et al. 2012). Moreover, considering that sources besides instrumental line broadening were not accounted for (e.g. disorder from micro-stresses (Warren 1990), twisting (Fernandes et al. 2011), structural inhomogeneities (Thomas et al. 2014), or contaminations from neighboring reflections), the reported values are likely an underestimate of the true dimensions and reported values should be interpreted as apparent minimum values.

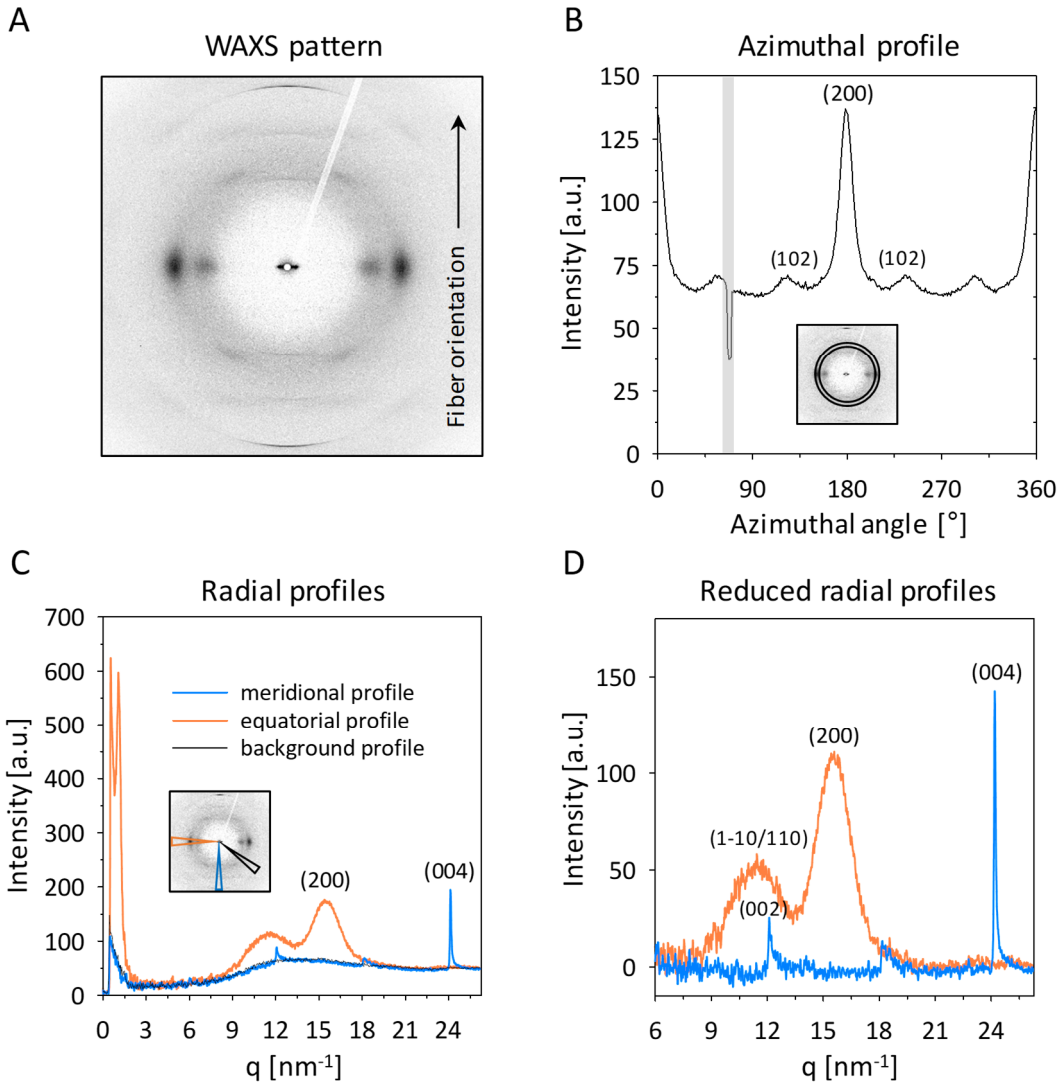

Figure 5-9: Viscin fiber wide angle X-ray scattering studies. A) WAXS pattern obtained from a mistletoe fiber. B) Azimuthal profile along the cellulose 200 reflection. Data regions which are influenced by the glass capillary holding the beam stop are marked in gray. C) Radial profiles along the equator, the meridian and a selected angular sector uesed for an estimation of background scattering intensity. D) Reduced equatorial and meridional profile after background subtraction.

Apart from the WAXS reflections, fiber scattering patterns exhibited intense lateral SAXS peaks centered at q ~ 1.1 nm^{-1} (Fig. 5-10A), interpreted as a highly regular packing of the CMFs with a mean center-to-center distance of ~5.7 nm when measured under ambient conditions (~50% RH). Experiments under changing RH conditions showed that the mean center-to-center distance changed reversibly from ~5.5 nm at ~30% RH to ~7.8 nm at ~95% RH as deduced from shifts of the SAXS peak (Fig. 5-10C). Due to very low scattering intensities it was impossible to analyze the peak position below ~30% RH. However, with rising RH the scattering intensity dramatically increased as illustrated by logarithmic scaling. With regard to the small crystallite width of ~2.5 nm the calculated mean center-to-center distances indicate an interfibrillar spacing ranging from ~3 nm to ~5.3 nm. These

values are considerably higher than what was measured with SAXS or small angle neutron scattering for other primary (Kennedy et al. 2007; Thomas et al. 2013) or secondary cell wall systems (Fernandes et al. 2011; Thomas et al. 2014; Thomas et al. 2015). Even in the dried state, these data suggest that the cellulose microfibrils always maintain a large and well-defined minimum distance and that there is little or no direct fibril-fibril contact.

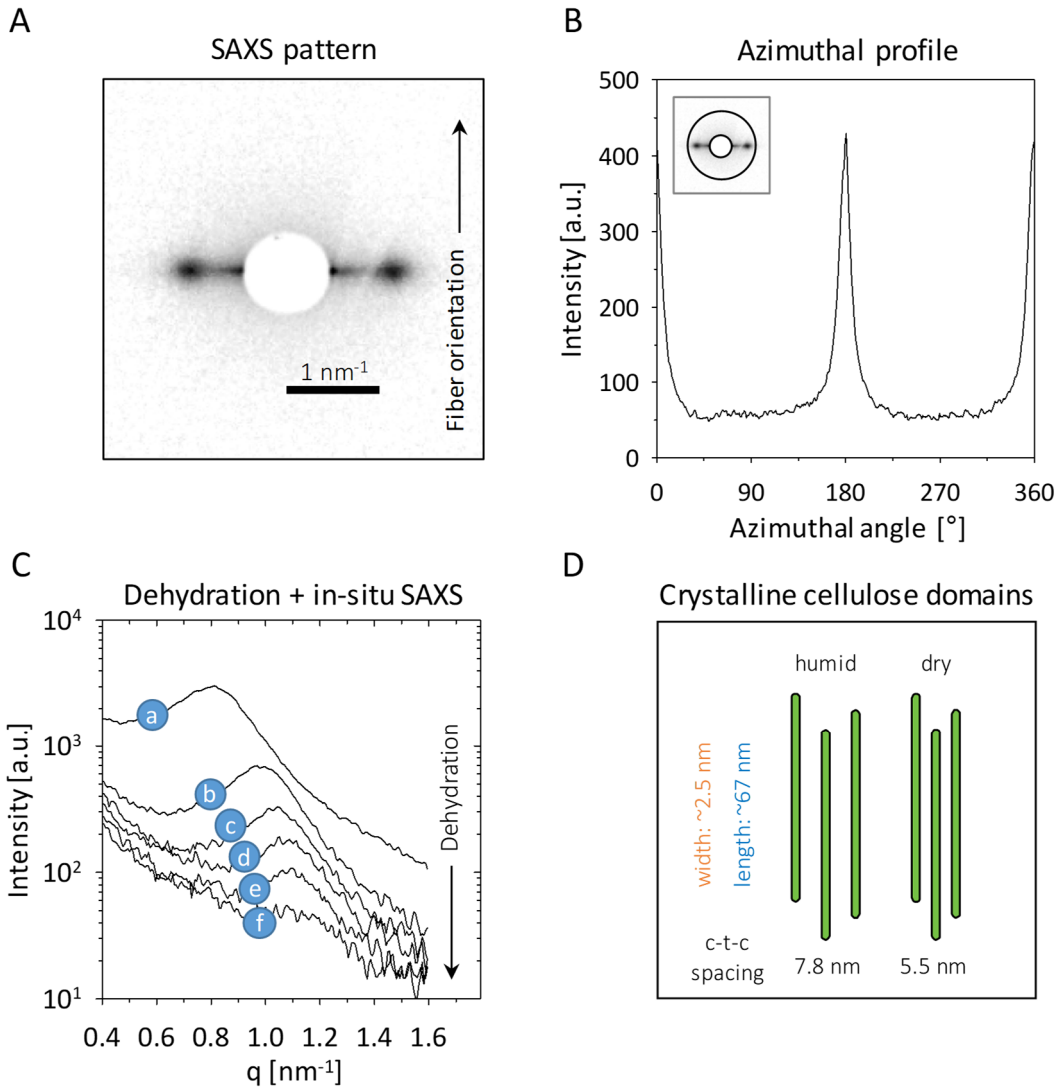

Figure 5-10: Viscin fiber small angle X-ray scattering studies. A) SAXS pattern of a mistletoe fiber. B) Azimuthal profile of (A). C) Radial profiles along the SAXS peaks from (A) as a function of the relative humidity (RH) reveals a shift of the peak center from ~ 0.8 at ~95% RH up to ~1.13 at ~ 30% RH. D) Summary of calculated parameters for the dimensions and spacings of cellulose crystalline domains from SAXS and WAXS.

5.3 Discussion

The findings of the current study reveal an extreme hydration dependent mechanical transformation, which under wet conditions facilitates simple low-force mechanical drawing of fibers of up to several meters in length from a starting tissue just a few millimeters long. In

the dry state (< 45% RH), on the other hand, the drawn fiber becomes remarkably stiff and strong, yet remains flexible. Remarkably, this hydration-dependent 35-fold change in stiffness, is fully reversible as humidity conditions are modulated. Concomitant with this moisture-dependent mechanical transformation is a drastic structural reorganization of the cellulose orientation and higher order packing as the material flows like a fluid polymer melt with liquid crystal-like properties and exhibits a remarkable draw ratio over a wide range of drawing speeds.

In this light, it is clear that mistletoe viscin exhibits a highly appealing ease of processing that is not currently found in the fabrication of typical polymeric materials, nor in current methods for producing cellulosic composites (Osorio-Madrazo et al. 2012; Hakansson et al. 2014; Mittal et al. 2018). Indeed, viscin fiber formation process functions under ambient conditions with water as an already integrated solvent. It does not require external heat since it naturally functions within a temperature range starting from below 0 °C outside in winter up until ~40 °C when passing a bird's digestive system before excretion, where it even tolerates short-term biochemical attack. Furthermore, it does not require a coagulation bath – rather, just a few minutes of air drying under ambient conditions to solidify. Thus, from the perspective of green and sustainable polymer fiber fabrication, mistletoe viscin presents an appealing role model for bio-inspired materials fabrication, and is especially relevant to current efforts aimed at developing nanocellulose-based composites as a veritable alternative to petroleum-based plastics.

The critical role of the non-cellulosic matrix in viscin fiber processing

Considering that microfluidic-based processing of cellulosic nanocrystallites can yield fibers with stiffness of over 80 GPa (following chemical cross-linking) (Mittal et al. 2018), it is not at all surprising that the aligned cellulose in mistletoe viscin leads to a stiffness of more than 14 GPa. However, what is surprising and quite remarkable is the ease of processing by which this is achieved. Most notable is the critical role of the water absorbent matrix in guiding this process. Based on the sharp SAXS reflections (Fig. 5-10), we can deduce that the mistletoe VCB and fibers consist of a homogeneous dispersion of CMFs with a highly defined interfibrillar spacing, which is completely controlled by a water-responsive matrix material. Indeed, the matrix appears to mediate the fully reversible interfibrillar swelling and deswelling during hydration cycles (Fig. 5-10C) correlated to the large water-dependent changes in fiber volume (Fig. 5-5A). The matrix additionally appears to prevent the CMFs from aggregating or fusing since even the lowest calculated mean center-to-center distance in the dry state suggests a minimum interfibrillar spacing on the order of ~3 nm. Furthermore, the exceptionally high length of the crystalline domains obtained from WAXS measurements hints that the matrix compounds bind to the CMFs such that their axial coherence is not disturbed. The resulting high aspect ratio of the crystalline domains is certainly beneficial for CMF reorientation along the drawing direction during the fiber formation process as illustrated in Figure 5-11. Likely, the matrix acts like a viscous stimuli-responsive gel in the wet state, whereas in the dry state it behaves like a strong cement,

binding the CMFs together. This is somewhat reminiscent of a glass transition, only that it does not depend on temperature, but rather on the moisture content.

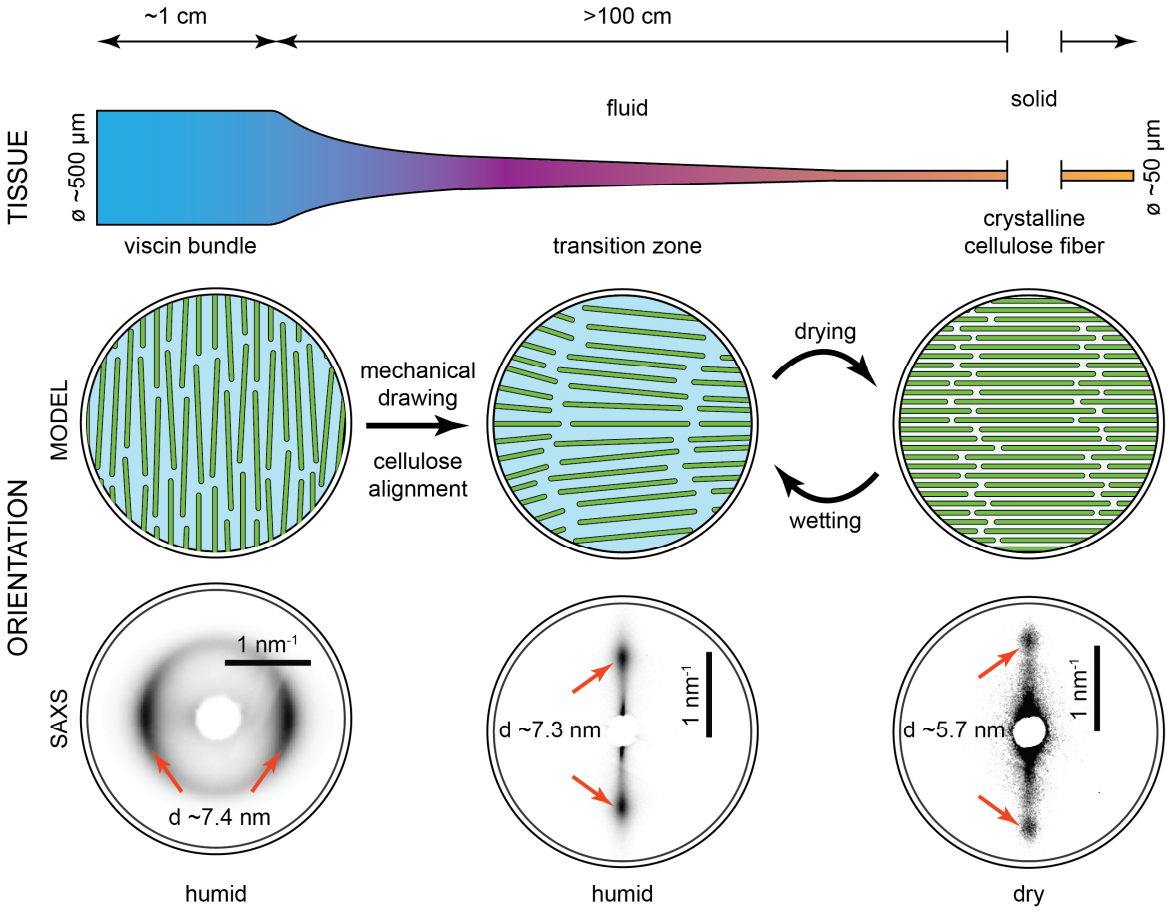

Figure 5-11: Schematic model of mistletoe viscin fiber formation. Based on current evidence, we favor an assembly model in which mistletoe viscin fiber assembly proceeds via hydration-dependent reorganization of crystalline domains of high aspect ratio from a perpendicular orientation relative to the fiber axis in the VCB to a highly aligned axial configuration in the fiber mediated through a structurally aligned, yet flowing phase in the transition zone. The VCB provides an astonishing degree of hidden length where the initial tissue undergoes an extreme >100-fold length increase and ~35-fold stiffness increase as it transforms into a fiber. SAXS data indicate this process depends on a decrease in the interfibrillar spacing during drying, proposed to arise from deswelling of the matrix material as it changes from a deformable hydrogel to a strong cement.

Clues to the molecular origin of this behavior can be extracted from previous compositional analysis of VCB tissue from different *V. album* variants (Azuma et al. 2000; Azuma and Sakamoto 2003), indicating that mistletoe viscin contains not only cellulose (~45-47% d.wt.), but also hemicelluloses (~53% d.wt.) and charged groups (e.g. 2% d.wt. uronic acid). The moisture-mediated reversibility of fiber drawing indicates non-covalent stabilization of the matrix. Thus, it seems plausible based on these compositional studies that the hemicelluloses and ionic groups may serve as a water-responsive matrix between CMFs as indicated by SAXS. Indeed, earlier studies appear to indicate that at least some hemicelluloses are covalently attached to the CMF surfaces (Azuma and Sakamoto 2003), which may explain why the interfibrillar distances extracted from SAXS are extremely well defined.

We hypothesize that electrostatic interactions mediated by charged groups in the matrix provide weak sacrificial cross-link in the presence of water (as has been observed in bone (Gupta and Zioupus 2008), wood (Keckes et al. 2003) and insect silks (Ashton et al. 2013), but upon drying, water loss results in a stronger interaction between electrostatic bonds which stabilizes the matrix. While this model of water-dependent fiber processing is intriguing based on the current data, further work is required to determine its validity.

Sacrificial bonds and hidden length as a means for fast fiber formation

It is worth considering, from a basic geometrical perspective, how the millimeter-scale VCB tissue is able to physically transform into a fiber of several meters. For reasons of simplicity, we consider an idealized cylindrical shape of a single viscin cell cross section with a typical diameter of ~25 µm in which the initial cross section area is reduced via drawing by a factor of 100 to a cylindrical filament with a diameter ~2.5 µm. If one further assumes volume conservation, a 1 mm long viscin cell would yield a 100 mm long filament. Considering the whole viscin cell bundle (diameter x length: ~500 µm x ~10 mm, see Fig. 5-11), one would predict a theoretical final length of 1 m with a corresponding fiber diameter of ~50 µm, which is in good agreement with observations of typical dimensions of mechanically drawn mistletoe fibers. Taking into consideration that often diameters of <50 µm are observed, even a fiber length of more than 2 m can easily be explained by these simplified considerations.

Put in a larger context, mistletoe viscin fiber formation has all the hallmarks of a process based on sacrificial bonds and hidden length – a recurring theme in biological materials science shown to play a critical role in material toughness, self-healing capacity and material formation (Fantner et al. 2005; Winegard et al. 2014; Reinecke et al. 2016). Sacrificial bonds are non-covalent interactions in materials that can be broken sacrificially, sparing the backbone covalent bonds and avoiding catastrophic material failure (Fantner et al. 2005; Reinecke et al. 2016). Hidden length, on the other hand, describes additional material extensibility that is inherent in the unraveling of higher order hierarchical organization in the molecular structure of the material. We surmise that the viscin cell wall with its peculiar perpendicular arrangement of densely packed cellulose fibrils provides an astonishing source of hidden length allowing a draw ratio of over 100-fold in the resulting mistletoe fibers. Indeed, an analogous assembly mechanism has been observed in the coiled thread skeins of hagfish slime (Winegard et al. 2014). Moreover, we believe that under hydrated conditions, non-covalent and reversible sacrificial bonds in the matrix (likely electrostatic) break and reform during fiber elongation maintaining the structural coherence of the fiber, but allowing a liquid-like flow.

6 Mistletoe viscin – A versatile natural fiber-reinforced adhesive

6.1 Introduction

Adhesives are a technically and biomedically important class of materials that perform diverse functions – e.g. engineering sealants, surgical glues and adhesive tapes. In recent years, scientists and engineers have looked to nature to address specific deficiencies in man-made adhesives, including adhesion in wet conditions and reversible adhesion (Favi et al, 2014; Zhao et al. 2017). Indeed, natural selection has resulted in the evolution of a number of versatile adhesives with properties unmatched by current synthetic means. Examples include the wet adhesives produced by mussels and velvet worms (Waite 2017, Baer et al. 2017), as well as the reversible dry adhesives utilized by geckos, insects and spiders (Gorb 2005; Autumn and Gravish 2008). Elucidation of the chemical and physical principles underlying adhesion in these systems has led directly to the invention and application of synthetic adhesives with both technical and biomedical functions (Lee et al. 2011; Haller et al. 2012; King et al. 2014). In the present study, I investigate the adhesive processing of mistletoe viscin – a fiber-forming cellulosic adhesive.

Mistletoe viscin is an extremely versatile adhesive produced by *V. album* L. plants (amongst other mistletoe species) and was even used in ancient times to produce birdlime – a gluey substance for capturing birds (Tubeuf 1923). Unlike most other biological adhesives, mistletoe viscin combines strong adhesion with the ability to be rapidly processed into incredibly stiff (E >14 GPa), yet flexible fibers by simple mechanical drawing (Chapters 4 & 5, Horbelt et al. 2019). This combination of properties has evidently evolved to facilitate the proliferation of mistletoe plants, which are hemiparasitic and rely on a host plant for their nutrition (Kuijt 1969; Heide-Jorgensen 2008). Typically, the mistletoe berries, which are a winter food source of many birds, quickly pass through the digestive tract and emerge at the other end as a sticky string containing several seeds that then becomes strongly adhered to a tree branch, enabling germination and fusion with the host plant (Fig. 6-1, Heide-Jorgensen 2008). Building off earlier work from Azuma and Chanzy (Azuma et al. 2000), we performed an in-depth structure-function investigation of the fiber formation process, revealing insights into the nanoscale mechanism and structure-function relationships (chapter 5, Horbelt et al. 2019). The impressive processability and multifunctionality of the viscin fiber material emerging from these studies are potentially relevant for current efforts to produce cellulosic composites. In this chapter, I explore the processability of viscin into more complex architectures and structures beyond simple fibers and investigate the adhesive properties of the viscin tissue and its potential as a biomedical sealant.

6.2 Results

The findings of the previous two chapters highlight the crucial importance of the swellable water-responsive matrix in the adhesive function and processability of mistletoe viscin. Indeed, these studies suggest that the non-cellulosic matrix material responds to changes of

the relative humidity, taking up water at about ~50% RH allowing microfibrils within the cells and even the contents of adjacent cells within the bundle to slide past one another at multiple length scales under hydrated conditions. Yet, upon drying, the matrix acts as a strong cement holding the cellulose microfibrils together, resulting in impressive tensile stiffness. The fact that the two VCBs from the same seed or numerous wet fibers from several seeds can merge to form a single functional fiber in the wet state further suggests that the water swellable adhesive matrix is also able to mediate self-adhesion. This ability is beautifully illustrated through observation of mistletoe feeding birds only a few minutes after they finished their last mistletoe meal. During the following excretion of their droppings one can observe the formation of characteristic chains containing several mistletoe seeds connected via sticky viscin fibers like pearls on a string (Fig. 6-1A). However, this natural phenomenon does not require the seed's passage through the bird's guts which can be easily demonstrated by the mechanical isolation and mixing of *V. album* seeds which leads to a similar seed chain, when artificially deposited on a tree branch (Fig. 6-1B).

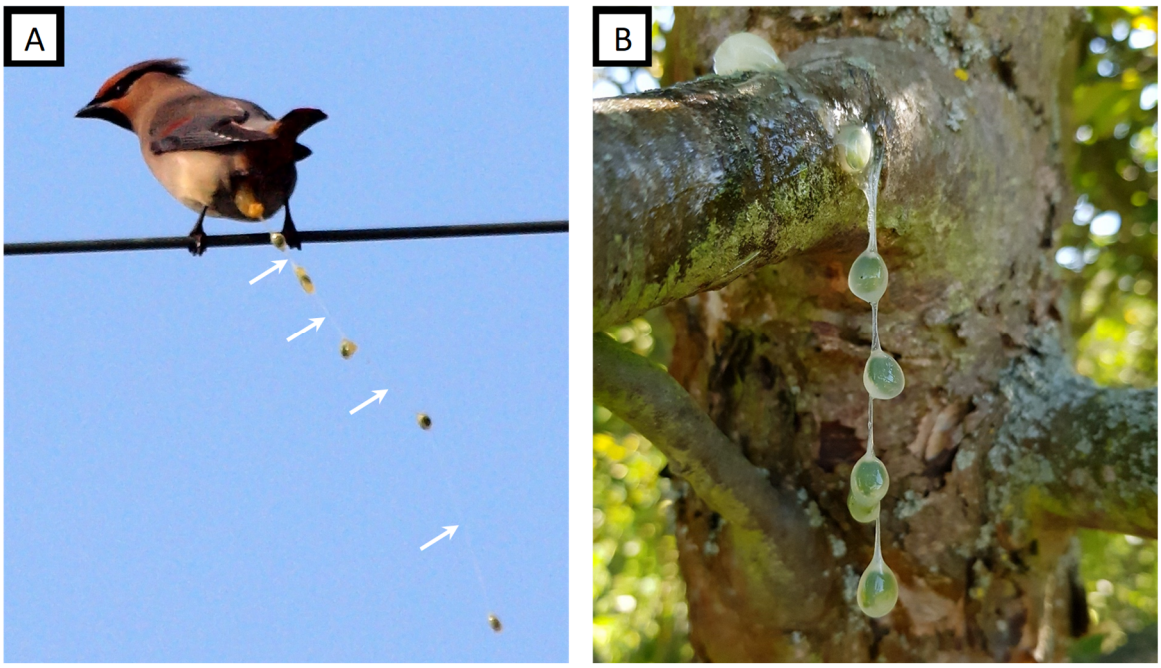

Figure 6-1: Mistletoe viscin "pearl chains". A) A Japanese waxwing (*Bombycilla japonica*) leaving a chain of mistletoe seeds connected via adhesive viscin fibers. White arrows: Thin barely visible viscin fibers. Adapted and reprinted under a CC BY 4.0 license. B) A chain of mechanically isolated *V. album* seeds manually deposited on an apple tree branch.

6.2.1 Exploring the self-adhesive properties of viscin

The self-adhesive character could not only be observed for freshly drawn fibers but also for dried fibers. It was observed that two fibers held together between the thumb and index finger will fuse with one another, presumably using just the humidity from the skin to initiate the adhesive interaction. To further investigate the ability to reactivate the self-adhesive properties of the fiber matrix, a "welding" experiment was performed in which a dried, non-sticky fiber was cut with a razor blade (Fig. 6-2A).

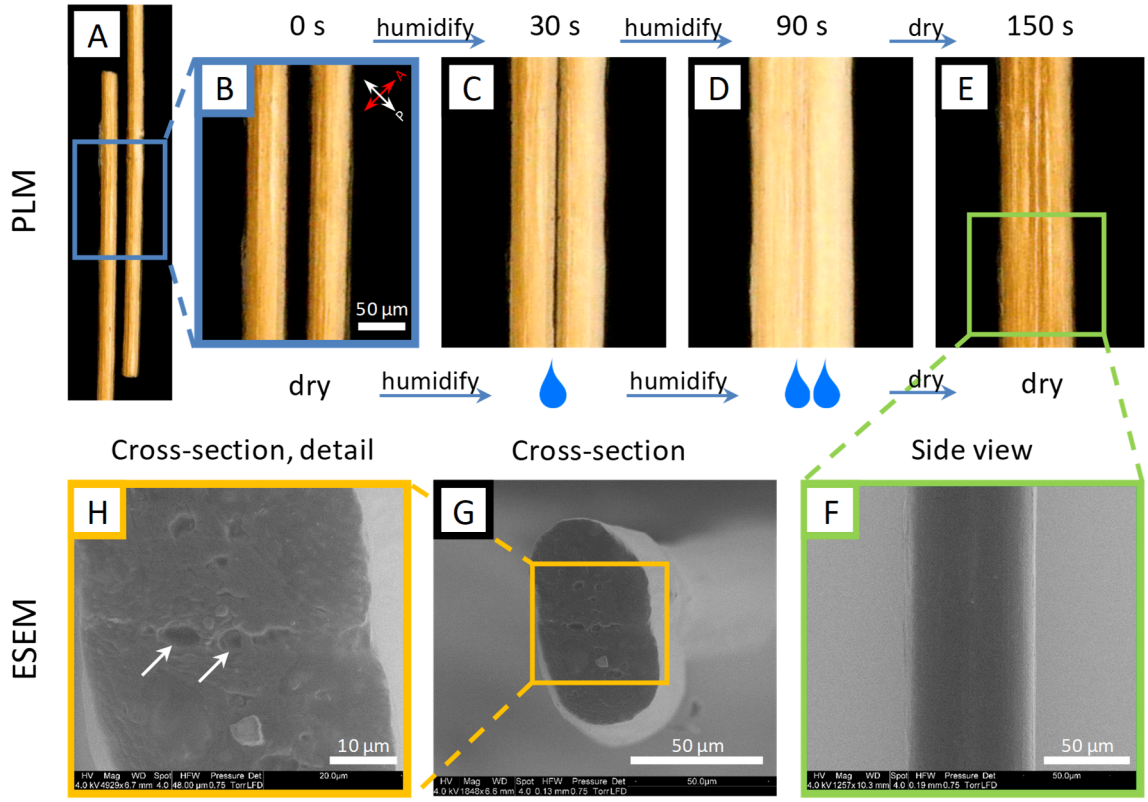

Figure 6-2: Hygro-activated fusion of viscin fibers. A) PLM image of 2 loose ends of dried viscin fibers oriented at 45° to the polarization filters. B) Detail of (A). Scale bar: 50 µm. C) Fibers were brought into contact. Slightly swollen fibers after 30 s of exposure to saturated water vapor (RH ~ 100%). The interface between the 2 fibers is still visible. D) Fibers at maximum swelling after 90 s of rehydration. The fibers fused in the contact zone and the interface gets lost. E) 60 s after maximum swelling (total experimental time of 150 s) the diameter of the fused fibers is reduced dramatically again. F) ESEM image showing a side view of the fused fibers. Scale bar: 50 µm. G) ESEM image of a fused fiber cross section. Scale bar: 50 µm. H) Detail of (G) revealing that the interface between the fused fibers gets lost. Arrows: voids due to possible inclusions at the former fiber-fiber interface. Scale bar: 10 µm.

The two resulting pieces of the stiff fiber do not interact adhesively in the dry state when they are brought into contact. However, by raising the RH to above ~40%, it could be observed that the fibers swell slightly (as previously reported) and when brought into contact begin to adhere and deform at the interface (Fig. 6-2C). Further raising the humidity by exposing the fiber ends to saturated water vapor (~100% RH) leads to an intense swelling of the fibers where the fibers further deform along the interface between the fibers, which gradually disappears (Fig. 6-4D). Cutting off the water vapor leads to a sudden drop of the RH back down below 40%, after which it was observed that the fibers become physically fused to one another (Fig. 6-2E+F). The fused fiber ends were cut and the cross-section was investigated with environmental scanning electron microscopy (ESEM), confirming that the interface between the formerly separate fibers is largely lost (Fig. 6-2G+H).

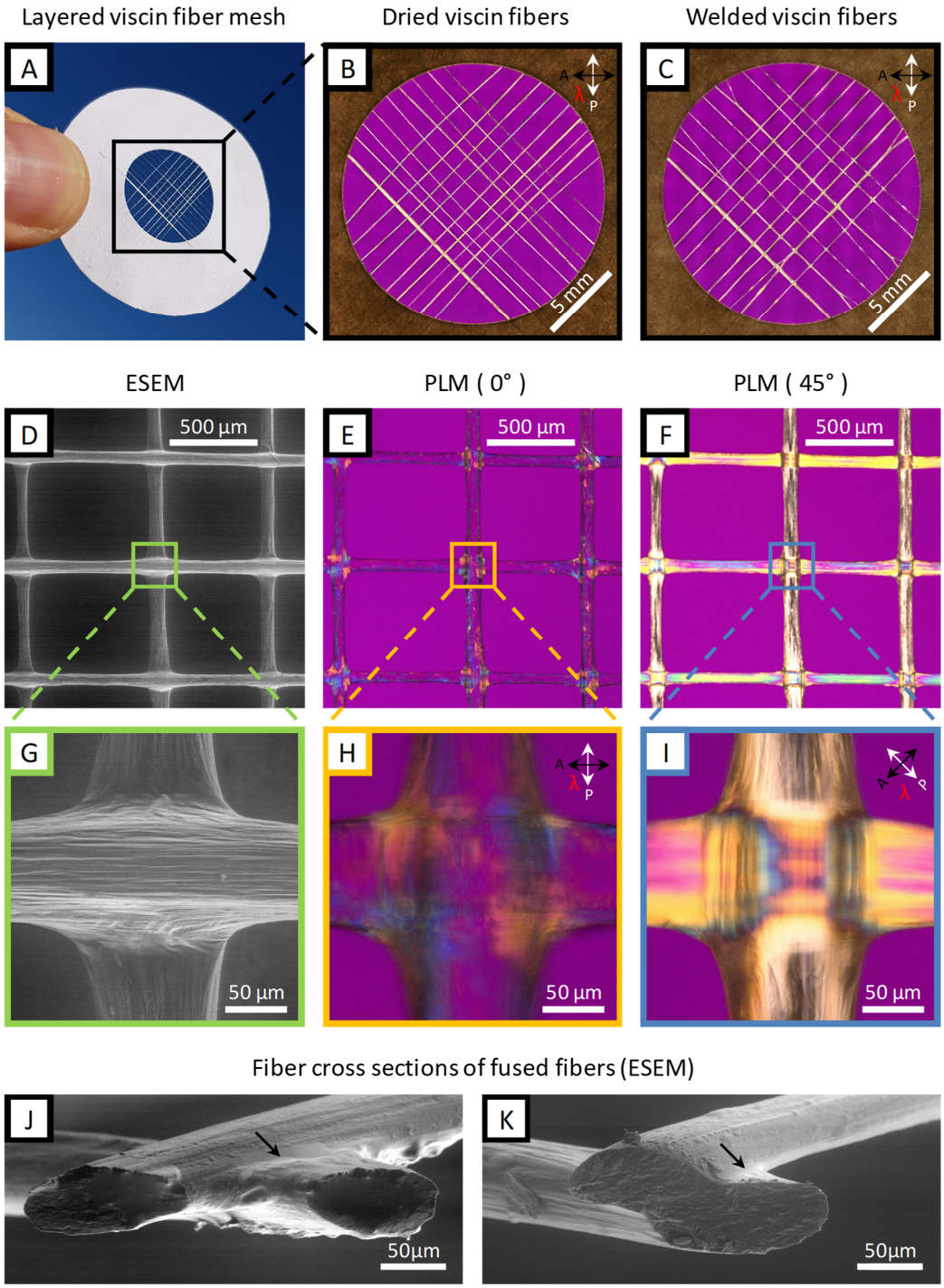

Figure 6-3: Structures made from viscin fibers. A) A mesh of viscin fiber segments arranged in a crosswise pattern glued on a card board frame. B) PLM overview image of the dried viscin web. C) PLM image of the welded viscin fiber web after short time rehydration. Scale bars in B+C: 5 mm. D) ESEM image of welded fiber nodes. E) PLM image of welded fiber nodes. F) PLM image of welded fiber nodes at an angle of 45° with respect to the polarization filters. Scale bars in D-F: 500 µm. G) ESEM detail of a fiber node showing the distorted viscin on the fiber surface around the node edges. H) PLM detail of a single node. I) PLM detail of single node. Scale bars in G-I: 50 µm. J) An oblique view on the cross-sections of 2 fused fibers crossing at an angle of ~90° and sectioned at an angle of ~45° close to the node. K) Oblique view as in (J) sectioned through the node. Scale bars in J+K: 50 µm.

Based on this water-initiated self-adhesion between viscin fibers, it was possible to construct two-dimensional objects from individual stiff mistletoe fibers, by simply arranging stiff pieces of mistletoe fiber in the dry state, exposing them to water vapor for a short time at the joints and then allowing them to air dry (Fig. 6-3A-C, for a more detailed description see chapter 3). The physical fusion of the fibers was confirmed using ESEM (Fig. 6-3D). Indeed, the fibers lose their circular cross-section at the welding point and appear to merge together showing distortion in the microfibrillar texture on the surface of the fiber (Fig. 6-3G). In order to investigate how the cellulose fibrils within the fibers are affected by this fusion process, we utilized PLM – clearly revealing that the cellulose becomes distorted at the nodes where two fibers are fused (Fig. 6-3E,F,H,I). Cross-sections of fused fiber nodes in ESEM clearly show that the interface between the two fibers is largely lost at the junction points (Fig. 6-3J+K). Interestingly, due to the strong plastic deformation of the individual fibers the ESEM images give the impression, that fibers interpenetrate each other at the junction points. These observations reveal that the mistletoe fibers are indeed self-welding using elevated moisture as a soldering agent at room temperature. Because the adhesive is integrated in the fiber, there is no need for additional glues, just water. This is a remarkable behavior for polymer fibers with a stiffness in the dry state of more than 14 GPa (i.e. exceeding that of Nylon by more than 3-fold (Najafi et al. 2017)

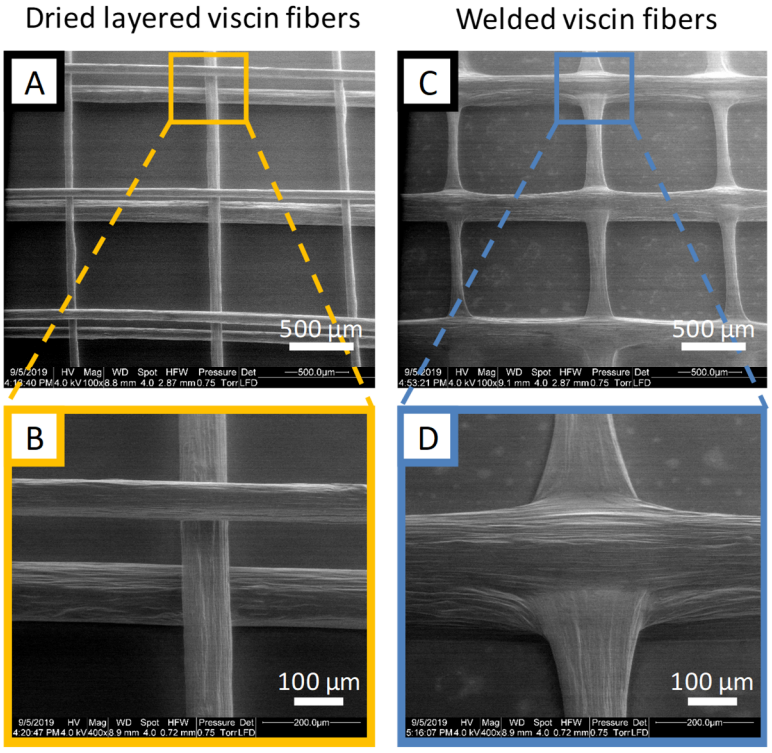

Figure 6-4: ESEM studies of the self-welding behavior of multilayered viscin fibers. A) 3 staggered layers of dried viscin fibers successively arranged perpendicular to the adjacent layer. Images A-D are oblique views taken at an angle of 25°. Scale bar: 500 µm. B) Detail of (A) showing the circular shaped fibers are not connected. Scale bar: 100 µm. C) Self-welded viscin fibers after rehydration due to short time exposure to saturated water vapor. Scale bar: 500 µm. D) detail of (C) showing all 3 fibers permanently fused. The formerly independent parallel bottom and top layered

fibers fused along their entire length. The center fiber gets fused to the adjacent fibers at the fiber crossings in a sandwich-like structure. The fibers get deformed after rehydration and appear flatter and broader than the original circular fibers which is particularly pronounced for the center fiber towards the crossings. Scale bar: 100 µm.

From a simple fiber, one can easily construct the aforementioned 2D structures. Additionally, these structures can be expanded into multilayer architectures similar to the additive manufacturing of 3D printed objects. Figure 6-4 shows a multilayer 2D mesh in which multiple fibers laid over one another can envelop another layer of fibers oriented orthogonally, creating more complex, and presumably more stable junction points. Moreover, dried viscin fibers can be used to construct three-dimensional objects by a stepwise premanufacturing of several 2D mesh structures, which can later be assembled into the desired 3D shape and welded by local rehydration along the junction zones. And of course, it also possible to build similar structures with freshly drawn self-adhesive viscin fibers (Fig. 6-5).

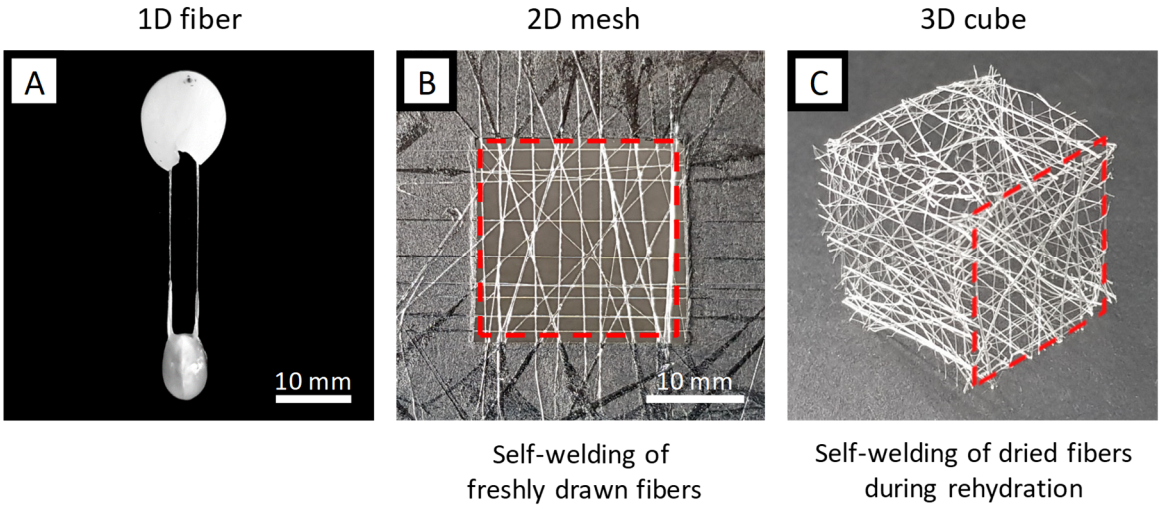

Figure 6-5: Structures made from drawn viscin fibers. A) Manually drawn viscin fibers. B) A two-dimensional mesh created from self-welding viscin fibers. After drying the mesh can be cut from the card board frame (red dotted line: cutting contour). C) A hollow cube formed of premanufactured two-dimensional meshs welded by rehydration (red dotted line: outlines of an individual 2D mesh from (B)). Scale bars: 10 mm.

6.2.2 Formation of free-standing films from mistletoe viscin

It was demonstrated in chapters 4 and 5 that the adhesive properties of mistletoe viscin and viscin fibers arise from the swellable matrix material, which is infused between and within micro- and nano-fibrils. It stands to reason that this can be applied not only to form fibers via elongational shear, but possibly also films by shearing perpendicular to the microfibrillar axis, as demonstrated by the flattening of fused fibers. This can be easily demonstrated by placing viscin tissue between fingers, adding a bit of shear by rubbing and then slowly separating the fingers. This results in the formation of an adhesive interaction with the mistletoe viscin at the fingertips, and the formation of a stable free-standing film between the

fingers (Fig. 6-6A), stabilized presumably by cohesive forces between the matrix and fibrils. Further separation of the fingers results in the eventual collapse of the films into a fiber.

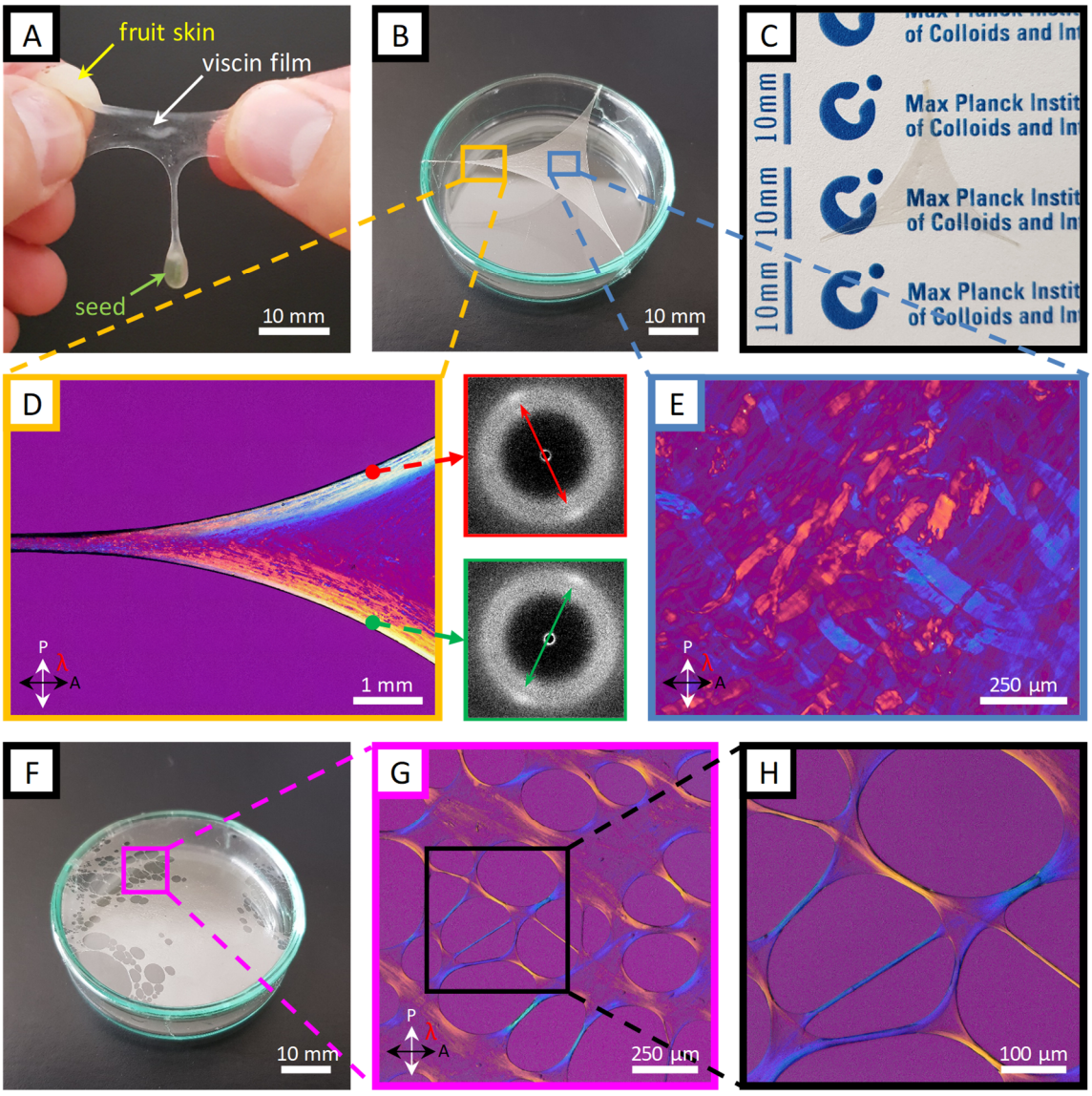

Figure 6-6: Viscin film properties examined with PLM and WAXS. A) Image of a freshly formed and flexible viscin film drawn from a compressed berry of *V. album*. Scale bar: 10 mm. B) Free standing viscin film drawn into a triangular shape and glued to the edge of a Petri dish making use of the natural adhesive properties. Scale bar: 10 mm. C) A dried viscin film is dimensionally stable and highly transparent. D) PLM image showing a detail of (B) revealing the cellulose orientation along the contours of a film. Scale bar 1 mm. Cellulose orientation was also confirmed with wide-angle X-ray diffraction shown in the adjacent diffraction pattern from 2 selected points along the film contour. The arrows in the diffraction patterns mark the distinct equatorial cellulose diffraction spots. E) PLM image of the film center from (B) where viscin cells are found to be randomly oriented and mostly unstretched. Scale bar: 250 µm. F) A viscin film which locally collapsed into a porous structure. Scale bar: 10 mm. G) PLM image showing a detail of a porous region from (F). Scale bar: 250 µm. H) Detail from (G) showing that the film locally collapsed into small fibers. The cellulose is highly aligned along the fiber directions and the pore contours as indicated by the polarization colors.

In a more controlled manner, it was possible to form thin films of viscin adhesive made from mechanically isolated viscin. The isolated viscin was drawn into short and thick strands and fixed on at least two different points (using the natural adhesive properties of the viscin) after which it was and pulled in an opposing direction and fixed on a third point (Fig. 6-6B, for a more detailed description see chapter 3, Fig. 3-4). This resulted in the formation of a freestanding film between the three anchoring points, which flows when hydrated and stretched. When dried, the transparent film stiffens, retaining its integrity and shape (Fig. 6-6C). PLM imaging of the film reveals orientation of the cellulose microfibrils along the local contours of the anchoring points (Fig. 6-6D). This orientation was verified with wide-angle X-ray scattering, showing that cellulose is aligned along the apparent stress fields. In the middle of the film, in contrast, numerous randomly oriented unstretched viscin cells could be observed (Fig. 6-6E) – which could ostensibly supply further extensibility of the film in the wet state. However, a viscin film, which is excessively stretched will fail at some point. The failure is not characterized by a total rupture of the film but is rather initiated by a local collapse of the film into a porous architecture (Fig. 6-6F). The arising pores are connected via thin highly oriented fiber segments ensuring the mechanical integrity of the remaining film (Fig. 6-6G+H). As revealed by PLM, the cellulose orientation follows the local contours of the pores. While the freshly isolated viscin can be readily stretched into continuous films, partially dried films (drying occurs quickly) tend to collapse into the porous structures as described above.

6.2.3 Mistletoe functions as a versatile adhesive on diverse surface chemistries

Based on the ability of the hydrated viscin fibers to stick to themselves, to tree branches and to fingertips (and other materials observed during my investigations, such as glass slides, tweezers and lab bench surfaces), I further explored the versatility of the viscin adhesive on a wide range of surfaces presenting different chemistries including metals (brass, aluminum, stainless steel), glass, polymers (polytetrafluoroethylene (PTFE), high density polyethylene (HDPE), polycarbonate (PC), polyamide (PA), polypropylene (PP), metal oxides (mica) and wood, as well as viscoelastic biomaterials (porcine cartilage and skin). For a number of selected materials, the viscin from a single berry was able to adhere to a small area and support the weight of 10 g of each material (Fig. 6-7A). Considering that the typical weight of a hydrated seed is in the order of 0.2 g the dried viscin can withstand loads at least 50x higher than required based on the assumed natural function and possibly more.

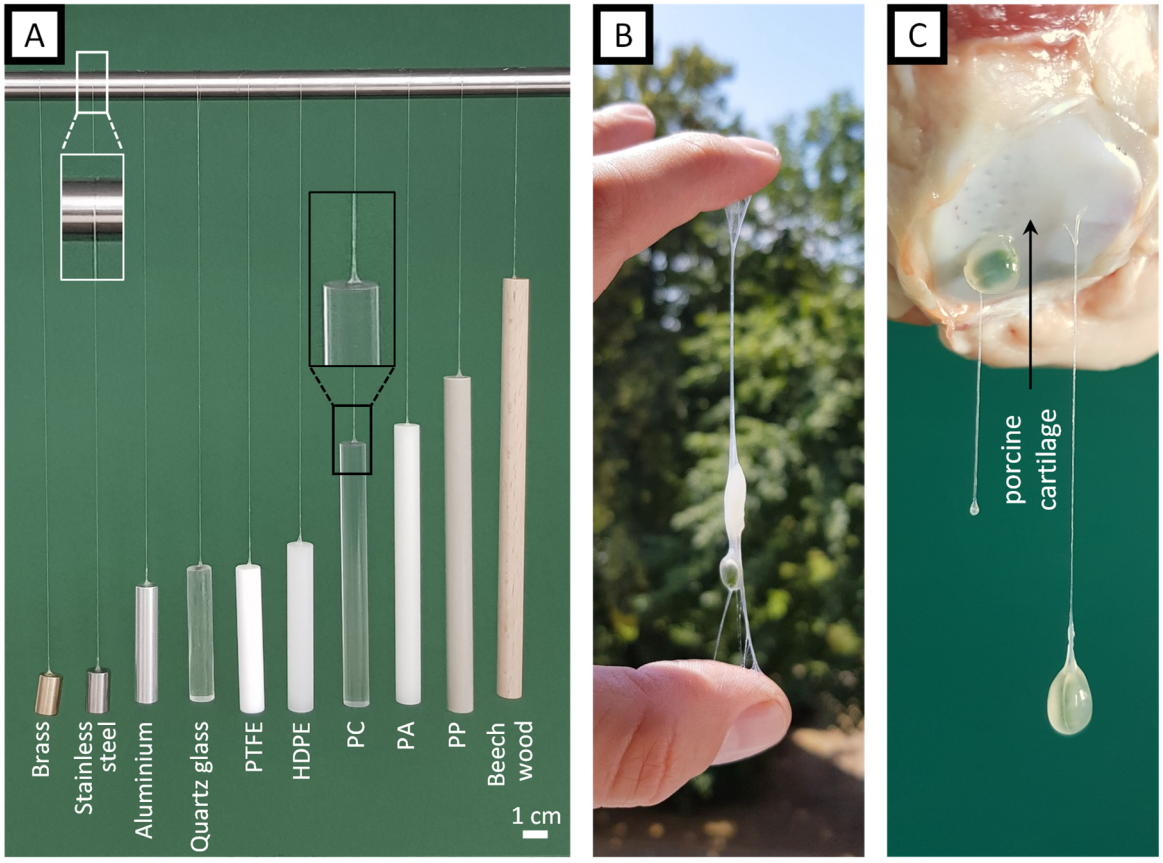

Figure 6-7: The multimaterial adhesive properties of viscin. A) Cylinders from 10 selected materials with different surface chemistries are supported by a viscin fiber each attached to the top surface of the cylinder and a laboratory stand. Cylinder diameter: 1 cm, cylinder weight: 10 g. Scale bar: 1 cm. B) A viscin fiber adhered between two fingers supporting the seed. C) Two *V. album* seeds adhering to porcine cartilage. One seed is directly attached to the cartilage via the hydrated viscin layer surrounding the seed. The other seed is connected via a freshly formed viscin fiber.

6.2.4 Biomedical potential of viscin coatings

The ability of mistletoe viscin to stick to skin and cartilage also makes it an interesting candidate as a wound sealant or biomedical adhesive. Indeed, there are reports of mistletoe viscin being used both as a birdlime and wound dressing in ancient times (reviewed in Tubeuf 1923, p. 41 ff.), and commercially available nitrocellulose-based sealants for small cuts can be found at most drugstores (Filmogel, Laboratoires Urgo, France). To investigate the potential of this natural fiber-reinforced adhesive as a wound sealant, incisions were made in porcine skin (non-living) using a razor blade (Fig. 6-8A). The incisions were sealed by spreading native isolated viscin tissue over the cut (Fig. 6-8B), and allowing it to dry (Fig. 6-8C). The silky, glossy viscin sealant remained attached upon drying and even when a load was applied to the skin, the cut remained sealed, while nearby unsealed incisions opened easily (Fig. 6-8D+E). Tested on live human skin (no incisions inflicted!), such a viscin sealant remained attached for a period of more than 3 days. The sealant always retained a minor tack on its surface. Aside from that, it remained flexible, allowing free movement when performing everyday tasks like using tools, cutlery or riding a bike and was

even resistant to short time rinsing with water, e.g. when washing the skin under running water. To remove the seal, friction could be used by simply rubbing the sealed area.

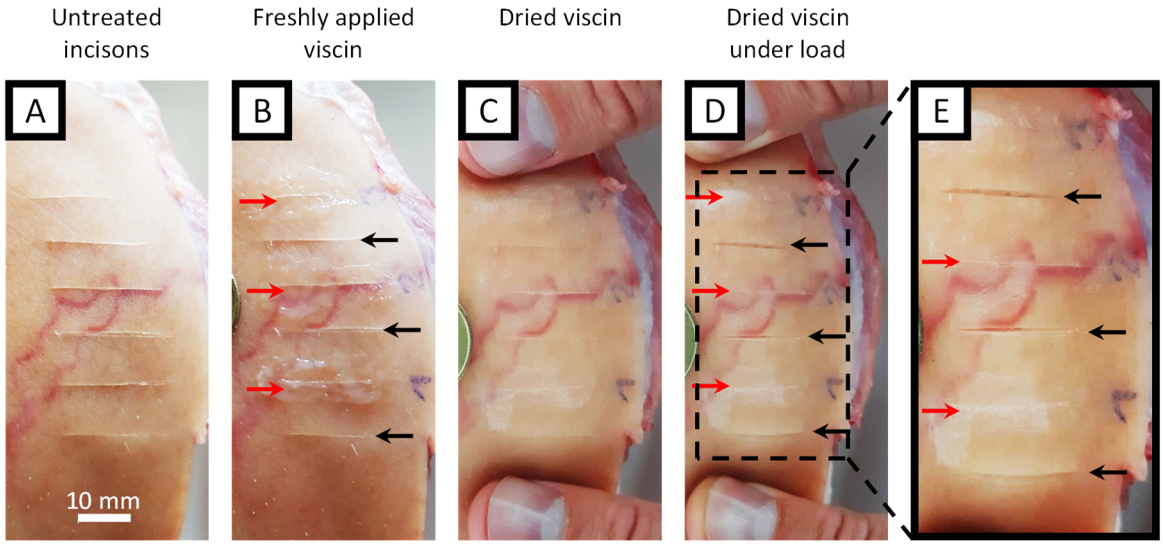

Figure 6-8: Image series of an artificial wound treatment with viscin. A) Parallel cuts were made with a razor blade on a porcine skin. Scale bar: 10 mm. B) Three incisions were selected as reference (black arrows) while the remaining incisions were used for viscin treatment (red arrows). Freshly isolated viscin from one berry each was spread over the selected incisions. C) Applied viscin after drying. D) Dried viscin sealant loaded perpendicular to the incisions. E) Detail from (D) showing the opened reference incisions under load while the dried viscin sealant keeps the incisions sealed and closed.

Native viscin already performs surprisingly well when used as a tissue sealant, considering this is presumably not the evolved function. However, the intrinsic property to stick to all kinds of surfaces and the ability to instantly form fibers makes it slightly delicate to handle and complicates the precise application onto only the designated area. Therefore, I followed remarks in the literature on ancient recipes for making viscin birdlime and coatings mentioning the use of natural oils as an additive (Theophrastus (371-287 BC): *De Causis Plantarum* and Pliny (AD 24-79): *Naturalis historia*, reviewed in Tubeuf 1923, p. 50). In a very simplistic approach, mechanically isolated viscin from multiple berries was submerged in walnut oil or olive oil for a few minutes (Fig. 6-9A+B).

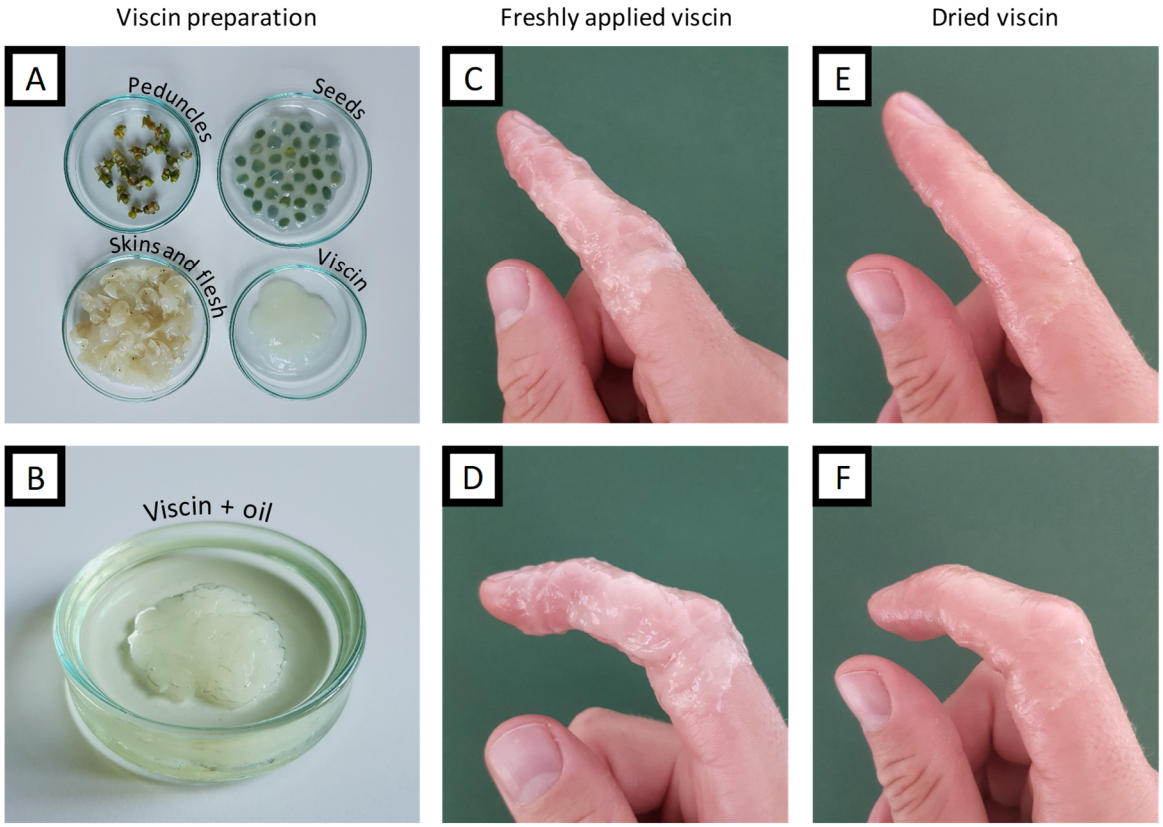

Figure 6-9: Preparation and application of viscin bandages. A) Mechanically separated fraction of the *V. album* berries: peduncles, seeds, skins and flesh and viscin. B) Viscin submerged in walnut oil. C) Translucent, milky viscin coating from (B) freshly applied to human skin, covering a finger. D) The freshly applied viscin allows free movement of the covered finger. E) The viscin coating dried into a thin transparent film. F) The dried flexible viscin coating still allows free movement of the finger without failure despite intense stretching and compression, e.g. around the knuckles.

The oil-treated viscin was not as sticky as the native viscin, allowed a much easier processing, but still revealed a notable adhesion to human skin. The oil-treated viscin exhibited only a weak tendency to form fibers combined with an improved coherence. The oil-processed viscin feels smooth and silky and can be kneaded like a dough, stretched into stable films and applied to the skin where it can be further redistributed over the designated area (Fig. 6-9C+D). Within only a few minutes even thickly applied viscin dries into a smooth transparent coating (Fig. 6-9E). In contrast to the native viscin, the oil-treated viscin does not show any perceptible tack, and allows one to grab or touch things without getting stuck to the surface and is so flexible that is does not restrict any movements (Fig. 6-9F). Indeed, it is not perceptible on the skin. Similar to the native viscin, defects can be repaired by adding further material (additive manufacturing) or by locally rehydrating the coating which enables further manipulation, consistent with the self-welding nature of the material. To wrap an entire finger with a viscin coating as presented in Figure 6-9C+D it requires the viscin of about 10-15 berries.

6.3 Discussion

In this chapter, I investigated mistletoe viscin primarily from the perspective of a fiber-reinforced adhesive. I investigated and demonstrated the versatile processability of the viscin adhesive, including the ability of water-based self-welding to form two-dimensional and three-dimensional structures, formation of free-standing films revealing dynamic and adaptive reorientation of CMFs, strong adhesion to a broad range of surface chemistries and finally, the ability to act as a biogenic adhesive that is effective on mammalian skin and cartilage. This multifunctionality, which is intimately related to the hierarchical structure comprised of cellulose nano- and microfibrils surrounded by a humidity-responsive adhesive, further underlines the enormous potential for bio-inspiration inherent in mistletoe viscin.

Reversible water-responsive adhesive

Results presented in chapters 4 and 5 clearly demonstrate the presence of a stimuli-responsive matrix that swells and becomes sticky and sacrificial at RH above ~50%. In the dry state, however, the matrix acts as a strong cement that holds CMFs together, which is not sticky or self-adhesive – e.g. two fibers can be held in contact, but will not adhere. In this state, the fibers are highly flexible, with stiffness values far exceeding those of most standard thermoplastics, with the exception of ultrahigh-performance technical plastics including polyaramids, such as Kevlar (Akato and Bhat 2017) and UHMWPE (Deitzel et al. 2017). However, unlike petroleum-based thermoplastics, viscin fibers are produced and processed under sustainable and environmentally friendly conditions and are additionally biorenewable and biodegradable. In contrast to the dry fiber state, the hygro-responsive matrix material can uptake moisture from the atmosphere at RH above ~50%, which converts it from a strong cement to a sticky sacrificial glue that allows the CMFs to flow past one another, enabling elongation of the tissue into fibers (chapter 5, Horbelt et al. 2019). However, this tendency of the hydrated matrix also enables the viscin to stick to other fibers, as well as a number of other surfaces. From an evolutionary perspective, it seems that this propensity of viscin from multiple berries to stick to one another may be advantageous in order to create a network of fibers in the bird's gut, that when released, increases the likelihood of adhesion to branches, and thus, seed propagation and germination. However, we discovered that the stimuli-responsive nature of the matrix and the resulting tendency of the viscin tissue to adhere indiscriminately to itself and various other surface chemistries in the hydrated state enables remarkable materials processing and possible biomedical applications that go well beyond the evolved biological function, which I will discuss below.

Fiber fusion and self-welding

Self-welding behavior under ambient conditions is not a typical property of most plastics, and fusion of two separate surfaces, would normally require bringing a thermoplastic to its melting point, and essentially remolding two surfaces into one (Troughton 2009). A notable exception is a class of supramolecular polymer elastomers known as vitrimers developed

initially by Leibler and colleagues, which exhibit self-welding and self-healing behaviors based on reversible hydrogen bonding interactions (Cordier et al. 2008). However, this response requires the presence of unpaired hydrogen bond donors and acceptors on the surface, which decay on a freshly cut surface relatively quickly if two surfaces are not brought together immediately because new bonds are formed in the bulk rather than between two surfaces (Cordier et al. 2008). In general, supramolecular polymers stabilized by reversible non-covalent interactions including H-bonding, metal coordination or ionic interactions will tend to be self-healing and possibly self-welding (Herbst et al. 2013); however, these materials are typically extremely soft.

In contrast to typical supramolecular polymers, mistletoe viscin fibers are extremely stiff, yet flexible due to reinforcement with CMFs, and the self-welding response is triggered by simply cycling between low and high humidity conditions, resulting in the melding of multiple fibers (Fig. 6-2). We presume that this response arises from the swellable hygro-responsive matrix material identified in previous studies as existing between CMFs (chapter 4 and 5, Horbelt et al. 2019). Yet, currently very little is understood about the chemical composition of the viscin matrix, as already pointed out in chapter 4. The limited chemical analysis performed on Viscaceae mistletoe species indicates the presence of various hemicelluloses and pectin in addition to cellulose, none of which is unusual for a material that has its basis in the primary cell wall (Gedalovich and Kuijt 1987; Gedalovich-Shedletzky et al. 1989; Azuma et al 2000; Azuma and Sakamoto 2003). Nonetheless, the combination of a water-responsive adhesive reinforced by stiff cellulosic fibrils provides an exciting paradigm for design of high-performance supramolecular composites, combining exceptional mechanical properties with intrinsic self-healing and self-welding response. Future work must elucidate the chemical constituents of the matrix.

Film formation

I was able to demonstrate also in this chapter that the ultra-soft cell walls of viscin cells from the viscin cell bundles (VCBs) and viscin cell clusters (VCCs) can be stretched not only into uniaxial fibers, but also into free-standing films via application of a multiaxial load and drying. Considering the viscin tissue as a composite of CMFs embedded in a supramolecular hygro-responsive matrix, one can envision the film formation process as a force-induced reorientation and uncoiling of VCBs into aligned CMFs along various directions corresponding to local stress/strain fields under multiaxial load, while the matrix maintains the integrity of the film, holding CMFs together. This is supported by the fact that CMFs orient along the fiber axis near anchoring points, but are less oriented in the middle and may remain as coiled viscin cells in the center of the film as demonstrated by WAXS and PLM measurements. This combination of fully stretched and locally aligned CMFs towards the film periphery with partly and mostly unstretched cells provides an enormous reservoir of hidden length to further expand the surface area of a dried film in any direction following rehydration under RH conditions above 50%. There is a limit of expansion at which the film becomes mechanically unstable; however, this does not result in the

complete failure of the film as a whole, but rather the local formation of pores on the scale of a few 100 µm in the film. Notably, the CMFs can become locally oriented along the struts of pores that form due to drying, likely due to the presence of local drying stresses (Fig. 6-6J+K).

Multimaterial adhesion

In addition to the already discussed self-adhesion, the natural substrate of the viscin adhesive is the tree bark covering the branches of host species, which is crucial for propagation and germination of the seeds (Kuijt 1969; Heide-Jorgensen 2008). However, we demonstrate here that viscin is essentially indiscriminate in terms of what surface chemistry it adheres to, showing adhesion to both biogenic materials such as wood, skin and cartilage, as well as completely synthetic materials including various plastics, metal alloys, and glass. Adhesion to skin may also be relevant evolutionarily since adhesion to bird feathers and beaks, which share a keratinous origin similar to mammalian skin (Wang et al. 2016), also constitutes a seed-spreading mechanism (e.g. a bird will dislodge a seed that has become adhered to its beak onto a branch). Yet, the adherence to various synthetic surfaces that represent both polar and non-polar surface chemistries is harder to explain from a biological adaptation standpoint and may simply represent a highly versatile adhesion chemistry, analogous to that observed in mussel adhesion (Waite 2017).

Currently, the chemical and physical mechanisms of viscin adhesion is completely unknown, which is not surprising considering how little is understood about the basic composition of the viscin matrix. Nonetheless, it seems likely that the ability of the viscin to adapt its shape to a surface it is in contact with in the wet state enables mechanical adhesion as the material dries and locks in to nano- and microscale pores on the surface (e.g. similar to cyanoacrylate glues). However, specific chemical adhesion mechanisms are also suggested since the viscin also binds to freshly cleaved mica, on which surface roughness is minimal and to cartilage, which most adhesives functioning purely based on mechanical mechanisms cannot adhere to. The ability to stick to both hydrophilic (e.g. mica, biological) and hydrophobic (PTFE) surfaces suggests that the adhesion is chemically versatile. This is not unprecedented in the biological world – DOPA-based mussel adhesives bind to hydrophilic surfaces via hydrogen bonds, ionic bonds or metal coordination, and bind to non-polar surfaces through the hydrophobic face of the aromatic rings of the catechol groups of the DOPA residues (Waite 2017). In fact, catechols have been detected in viscin of certain mistletoe species (Gedalovich-Shedletzky et al. 1989). However, at this point there are no clear connections between adhesion and any aspect of the viscin chemical composition. In addition to the chemical adhesion mechanisms, mechanical reinforcement of adhesives can be a critical feature in their performance. As demonstrated with gecko and gecko-inspired adhesion, the compliance of an adhesive is inversely related to the pull-off force (Gilman et al. 2015). In this light, the inclusion of stiff CMFs in the viscin adhesive likely contributes positively to the adhesive behavior of mistletoe viscin as well.

Biomedical potential for viscin

Probably the most exciting observation of the adhesion studies with respect to potential applications is the demonstration that viscin can adhere to biological tissues including cartilage and skin. In particular, the observation that mistletoe viscin can adhere to cartilage is especially remarkable considering the enormous challenges in developing effective adhesives for wet surfaces in biological tissues (Li et al. 2017; Yuk et al. 2019). While much more needs to be done to investigate the potential of this approach, interaction with cartilage makes it an interesting model system towards the development of bio-inspired intervertebral disc fluids or synovial fluids.

With regards to skin coatings and wound sealants, the processability of viscin into a coating is incredibly facile, as demonstrated with film formation. No further additives are required – as long as the viscin stays hydrated, the coatings can be formed and applied under ambient conditions. Indeed, the humidity from skin moisture appear to be enough to keep the viscin film pliable and sticky for at least several days. The mechanical integrity of the coatings is easily demonstrated and arises presumably from the presence of CMFs within the films. The coatings remain firmly attached during brief washing in water (e.g. hand washing); yet, are easily removable with a bit of friction, providing the ideal properties for a tissue sealant. The viscin from a single berry can be used to produce a film with a limited surface area (as already discussed). However, based on ancient recipes of birdlime, treatment of viscin from many berries with olive oil or walnut oil, produces a larger, less sticky, smooth film that is comfortable to "wear" and more flexible. This means that there are no restrictions in using coated hands besides ensuring not to soak the film for too long in water since it completely rehydrates and swells dramatically, and will wash it off at some point. As opposed to currently available nitrocellulose-based wound sealants, the viscin films are sustainable natural products with no synthetic additives, are environmentally friendly, are apparently biocompatible (no skin irritations were observed), are biodegradable and even function under wet conditions (suggesting these would still work in the presence of bodily fluids such as blood). Furthermore, the fact that potential anti-cancer and other therapeutic compounds and have been previously extracted from mistletoe viscin (Büssing 2000; Horneber et al. 2008; Nazaruk and Orlikowski 2016), perhaps adds a further dimension to the potential biomedical applications of these bio-coatings. However, there are also critical reports about a considerable potential of harm of mistletoe extracts used for medical applications (Ernst 2006) and reviews which conclude, that reliable controlled clinical trials do not show a significant benefit in anti-cancer treatment (Kleijnen and Knipschild 1994; Ernst et al. 2003).

7 Conclusions and outlook

The fields of biomimicry and bio-inspiration are founded on the concept that nature can offer humans novel insights into more effective and sustainable ways of doing things. In particular, bio-inspired materials research provides design principles and structure-function paradigms that can transform and improve the materials we use and how we make and dispose of them. In this light, the material properties and structure of mistletoe berries from the European mistletoe (*V. album* L.) were investigated in this thesis with a specific focus on the adhesive viscin tissue surrounding the seed inside the mistletoe berry. The viscin adhesive not only plays a crucial role in the seed-host attachment of this hemiparasitic plant species, but as highlighted in the thesis, may also offer important inspiration for the sustainable design of next generation adhesives and cellulosic composites toward potential technical and biomedical applications. Indeed, during the natural dissemination of the mistletoe seeds (through the help of birds), the viscin tissue shows the remarkable ability to form adhesive fibers and films which help to glue the seed firmly onto a suitable host. However, it was also demonstrated clearly in this thesis that the adhesive is remarkably versatile, sticking to a broad range of surface chemistries beyond what it presumably evolved for, including metals, glass, plastics and even living tissue. Based on the multiscale material analysis performed here, this work provides valuable new insights into this fascinating fiber and film formation process. Below, I will summarize the key findings from each data chapter and will highlight the unifying concepts elucidated as a whole. Finally, I will provide an outlook on the potential for bio-inspiration and on future directions.

In chapter 4, a comparative study of mistletoe berries of two closely related subspecies of *V. album* L. was performed to identify differences in the structural organization, as well as the functional adhesive performance of the fiber forming subspecies *V. album* compared to the non-fiber forming subspecies *V. austriacum*. A method was developed to define a set of anatomical planes of the *V. album* berry, which enabled for the first time, the systematic histological characterization of the structural organization of the berry, achieved via hand sectioning of frozen berries. Mechanical investigation revealed that the ability to form long adhesive fibers was clearly linked to a specific tissue in the viscin of *V. album*, which was completely absent in *V. austriacum*. As shown with PLM, the tissue consists of viscin cell bundles (VCB) and viscin cell clusters (VCC), which connect the berry endocarp surrounding the seed to the epicarp. PLM, CFM and SHGM showed that both VCB and VCC are comprised of elongated cells with massive cell walls where submicron sized cellulosic fibrils were coiled perpendicular to the cell long axis embedded into a non-cellulosic matrix. When the seed was mechanically removed from the surrounding berry tissue – as is assumed to occur in nature during feeding or subsequent defecation of mistletoe berries by birds – the cell walls of the individual viscin cells of VCB and VCC are massively stretched. This leads to an uncoiling of the cellulose fibrils in which each cell can be drawn into a small filament of ~2-3 µm in diameter. These filaments aggregate parallel to the drawing direction and are glued to together by a non-cellulosic matrix to form macroscopic fibers.

In addition to the observed structural variation, functional differences in the adhesive behavior of the viscin tissue extracted from the two subspecies was observed, which may be linked to their efficacy in successfully germinating on specific host species. To summarize the findings, *V. album* berries attached very firmly on surfaces, while *V. austriacum* berries tended to attach, but then slide along a surface under the effects of gravity. It is tempting to speculate that the differences in adhesive response, as well as the tendency to form fibers, may represent host-specific strategies for attachment to deciduous hardwoods versus coniferous hosts. Indeed, one could speculate that sticky fibers of multiple linked *V. album* seeds are more effective at attaching to the bare branches of a hardwood in the winter. On the other hand, the sliding berries of *V. austriacum* would appear to have an advantage on pine host branches, which are covered with needles throughout the year.

While these conjectures about functional relevance clearly require more intensive field-based studies to confirm, an equally interesting question concerns the genetic basis of these functional and structural differences. Are *V. album* and *V. austriacum* in fact genetically distinct as some studies seem to suggest (Zuber and Widmer 2000, Zuber and Widmer 2009; Maul et al. 2019) or could these functional differences result from host-specific epigenetic effects, for example? Interestingly, there is one host species *Genista cinerea* that serves as the only identified natural common host for both subspecies (Grazi and Zemp 1986). One could imagine a very interesting series of experiments comparing the behavior and development of *V. album* and *V. austriacum* seeds on *G. cinerea*; however, this would require long term investigations (first fruiting after 4-5 years). In addition, the overall approach developed in this thesis might help to elucidate the morphological differences between other species and subspecies to gain a broader understanding of the structure-function relationships within the viscin tissue across different mistletoe families. It would be highly interesting to combine these structural studies with systematic investigations on the development of berries from both species in more detail similar to the work of Gedalovich and Kuijt (1987) for *P. pyrifolia* to gain a better understanding of the structural organization.

At the moment, lower hanging fruit in terms of research efforts would focus on the compositional and nanostructural sources of the different adhesive performance and fiber formation capacity of the two species. Specifically, what chemical groups are present in the viscin tissue of *V. album* vis-à-vis V. *austriacum* differences and how might one connect them to the very different adhesive functions? There are extremely few studies on the chemical composition of the mistletoe viscin tissue (Gedalovich and Kuijt 1988; Gedalovich-Shedletzky et al. 1988; Azuma et al. 2000; Azuma and Sakamoto 2003), and these studies were made on a broad range of species and were inconsistent with the specific part of the viscin tissue that was examined, which has led to highly disparate results in terms of basic composition. However, this information will be very relevant for efforts to develop new adhesive inspired by the mistletoe, as highlighted in chapter 6. Regarding the fiber-forming capacity of *V. album* viscin tissue – this is highly relevant for ongoing efforts to produce

fibers and composites from bio-sourced cellulose nanocrystals (CNCs) and cellulose nanofibrils (CNFs), and thus, understanding the nanoscale structural changes during fiber fabrication is the precise focus on chapter 5 of this thesis.

After localization and structural characterization of the tissue involved in the fiber formation in chapter 4, the second data chapter elucidates the rapid fiber-assembly process in more detail (chapter 5) with a focus on extracting a multiscale understanding cellulose organization. To achieve this goal, specific protocols were developed for both manual and semi-automated viscin fiber drawing. The latter involved the development of a custom-built Lego® fiber drawing device to follow the rapid transition from ultra-soft cells to stiff fibers with in situ PLM video imaging. Complementary PLM and synchrotron based XRD experiments revealed the change in cellulose orientation from transverse orientation in the native VCB tissue to an almost perfect orientation along the drawing direction of the resulting fiber. Remarkably, the drawing forces required to induce fiber formation were close to the lower detection limit of the sensitive load cell on the order of ~10 mN while after only a few minutes of drying under ambient conditions the fibers became extremely stiff – up to 20 GPa in some cases. Tensile tests of viscin fibers under controlled environmental conditions (T and RH) revealed a decrease in average tensile stiffness from ~14 GPa in the dry state (0% RH) to ~0.4 GPa in the wet state (90% RH) where the stiffness suddenly plummets at 45% RH. The suggested influence of the moisture content on the tensile stiffness was further supported by microscopic investigations of fiber swelling and fiber sorption experiments using DSC-TGA showing an increase in fiber diameter and a water uptake above 30% RH, respectively, which most likely induces the mechanical softening of the fibers.

Synchrotron based XRD experiments were conducted to examine the fiber ultrastructure in more detail. WAXS results showed, that the fibers consist of highly oriented thin CMFs of low crystallinity but with a remarkably high aspect ratio of the crystalline domains (L: ~67 nm / W: ~2.5 nm) along the CMF long axis. As observed from humidity controlled SAXS measurements these CMFs showed a highly regular parallel stacking. Changes of the RH led to a fully reversible change of the CMF spacing where the individual CMFs were always kept at a minimum distance around 3 nm. This led to the supposition that there must be a fixed, swellable matrix materials between the CMFs (maybe covalently attached to their surface) that enables the flow and reorganization of CMFs past one another under mechanical load in hydrated conditions, yet acts a strong binding agent under dry conditions, providing the mechanical integrity of the fiber. Indeed, the key to understanding (and eventually mimicking) the fiber fabrication process with bio-sourced CNCs is to determine the nature of this swellable matrix and understand how it functions together with the cellulose. One interesting observation from nature that points to an even more complex multifunctional behavior of this matrix material is the tendency of fibers from multiple berries to adhere to one another after passing through a bird's gut, forming a single fiber. This self-adhering behavior of the fibers and their adhesive behavior in general form the basis for the investigations in the final data chapter.

In chapter 6, mistletoe viscin was investigated from the standpoint of a natural fiber-reinforced adhesive with the goal of assessing the potential of processing and possible applications. Sparked by the observation of viscin fibers fusing in natural circumstances (i.e. bird droppings) and during artificially induced fusing (e.g. when holding two fibers in contact between fingers), the investigation first focused on the factors that control fiber self-adhesion. PLM and ESEM investigations showed that it was possible to reactivate the viscin adhesive properties of dried fibers (which lose their tackiness) by simply exposing them to water vapor. Two humidity-activated fibers held in close proximity will bind to one another, and after rapid drying, the fused fibers showed a combined cross-section where the former fiber-fiber interface was completely lost – indicating a self-welding behavior. This goes beyond the fibers simply sticking to one another. Rather, the welded fibers exhibit clear structural reorganization at the nano- and microscale, behaving structurally and mechanically as a single element. These insights were used to build larger 2D structures from many dried fibers, by stacking fibers into mesh-like structures, which could then be permanently fused at the fiber-fiber joints. Furthermore, these 2D structures could be successively assembled into even larger free-standing 3D structures. It was observed that freshly drawn fibers do not require the addition of water to fuse and that self-adhesiveness is an intrinsic property of fresh viscin, likely relevant for its biological function. Indeed, freshly drawn fibers could be rapidly stacked into complex shapes, which become physically cross-linked by quick subsequent drying of the in-built adhesive. This makes viscin and interesting candidate for applications such as additive manufacturing with possible applications as biocompatible scaffolds.

Apart from the self-adhesive properties, it was also demonstrated in chapter 6 that viscin is actually able to adhere to a broad range of both natural and synthetic materials presenting extremely different surface chemistries, including wood, glass, various polymer thermoplastics and thermosets, metal alloys and even biological tissues including skin and cartilage. This is a remarkable and surprising range of adhesive substrates for a biological material that has ostensibly evolved to adhere to tree branches (from specific hosts) and possibly, bird feathers and beaks. From a bio-inspiration standpoint, these observations mark mistletoe viscin as an exciting new model system for understanding and mimicking bioadhesion. This has been pursued successfully in many marine adhesive systems, most notably the mussel byssus, resulting in the discovery of chemical adhesion mechanisms that are currently being applied for producing technical and biomedical adhesive, including prenatal surgical glues (Lee et al. 2011). However, unlike most other bioadhesives viscin not only sticks well, but is mechanically reinforced with cellulose fibers, providing an exceptional combination of stiffness and flexibility that is humidity dependent. As already mentioned, further investigations are necessary to understand the complex chemical interactions underlying the adhesive behavior of viscin. A first step towards a better understanding will be the careful mechanical characterization of the adhesive strength in combination with different surfaces chemistries, while determining the chemical composition of the polysaccharidic matrix will hopefully provide molecular level mechanistic insights.

Another important finding of this investigation was the discovery that while viscin tissue is adept at forming fibers under uniaxial load, it can also be processed into free-standing films under biaxial loading. In this context, a protocol was developed to isolate viscin mechanically from the surrounding tissue of the berry, and it was demonstrated how the isolated material could be easily drawn into 2D films with a defined geometry. The initially viscous films were allowed to dry under ambient conditions resulting in thin, transparent and dimensionally stable films. PLM and WAXD investigations showed that the cellulose was highly oriented along the local contours of the films indicating that the cellulose responds to the local force and strain fields acting on the material during multiaxial loading in the wet state. This is consistent with the findings in chapter 5 on fiber drawing and suggests that the water swellable matrix between CMFs play a key role in enabling film formation. Notably, towards the center of the films numerous viscin cells with their characteristic transverse cellulose orientation can be found, which presumably did not experience sufficient mechanical loading to unravel and align. However, these pristine or partially stretched cells will likely act as a reservoir for hidden length within the film allowing further stretching of the films if the viscin were to be rehydrated.

Combining the observations that viscin adheres effectively to human skin and is able to be processed into complex film geometries via multiaxial loading suggests a clear potential in the realm of biomedical applications. Along these lines, it was demonstrated that freshly isolated viscin could be used to cover artificially inflicted incisions on (non-living) porcine skin by simply distributing the viscin over the dedicated area. After drying, the viscin formed a thin coating which was able to withstand mechanical loading and to keep the incisions closed and even tolerated sustained washing with water. It can be assumed that the numerous stretched cellulosic filaments present in the viscin film act as the main load bearing component that adds mechanical integrity to the wound covering. In a slightly advanced procedure, following ancient reports on the making of birdlime and bandages from viscin, the viscin was given into vegetable oil after isolation and before application which improved the processability of the viscin as a coating even further, allowing it to be easily stretched over an entire finger on which it remained stiff, yet flexible. In the context of biomedical applications such as wound sealants and wound dressings, the fact that the viscin tissue combines mechanical fiber reinforcement with an integrated versatile adhesive makes it a very intriguing system for biomedical inspiration. In this light, there is an enormous literature on the use of chitin and chitosan for the production of anti-microbial wound dressings, showing the clear potential of such an approach (Jayakumar et al. 2011).

The findings outlined in this thesis provide crucial new insights for understanding the biological role of mistletoe, and clearly demonstrate the potential of this system in terms of bio-inspiration. Through evolution, mistletoe viscin has achieved a level of simplicity and economy in material processing that is, as of yet, unattainable by polymer scientists. In terms of fiber formation, this is dependent on a massive, moisture-dependent reorganization of cellulose microfibrils containing crystalline domains of high aspect ratio through simple mechanical drawing. Key to this process is a water-responsive interfibrillar matrix material

that functions alternatively as a sacrificial binder allowing CMFs to flow and reorient in the hydrated state and a strong cement providing mechanical integrity in the dry state. This combination of sacrificial bonds and hidden length allows for a >100-fold draw ratio and 35-fold increase in stiffness by simple mechanical drawing and drying of viscin fibers at ambient conditions. The ability to mimic this process in industrial level manufacturing of cellulose-based composite materials would represent a paradigm shift in efforts to mass produce sustainable material alternatives to petroleum-derived plastics. Indeed, materials based on biorenewable cellulose sources from wood pulp, tunicates and even microbes hold great potential for replacing humanity's plastic addiction; yet, there are major challenges in processing the precursors into useful materials (Moon et al 2011; Thomas et al. 2018; Klemm et al. 2018). Mistletoe may provide some answers and ideas for novel processing strategies. However, before this can happen, the intricate biochemical and biological details of the viscin fiber and film formation process must be further elucidated – in particular, the nature of the interfibrillar matrix material and the mechanism of moisture-dependent deformation must be determined. Along these lines, comparative studies of other mistletoe species that form adhesive fibers (and potentially films) (e.g. *Phthirusa pyrifolia* in Gedalovich and Kuijt (1987), *Viscum coloratum* in Azuma and Sakamoto (2003) and *Viscum minimum* in Heide-Jorgensen (2008)) are likely to reveal further important insights into the underlying mechanisms of fiber and film formation, enabling the eventual transfer of these design principles towards green manufacture of materials using biorenewable starting materials.

In addition, mistletoe viscin clearly holds potential beyond inspiring processing of sustainable building materials, especially with regards to its potential as a biomedical adhesive or wound dressing. Given the observed dissemination of the mistletoe seeds by sticking to bird feathers and beak, the viscin adhesive may be optimized for not only adhering to tree bark, but also to keratin-based materials, which would also include mammalian skin. While this is only speculation at this point, results from chapter 6 clearly reveal the efficacy of viscin-skin attachment and the potential role of viscin as a fiber-reinforced wound dressing. However, before this can be realized effectively, it is essential to understand the molecular mechanisms of film formation and adhesion, which will also depend on characterizing the water swellable matrix of the viscin cell bundle. Thus, with these challenges in sight, the future of mistletoe berry research and bio-inspiration is sure to be quite fruitful.

References

Akato, K., and G. Bhat. 2017. 'High-performance fibers from aramid polymers.' in G. Bhat (ed.), *Structure and Properties of High-Performance Fibers* (Woodhead Publishing: Oxford).

Albersheim, P., A. Darvill, K. Roberts, R. Sederoff, and A. Staehelin. 2011. *Plant Cell Walls: From Chemistry to Biology* (Garland Science).

Allen, G.M. 1962. *Bats* (Dover Publications).

Amico, G., and M. A. Aizen. 2000. 'Mistletoe seed dispersal by a marsupial', *Nature*, 408: 929-30.

Andersson, S., R. Serimaa, T. Paakkari, P. Saranpaa, and E. Pesonen. 2003. 'Crystallinity of wood and the size of cellulose crystallites in Norway spruce (Picea abies)', *Journal of Wood Science*, 49: 531-37.

Ashton, N. N., D. R. Roe, R. B. Weiss, T. E. Cheatham, and R. J. Stewart. 2013. 'Self-Tensioning Aquatic Caddisfly Silk: Ca2+-Dependent Structure, Strength, and Load Cycle Hysteresis', *Biomacromolecules*, 14: 3668-81.

Atmodjo, M. A., Z. Hao, and D. Mohnen. 2013. 'Evolving views of pectin biosynthesis', *Annu Rev Plant Biol*, 64: 747-79.

Aukema, J. E. 2003. 'Vectors, viscin, and Viscaceae: mistletoes as parasites, mutualists, and resources', *Frontiers in Ecology and the Environment*, 1: 212-19.

Autumn, K., and N. Gravish. 2008. 'Gecko adhesion: evolutionary nanotechnology', *Philosophical Transactions of the Royal Society A: Mathematical, Physical and Engineering Sciences*, 366: 1575-90.

Azuma, J., N.-H. Kim, L. Heux, R. Vuong, and H. Chanzy. 2000. 'The cellulose system in viscin from mistletoe berries', *Cellulose*, 7: 3-19.

Azuma, J., and M. Sakamoto. 2003. 'Cellulosic Hydrocolloid System Present in Seed of Plants', *Trends in Glycoscience and Glycotechnology*, 15: 1-14.

Baer, A., S. Schmidt, S. Haensch, M. Eder, G. Mayer, and M. J. Harrington. 2017. 'Mechanoresponsive lipid-protein nanoglobules facilitate reversible fibre formation in velvet worm slime', *Nature Communications*, 8: 7.

Barlow, B. A. 1983. 'Biogeography of Loranthaceae and Viscaceae.' in M. Calder and P. Bernhardt (eds.), *The Biology of Mistletoes* (Academic Press: Sydney).

Barney, C. W., F. G. Hawksworth, and B. W. Geils. 1998. 'Hosts of *Viscum album*', *European Journal of Forest Pathology*, 28: 187-208.

Becker, H. 1986. 'Botany of European Mistletoe (*Viscum album* L.)', *Oncology*, 43: 2-7.

Benecke, G., W. Wagermaier, C. H. Li, M. Schwartzkopf, G. Flucke, R. Hoerth, I. Zizak, M. Burghammer, E. Metwalli, P. Muller-Buschbaum, M. Trebbin, S. Forster, O. Paris, S. V. Roth, and P. Fratzl. 2014. 'A customizable software for fast reduction and analysis of large X-ray scattering data sets: applications of the new DPDAK package to small-angle X-ray scattering and grazing-incidence small-angle X-ray scattering', *Journal of Applied Crystallography*, 47: 1797-803.

Bergander, A., and L. Salmén. 2002. 'Cell wall properties and their effects on the mechanical properties of fibers', *Journal of Materials Science*, 37: 151-56.

Bland, R. 1814. *Proverbs, chiefly taken from the Adagia of Erasmus* (T. Egerton: London).

Boespflug, R. 1964. 'Geheimnisvolle Mistelbeere', *Mikrokosmos*, 53.

Böhling, N., W. Greuter, T. Raus, B. Snogerup, S. Snogerup, and D. Zuber. 2002. 'Notes on the Cretan mistletoe, *Viscum album* subsp *creticum* subsp *nova* (Loranthaceae/Viscaceae)', *Israel Journal of Plant Sciences*, 50: S77-S84.

Bull, H. G. 1864. 'The mistletoe in Herefordshire', *Transactions of the Woolhope Naturalists' Field Club, 1852-1865*: 312-47.

Burgert, I., M. Eder, K. Frühmann, J. Keckes, P. Fratzl, and S. Stanzl-Tschegg. 2005. 'Properties of chemically and mechanically isolated fibres of spruce (*Picea abies* [L] Karst.). Part 3: Mechanical characterisation', *Holzforschung*, 59: 354 - 57.

Büssing, A. 2000. *Mistletoe: The Genus Viscum* (Harwood Academic Publishers: Amsterdam).

Calder, D. M. 1983. 'Mistletoe in Focus: An Introduction.' in M. Calder and P. Bernhardt (eds.), *The Biology of Mistletoes* (Academic Press: Sydney).

Cave, I. D. 1997. 'Theory of X-ray measurement of microfibril angle in wood .2. The diffraction diagram - X-ray diffraction by materials with fibre type symmetry', *Wood Science and Technology*, 31: 225-34.

Cordier, P., F. Tournilhac, C. Soulié-Ziakovic, and L. Leibler. 2008. 'Self-healing and thermoreversible rubber from supramolecular assembly', *Nature*, 451: 977-80.

Cosgrove, D. J. 2005. 'Growth of the plant cell wall', *Nature Reviews Molecular Cell Biology*, 6: 850-61.

Cosgrove, D. J. 2014. 'Re-constructing our models of cellulose and primary cell wall assembly', *Current Opinion in Plant Biology*, 22: 122-31.

Cosgrove, D. J., and M. C. Jarvis. 2012. 'Comparative structure and biomechanics of plant primary and secondary cell walls', *Front Plant Sci*, 3: 204.

Cox, G., N. Moreno, and J. Feijo. 2005. 'Second-harmonic imaging of plant polysaccharides', *Journal of Biomedical Optics*, 10: 6.

Darwin, C. 1859. *On the origin of species by means of natural selection, or preservation of favoured races in the struggle for life* (John Murray: London).

Deitzel, J. M., P. McDaniel, and J. W. Gillespie. 2017. 'High-performance polyethylene fibers.' in G. Bhat (ed.), *Structure and Properties of High-Performance Fibers* (Woodhead Publishing: Oxford).

Docters van Leeuwen, W. M. . 1954. 'On the Biology of some Javanese Loranthaceae and the role birds play in their life-historie', *Beaufortia*, 4: 103-207.

Driemeier, C., W. D. Santos, and M. S. Buckeridge. 2012. 'Cellulose crystals in fibrovascular bundles of sugarcane culms: orientation, size, distortion, and variability', *Cellulose*, 19: 1507-15.

Driouich, A., M.-L. Follet-Gueye, S. Bernard, S. Kousar, L. Chevalier, M. Vicré-Gibouin, and O. Lerouxel. 2012. 'Golgi-mediated synthesis and secretion of matrix polysaccharides of the primary cell wall of higher plants', *Frontiers in Plant Science*, 3: 79-79.

Eder, M. 2007. 'Structure, properties and function of single wood fibres of Norway spruce (*Picea abies* [L.] Karst.)', PhD-Thesis, BOKU-University of Natural Resources and Applied Life Sciences.

Eder, M., O. Arnould, J. W. C. Dunlop, J. Hornatowska, and L. Salmén. 2013. 'Experimental micromechanical characterisation of wood cell walls', *Wood Science and Technology*, 47: 163-82.

Eichhorn, S. J., A. Dufresne, M. Aranguren, N. E. Marcovich, J. R. Capadona, S. J. Rowan, C. Weder, W. Thielemans, M. Roman, S. Renneckar, W. Gindl, S. Veigel, J. Keckes, H. Yano, K. Abe, M. Nogi, A. N. Nakagaito, A. Mangalam, J. Simonsen, A. S. Benight, A. Bismarck, L. A. Berglund, and T. Peijs. 2010. 'Review: current international research into cellulose nanofibres and nanocomposites', *Journal of Materials Science*, 45: 1-33.

Ernst, E. 2006. 'Mistletoe as a treatment for cancer', *BMJ (Clinical research ed.)*, 333: 1282-83.

Ernst, E., K. Schmidt, and M. K. Steuer-Vogt. 2003. 'Mistletoe for cancer? A systematic review of randomised clinical trials', *International Journal of Cancer*, 107: 262-7.

Fantner, G. E., T. Hassenkam, J. H. Kindt, J. C. Weaver, H. Birkedal, L. Pechenik, J. A. Cutroni, G. A. G. Cidade, G. D. Stucky, D. E. Morse, and P. K. Hansma. 2005. 'Sacrificial bonds and hidden length dissipate energy as mineralized fibrils separate during bone fracture', *Nature materials*, 4: 612-16.

Favi, P. M., S. Yi, S. C. Lenaghan, L. Xia, and M. Zhang. 2014. 'Inspiration from the natural world: from bio-adhesives to bio-inspired adhesives', *Journal of Adhesion Science and Technology*, 28: 290-319.

Fengel, D., and G. Wegener. 1989. *Wood - Chemistry, Ultrastructure, Reaction* (De Gruyter: Berlin).

Fernandes, A. N., L. H. Thomas, C. M. Altaner, P. Callow, V. T. Forsyth, D. C. Apperley, C. J. Kennedy, and M. C. Jarvis. 2011. 'Nanostructure of cellulose microfibrils in spruce wood', *Proceedings of the National Academy of Sciences of the United States of America*, 108: E1195-E203.

Fratzl, P., and R. Weinkamer. 2007. 'Nature's hierarchical materials', *Progress in Materials Science*, 52: 1263-334.

Gedalovich-Shedletzky, E., D.P. Delmer, and J. Kuijt. 1989. 'Chemical Composition of Viscin Mucilage from Three Mistletoe Species - A comparison', *Annals of Botany*, 64: 249-52.

Gedalovich, E., and J. Kuijt. 1987. 'An Ultrastructural Study of the Viscin Tissue of *Phthirusa Pyrifolia* (HBK) Eichler (Loranthaceae)', *Protoplasma*, 137: 145-55.

Gedalovich, E., J. Kuijt, and N. C. Carpita. 1988. 'Chemical composition of viscin, an adhesive involved in dispersal of the parasite *Phoradendron californicum* (Viscaceae)', *Physiological and Molecular Plant Pathology*, 32: 61-76.

Gibson, L. J. 2012. 'The hierarchical structure and mechanics of plant materials', *Journal of the Royal Society, Interface*, 9: 2749-66.

Gilman, C. A., M. J. Imburgia, M. D. Bartlett, D. R. King, A. J. Crosby, and D. J. Irschick. 2015. 'Geckos as Springs: Mechanics Explain Across-Species Scaling of Adhesion', *Plos One*, 10: e0134604.

Gjokic, G. 1896. 'Zur Anatomie der Frucht und des Samens von *Viscum*', *Sitzungsberichte der Akademie der Wissenschaften mathematisch-naturwissenschaftliche Klasse*, 105: 447-64.

Gorb, S. N. 2005. 'Uncovering Insect Stickiness: Structure and Properties of Hairy Attachment Devices', *American Entomologist*, 51: 31-35.

Goscinny, R., and A. Uderzo. 1961. *Astérix le Gaulois* (Hachette Livre: Paris).

Grazi, G., and K. Urech. 1981. 'Einige morphologische Merkmale der Mistelbeere (*Viscum album* L.) und deren taxonomische Bedeutung', *Beiträge zur Biologie der Pflanzen*, 56: 293-306.

Grazi, G., and M. Zemp. 1986. '*Genista cinerea* DC., ein natürlicher Sammelwirt für *Viscum album* L. ssp. *album* und *Viscum album* ssp. *austriacum* (Wiesb.) Vollmann', *Berichte der Deutschen Botanischen Gesellschaft*, 99: 99-103.

Gupta, H. S., and P. Zioupos. 2008. 'Fracture of bone tissue: The 'hows' and the 'whys'', *Medical Engineering & Physics*, 30: 1209-26.

Hakansson, K. M. O., A. B. Fall, F. Lundell, S. Yu, C. Krywka, S. V. Roth, G. Santoro, M. Kvick, L. P. Wittberg, L. Wagberg, and L. D. Soderberg. 2014. 'Hydrodynamic alignment and assembly of nanofibrils resulting in strong cellulose filaments', *Nature Communications*, 5: 10.

Haller, C. M., W. Buerzle, A. Kivelio, M. Perrini, C. E. Brubaker, R. J. Gubeli, A. S. Mallik, W. Weber, P. B. Messersmith, E. Mazza, N. Ochsenbein-Koelble, R. Zimmermann, and M. Ehrbar. 2012. 'Mussel-mimetic tissue adhesive for fetal membrane repair: an ex vivo evaluation', *Acta Biomater*, 8: 4365-70.

Hawksworth, F. G. 1983. 'Mistletoe as Forest Parasites.' in M. Calder and P. Bernhardt (eds.), *The Biology of Mistletoes* (Academic Press: Sydney).

Hawksworth, F. G., and R. F. Scharpf. 1986. 'Spread of European mistletoe (*Viscum album*) in California, U.S.A', *European Journal of Forest Pathology*, 16: 1-5.

Heide-Jorgensen, H. S. 2008. *Parasitic Flowering Plants* (Brill: Leiden, The Netherlands).

Heide-Jorgensen, H. S. 2015. 'The Mistletoe *Viscum album*', Accessed 31.01.2020. http://www.viscum.dk/abstracts/text/viscum_2015_english.pdf.

Heinricher, E. 1911. 'Experimentelle Beiträge zur Frage nach den Rassen und der Rassenbildung der Mistel', *Centralblatt für Bakteriologie Abt. II*, 31: 254–86.

Heinricher, E. 1912. 'Samenreife und Samenruhe der Mistel (*Viscum album* L.) und die Umstände, welche die Keimung beeinflussen', *Sitzungsberichte der Akademie der Wissenschaften, mathematisch-naturwissenschaftliche Klasse*, 121: 573–613.

Herbst, F., D. Döhler, P. Michael, and W. H. Binder. 2013. 'Self-Healing Polymers via Supramolecular Forces', *Macromolecular Rapid Communications*, 34: 203-20.

Hinds, T. E., F. G. Hawksworth, and W. J. McGinnies. 1963. 'Seed Discharge in *Arceuthobium*: A Photographic Study', *Science*, 140: 1236.

Höfte, H., A. Peaucelle, and S. Braybrook. 2012. 'Cell wall mechanics and growth control in plants: the role of pectins revisited', *Frontiers in Plant Science*, 3.

Horbelt, N., M. Eder, L. Bertinetti, P. Fratzl, and M. J. Harrington. 2019. 'Unraveling the Rapid Assembly Process of Stiff Cellulosic Fibers from Mistletoe Berries', *Biomacromolecules*, 20: 3094-103.

Horneber, M., G. Bueschel, R. Huber, K. Linde, and M. Rostock. 2008. 'Mistletoe therapy in oncology', *Cochrane Database of Systematic Reviews*.

Jakob, H. F., D. Fengel, S. E. Tschegg, and P. Fratzl. 1995. 'The elementary cellulose fibril in Picea abies: Comparison of transmission electron microscopy, small-angle X-ray scattering, and wide-angle X-ray scattering results', *Macromolecules*, 28: 8782-87.

Jarvis, M. C. 2018. 'Structure of native cellulose microfibrils, the starting point for nanocellulose manufacture', *Philosophical Transactions of the Royal Society a-Mathematical Physical and Engineering Sciences*, 376: 13.

Jayakumar, R., M. Prabaharan, P. T. Sudheesh Kumar, S. V. Nair, and H. Tamura. 2011. 'Biomaterials based on chitin and chitosan in wound dressing applications', *Biotechnology Advances*, 29: 322-37.

Jonoobi, M., R. Oladi, Y. Davoudpour, K. Oksman, A. Dufresne, Y. Hamzeh, and R. Davoodi. 2015. 'Different preparation methods and properties of nanostructured cellulose from various natural resources and residues: a review', *Cellulose*, 22: 935-69.

Keckes, J., I. Burgert, K. Frühmann, M. Müller, K. Kölln, M. Hamilton, M. Burghammer, S. V. Roth, S. Stanzl-Tschegg, and P. Fratzl. 2003. 'Cell-wall recovery after irresversible deformation of wood', *Nature materials*, 2: 810-14.

Kennedy, C. J., G. J. Cameron, A. Sturcova, D. C. Apperley, C. Altaner, T. J. Wess, and M. C. Jarvis. 2007. 'Microfibril diameter in celery collenchyma cellulose: X-ray scattering and NMR evidence', *Cellulose*, 14: 235-46.

Kim, S. J., and F. Brandizzi. 2016. 'The plant secretory pathway for the trafficking of cell wall polysaccharides and glycoproteins', *Glycobiology*, 26: 940-49.

King, D. R., M. D. Bartlett, C. A. Gilman, D. J. Irschick, and A. J. Crosby. 2014. 'Creating Gecko-Like Adhesives for "Real World" Surfaces', *Advanced Materials*, 26: 4345-51.

Kleijnen, J., and P. Knipschild. 1994. 'Mistletoe treatment for cancer review of controlled trials in humans', *Phytomedicine*, 1: 255-60.

Klemm, D., E. D. Cranston, D. Fischer, M. Gama, S. A. Kedzior, D. Kralisch, F. Kramer, T. Kondo, T. Lindström, S. Nietzsche, K. Petzold-Welcke, and F. Rauchfuß. 2018. 'Nanocellulose as a natural source for groundbreaking applications in materials science: Today's state', *Materials Today*, 21: 720-48.

Klemm, D., F. Kramer, S. Moritz, T. Lindstrom, M. Ankerfors, D. Gray, and A. Dorris. 2011. 'Nanocelluloses: A New Family of Nature-Based Materials', *Angewandte Chemie-International Edition*, 50: 5438-66.

Kronfeld, E. F. M. 1888. 'Zur Biologie der Mistel (*Viscum album*)', *Biologisches Centralblatt*, 7: 449 - 64.

Kuijt, J. 1969. *The Biology of Parasitic Flowering Plants* (University of California Press: Berkeley).

Ladley, J. J., and D. Kelly. 1996. 'Dispersal, Germination and Survival of New Zealand Mistletoes (Loranthaceae): Dependence on Birds', *New Zealand Journal of Ecology*, 20: 69-79.

Lamont, B. 1983. 'Germination of Mistletoes.' in M. Calder and P. Bernhardt (eds.), *The Biology of Mistletoes* (Academic Press: Sydney).

Lee, B. P. , P. B. Messersmith, J. N. Israelachvili, and J. H. Waite. 2011. 'Mussel-Inspired Adhesives and Coatings', *Annual Review of Materials Research*, 41: 99-132.

LeStrange, R. 1977. *A History of Herbal Plants* (Angus and Robertson: Sydney).

Li, J., A. D. Celiz, J. Yang, Q. Yang, I. Wamala, W. Whyte, B. R. Seo, N. V. Vasilyev, J. J. Vlassak, Z. Suo, and D. J. Mooney. 2017. 'Tough adhesives for diverse wet surfaces', *Science*, 357: 378-81.

Li, S., L. Bashline, Y. Zheng, X. Xin, S. Huang, Z. Kong, S. H. Kim, D. J. Cosgrove, and Y. Gu. 2016. 'Cellulose synthase complexes act in a concerted fashion to synthesize highly aggregated cellulose in secondary cell walls of plants', *Proceedings of the National Academy of Sciences*, 113: 11348-53.

Lichtenegger, H. C., A. Reiterer, S. E. Stanzl-Tschegg, and P. Fratzl. 1999a. 'Variation of Cellulose Microfibril Angles in Softwoods and Hardwoods - A Possible Strategy of Mechanical Optimization', *Journal of Structural Biology*, 129: 257 - 69.

Lichtenegger, H., M. Müller, O. Paris, C. Riekel, and P. Fratzl. 1999b. 'Imaging of the helical arrangement of cellulose fibrils in wood by synchrotron X-ray microdiffraction', *Journal of Applied Crystallography*, 32: 1127-33.

Lindh, E. L., and L. Salmén. 2017. 'Surface accessibility of cellulose fibrils studied by hydrogen–deuterium exchange with water', *Cellulose*, 24: 21-33.

Mangenot, G., J. Rebiffe, and A. Roudier. 1948. 'Sur le mucilage du Gui', *Comptes Rendus Hebdomadaires Des Seances De L'Academie Des Sciences*, 227: 439-41.

Martínez del Rio, C., A. Silva, R. Medel, and M. Hourdequin. 1996. 'Seed Dispersers as Disease Vectors: Bird Transmission of Mistletoe Seeds to Plant Hosts', *Ecology*, 77: 912-21.

Mathiasen, R. L., D. L. Nickrent, D. C. Shaw, and D. M. Watson. 2008. 'Mistletoes: Pathology, systematics, ecology, and management', *Plant Disease*, 92: 988-1006.

Maul, K., M. Krug, D. L. Nickrent, K. F. Muller, D. Quandt, and S. Wicke. 2019. 'Morphology, geographic distribution, and host preferences are poor predictors of phylogenetic relatedness in the mistletoe genus *Viscum* L', *Molecular Phylogenetics and Evolution*, 131: 106-15.

Mittal, N., F. Ansari, V. K. Gowda, C. Brouzet, P. Chen, P. T. Larsson, S. V. Roth, F. Lundell, L. Wagberg, N. A. Kotov, and L. D. Soderberg. 2018. 'Multiscale Control of Nanocellulose Assembly: Transferring Remarkable Nanoscale Fibril Mechanics to Macroscale Fibers', *Acs Nano*, 12: 6378-88.

Moon, R. J., A. Martini, J. Nairn, J. Simonsen, and J. Youngblood. 2011. 'Cellulose nanomaterials review: structure, properties and nanocomposites', *Chemical Society Reviews*, 40: 3941-94.

Najafi, M., L. Nasri, and R. Kotek. 2017. 'High-performance nylon fibers.' in G. Bhat (ed.), *Structure and Properties of High-Performance Fibers* (Elsevier Science: Oxford).

Nakano, Y., M. Yamaguchi, H. Endo, N. A. Rejab, and M. Ohtani. 2015. 'NAC-MYB-based transcriptional regulation of secondary cell wall biosynthesis in land plants', *Frontiers in Plant Science*, 6.

Nazaruk, J., and P. Orlikowski. 2016. 'Phytochemical profile and therapeutic potential of *Viscum album* L', *Natural Product Research*, 30: 373-85.

Newman, R. H. 2008. 'Simulation of X-ray diffractograms relevant to the purported polymorphs cellulose IVI and IVII', *Cellulose*, 15: 769-78.

Newman, R. H., S. J. Hill, and P. J. Harris. 2013. 'Wide-Angle X-Ray Scattering and Solid-State Nuclear Magnetic Resonance Data Combined to Test Models for Cellulose Microfibrils in Mung Bean Cell Walls', *Plant Physiology*, 163: 1558.

Nickrent, D. L. 2002. "Mistletoe phylogenetics: Current relationships gained from analysis of DNA sequences." In *46th Western International Forest Disease Work Conference*, 48-57. Waikoloa, Hawaii.

Nickrent, D. L. 2011. 'Santalales (Including Mistletoes).' in, *eLS*.

Nierhaus-Wunderwald, D., and P. Lawrenz. 1997. *Zur Biologie der Mistel. Merkblatt für die Praxis, 28* (Eidg. Forschungsanstalt WSL: Birmensdorf).

Nishiyama, Y. 2009. 'Structure and properties of the cellulose microfibril', *Journal of Wood Science*, 55: 241-49.

Nishiyama, Y., P. Langan, and H. Chanzy. 2002. 'Crystal Structure and Hydrogen-Bonding System in Cellulose Iβ from Synchrotron X-ray and Neutron Fiber Diffraction', *Journal of the American Chemical Society*, 124: 9074-82.

Norton, D. A., and M. A. Carpenter. 1998. 'Mistletoes as parasites: Host specificity and speciation', *Trends Ecol Evol*, 13: 101-5.

Osorio-Madrazo, A., M. Eder, M. Rueggeberg, J. K. Pandey, M. J. Harrington, Y. Nishiyama, J. L. Putaux, C. Rochas, and I. Burgert. 2012. 'Reorientation of Cellulose Nanowhiskers in Agarose Hydrogels under Tensile Loading', *Biomacromolecules*, 13: 850-56.

Paquet, P. J., D. M. Knutson, R. O. Tinnin, and R. D. Tocher. 1986. 'Characteristics of Viscin from the Seeds of Dwarf Mistletoe', *Botanical Gazette*, 147: 156-58.

Paris, O., C. H. Li, S. Siegel, G. Weseloh, F. Emmerling, H. Riesemeier, A. Erko, and P. Fratzl. 2007. 'A new experimental station for simultaneous X-ray microbeam scanning for small- and wide-angle scattering and fluorescence at BESSY II', *Journal of Applied Crystallography*, 40: s466-s70.

Postek, M. T., A. E. Vládar, J. A. Dagata, N. Farkas, B. Ming, R. G. Wagner, A. Raman, R. J. Moon, R. C. Sabo, T. H. Wegner, and J. f. Beecher. 2011. 'Development of the metrology and imaging of cellulose nanocrystals', *Measurement Science and Technology*, 22: 024005.

Qiu, H., and M. G. Gilbert. 2003. '*Viscum*.' in W. Zhengyi, P. H. Raven and D. Hong (eds.), *Flora of China* (Science Press/Missouri Botanical Garden Press: Beijing).

Ramm, H., K. Urech, M. Scheibler, and G. Grazi. 2000. 'Cultivation and Development of *Viscum album* L.' in A. Büssing (ed.), *Mistletoe: The Genus Viscum* (Harwood Academic Publishers: Amsterdam).

Reid, N. 1991. 'Coevolution of mistletoes and frugivorous birds?', *Australian Journal of Ecology*, 16: 457-69.

Reid, N., N. M. Smith, and Z. Yan. 1995. 'Ecology and Population Biology of Mistletoes.' in M. D. Lowman and N. M. Nadkarni (eds.), *Forest Canopies* (Academic Press: San Diego).

Reinecke, A., L. Bertinetti, P. Fratzl, and M. J. Harrington. 2016. 'Cooperative behavior of a sacrificial bond network and elastic framework in providing self-healing capacity in mussel byssal threads', *Journal of Structural Biology*, 196: 329-39.

Reiterer, A., H. C. Lichtenegger, S. Stanzl-Tschegg, and P. Fratzl. 1999. 'Experimental evidence for a mechanical function of the cellulose microfibril angle in wood cell walls', *Philosophical Magazine A*, 79: 2173 - 84.

Restrepo, C., S. Sargent, D. J. Levey, and D.M. Watson. 2002. 'The role of vertebrates in the diversification of New World mistletoes.' in D. J. Levey, W. R. Silva and M. Galetti (eds.), *Seed dispersal and frugivory: ecology, evolution and conservation* (CAB International Press: Oxfordshire).

Ross, C. M. 2006. 'Viscin cells in the dwarf mistletoe Arceuthobium americanum - green springs'' with potential roles in explosive seed discharge and seed adhesion', *Davidsonia*, 7: 75-86.

Sallé, G. 1983. 'Germination and Establishment of *Viscum album* L.' in D. Calder and P. Bernhardt (eds.), *The Biology of Mistletoes* (Academic Press: Sydney).

Salmén, L. 2004. 'Micromechanical understanding of the cell-wall structure', *C. R. Biologies*, 327: 873 - 80.

Salmén, L. 2018. 'Wood Cell Wall Structure and Organisation in Relation to Mechanics.' in Anja Geitmann and Joseph Gril (eds.), *Plant Biomechanics: From Structure to Function at Multiple Scales* (Springer International Publishing: Cham).

Scharpf, R. F., and F. G. Hawksworth. 1976. 'Luther Burbank introduced European mistletoe into California', *Plant Disease Reporter*, 60: 740-42.

Scheller, H. V., and P. Ulvskov. 2010. 'Hemicelluloses', *Annual Review of Plant Biology*, 61: 263-89.

Snow, B. K., and D. W. Snow. 1984. 'Long-term defense of fruit by mistle thrushes *Turdus viscivorus*', *Ibis*, 126: 39-49.

Snow, B. K., and D. W. Snow. 1988. *Birds and Berries: : A Study of an Ecological Interaction* (T. and A. D. Poyser: Carolton UK).

Speck, T., and I. Burgert. 2011. 'Plant Stems: Functional Design and Mechanics', *Annual Review of Materials Research*, 41: 169-93.

Spieß, L, T Teichert, R Schwarzer, H Behnken, and G Genzel. 2009. *Moderne Röntgenbeugung* (Springer Spektrum: Heidelberg).

Stewart, R. J., J. C. Weaver, D. E. Morse, and J. H. Waite. 2004. 'The tube cement of *Phragmatopoma californica*: a solid foam', *J Exp Biol*, 207: 4727-34.

Sugiyama, J., R. Vuong, and H. Chanzy. 1991. 'Electron-Diffraction Study on the 2 Crystalline Phases Occurring in Native Cellulose from an Algal Cell-Wall', *Macromolecules*, 24: 4168-75.

Tan, L., S. Eberhard, S. Pattathil, C. Warder, J. Glushka, C. Yuan, Z. Hao, X. Zhu, U. Avci, J. S. Miller, D. Baldwin, C. Pham, R. Orlando, A. Darvill, M. G. Hahn, M. J. Kieliszewski, and D. Mohnen. 2013. 'An *Arabidopsis* Cell Wall Proteoglycan Consists of Pectin and Arabinoxylan Covalently Linked to an Arabinogalactan Protein', *The Plant Cell*, 25: 270-87.

Thoday, D. 1951. 'The endophytic system of *Viscum album*', *Journal of experimental botany*, 2: 1-19.

Thomas, B., M. C. Raj, A. K. B, R. M. H, J. Joy, A. Moores, G. L. Drisko, and C. Sanchez. 2018. 'Nanocellulose, a Versatile Green Platform: From Biosources to Materials and Their Applications', *Chemical Reviews*, 118: 11575-625.

Thomas, L. H., V. T. Forsyth, A. Martel, I. Grillo, C. M. Altaner, and M. C. Jarvis. 2014. 'Structure and spacing of cellulose microfibrils in woody cell walls of dicots', *Cellulose*, 21: 3887-95.

Thomas, L. H., V. T. Forsyth, A. Martel, I. Grillo, C. M. Altaner, and M. C. Jarvis. 2015. 'Diffraction evidence for the structure of cellulose microfibrils in bamboo, a model for grass and cereal celluloses', *Bmc Plant Biology*, 15: 7.

Thomas, L. H., V. T. Forsyth, A. Sturcova, C. J. Kennedy, R. P. May, C. M. Altaner, D. C. Apperley, T. J. Wess, and M. C. Jarvis. 2013. 'Structure of Cellulose Microfibrils in Primary Cell Walls from Collenchyma', *Plant Physiology*, 161: 465-76.

Thygesen, L. G., and P. Hoffmeyer. 2005. 'Image analysis for the quantification of dislocations in hemp fibres', *Industrial Crops and Products*, 21: 173-84.

Tomann, G. 1906. 'Vergleichende Untersuchungen über die Beschaffenheit des Fruchtschleimes von *Viscum album* L. und *Loranthus europaeus* L. und dessen biologische Bedeutung', *Sitzungsberichte der Akademie der Wissenschaften mathematisch-naturwissenschaftliche Klasse*, 115: 353-65.

Troughton, M. J. 2009. *Handbook of Plastics Joining* (William Andrew Publishing: Boston).

Tubeuf, K. Freiherr v. 1923. *Monographie der Mistel* (R. Oldenbourg: München).

Vehoff, T., A. Glišović, H. Schollmeyer, A. Zippelius, and T. Salditt. 2007. 'Mechanical Properties of Spider Dragline Silk: Humidity, Hysteresis, and Relaxation', *Biophysical Journal*, 93: 4425-32.

Voragen, A. G. J., G.-J. Coenen, R. P. Verhoef, and H. A. Schols. 2009. 'Pectin, a versatile polysaccharide present in plant cell walls', *Structural Chemistry*, 20: 263.

Waite, J. H. 2017. 'Mussel adhesion – essential footwork', *The Journal of Experimental Biology*, 220: 517-30.

Wang, B., W. Yang, J. McKittrick, and M. A. Meyers. 2016. 'Keratin: Structure, mechanical properties, occurrence in biological organisms, and efforts at bioinspiration', *Progress in Materials Science*, 76: 229-318.

Wang, Y., K. Leppänen, S. Andersson, R. Serimaa, H. Ren, and B. Fei. 2012. 'Studies on the nanostructure of the cell wall of bamboo using X-ray scattering', *Wood Science and Technology*, 46: 317-32.

Wangerin, W. 1937. 'Loranthaceae.' in O. Kirchner, E. Loew and C. Schroeter (eds.), *Lebensgeschichte der Blütenpflanzen Mitteleuropas* (Verlag E. Ulmer: Stuttgart).

Warren, B. E. 1990. *X-ray diffraction* (Dover Publications: New York).

Watson, D. M. 2004. 'Mistletoe: A Unique Constituent of Canopies Worldwide.' in Margaret D. Lowman and H. Bruce Rinker (eds.), *Forest Canopies* (Academic Press: San Diego).

Winegard, T., J. Herr, C. Mena, B. P. Lee, I. Dinov, D. Bird, M. Bernards Jr, S. Hobel, B. Van Valkenburgh, A. Toga, and D. Fudge. 2014. 'Coiling and maturation of a high-performance fibre in hagfish slime gland thread cells', *Nature Communications*, 5: 3534.

Xie, Y. J., C. A. S. Hill, Z. Jalaludin, S. F. Curling, R. D. Anandjiwala, A. J. Norton, and G. Newman. 2011. 'The dynamic water vapour sorption behaviour of natural fibres and kinetic analysis using the parallel exponential kinetics model', *Journal of Materials Science*, 46: 479-89.

Yuk, H., C. E. Varela, C. S. Nabzdyk, X. Mao, R. F. Padera, E. T. Roche, and X. Zhao. 2019. 'Dry double-sided tape for adhesion of wet tissues and devices', *Nature*, 575: 169-74.

Zhao, Q., D. W. Lee, B. K. Ahn, S. Seo, Y. Kaufman, J. N. Israelachvili, and J. H. Waite. 2016. 'Underwater contact adhesion and microarchitecture in polyelectrolyte complexes actuated by solvent exchange', *Nature materials*, 15: 407-12.

Zuber, D. 2004. 'Biological flora of central Europe: *Viscum album* L.', *Flora*, 199: 181-203.

Zuber, D., and A. Widmer. 2000. 'Genetic evidence for host specificity in the hemi-parasitic *Viscum album* L. (Viscaceae)', *Mol Ecol*, 9: 1069-73.

Zuber, D., and A. Widmer. 2009. 'Phylogeography and host race differentiation in the European mistletoe (*Viscum album* L.)', *Mol Ecol*, 18: 1946-62.

List of abbreviations

CFM	confocal fluorescence microscopy
CMF	cellulose microfibrils
CNF	cellulose nanofibrils
CNC	cellulose nanocrystals
d.wt.	dry weight
ESEM	environmental scanning electron microscopy
GPa	GigaPascal, 1 GPa = 1000 N/mm²
HC	hairy cells
MC	moisture content
MPa	MegaPascal, 1 MPa = 1 N/mm²
PLM	polarized light microscopy
RH	relative humidity
SAXS	small angle X-ray scattering
SHGM	second-harmonic generation microscopy
VaC	vacuolated cells
VCB	viscin cell bundle
VCC	viscin cell cluster
WAXS	wide angle X-ray scattering
XRD	X-ray diffraction

Danksagungen

Mein besonderer Dank gilt meiner großen und meiner „kleinen“ Liebe: Steffi und Ella, ihr seid meine Anker. Eure bedingungslose Liebe gibt mir jeden Tag die Kraft, an mich zu glauben, so dass diese Arbeit entstehen konnte.

Mein größter Dank gilt meinem Betreuer und Arbeitsgruppenleiter Matthew J. Harrington, dir mir, inspiriert durch die Sendung mit der Maus, diesen klebrigen Spaß eingebrockt hat. Ihm verdanke ich, dass sich mein persönlicher Forschungshorizont entscheidend erweitert hat. Vor allem danke ich dir dafür, dass ich fachlich aber vor allem menschlich so viel von dir lernen durfte.

Danke an Prof. Alexander Pfriem von der Hochschule in Eberswalde, der meine Begeisterung für die Wissenschaft entscheidend geprägt hat und durch den ich den Weg ans MPI gefunden habe.

Vielen Dank an meine wichtige Förderin Michaela Eder, dass ich all die Jahre immer zu dir kommen konnte und du mir bei der Lösung vieler kleiner aber auch großer Probleme geholfen hast und mir neue Perspektiven aufgezeigt hast.

Vielen Dank auch an Peter Fratzl, der mir in vielerlei Hinsicht eine wichtige Stütze und echter Mentor ist. Oft gelobt und immer noch gültig: ihm ist es zu verdanken, dass die Arbeitsatmosphäre im Department für Biomaterialien in Golm so einzigartig ist und es ein Privileg und eine Freude ist, an diesem Ort forschen zu dürfen.

Vielen Dank an meine derzeitigen und früheren Kollegen, dass es so ein schönes Gefühl ist, nach Golm rauszufahren. Besonderer Dank gilt Kerstin Gabbe, Susann Weichold, Jeannette Steffen, Petra Leibner, Christine Pilz-Allen, Ingrid Zenke, Anette Pape, Silke Nienhaus, Luca Bertinetti, Clemens Schmitt, Franziska Jehle, Tobias Priemel, Oliver Späker, Friedrich Reppe, Lucas Kuhrts sowie Stefan Siegel und Chenghao Li für die vielen schönen gemeinsamen Tage und Nächte am Bessy. Klaus Bienert gebührt großer Dank für die vielen Stunden Tüftelei am Feuchtegenerator und der technischen Unterstützung bei der mechanischen Charakterisierung. Gleiches gilt für die Kollegen aus der Metallwerkstatt: Günther Haseloff, Jan von Szada-Borryszkowksi, Marco Bott und Tobias Schmidt sowie unserem Glasbläser Cliff Janiszewski. Ohne unsere IT-Experten wäre das Experimentieren oft ein Trauerspiel: Vielen Dank an René Genz, Paul Meißner, Ralf Ditsch, Ingo Fiedler und Fridtjof Neuber.

Youssef Chebli und Anja Geitmann von der McGill Universität in Montreal danke ich für die Unterstützung zur Fluoreszenzmikroskopie. Selbiges gilt für Alexei Kazarine und Paul Wiseman von der McGill Universität für die Aufnahmen per second-harmonic generation imaging.

Und zu guter Letzt möchte ich mich bei meiner Familie bedanken: Müt, für deine offenen Ohren und dass du mir hilfst, zu erkennen, wer ich bin. Claudi und Micha für eure wertvolle Unterstützung im Alltag und euren unerschütterlichen Glauben an mich.

Eidesstattliche Erklärung

Ich erkläre an Eides statt, dass die vorliegende Dissertation in allen Teilen von mir selbständig angefertigt wurde und die benutzen Hilfsmittel vollständig angegeben worden sind. Weiter erkläre ich, dass die Angaben zu den Eigenanteilen bei Co-Autorenschaft zutreffend sind und ich nicht schon anderweitig einmal die Promotionsabsicht angemeldet oder ein Promotionseröffnungsverfahren beantragt habe. Mir ist auch bekannt, dass fahrlässige oder vorsätzlich falsche Angaben strafrechtlich verfolgt werden können.

Ort, Datum, Unterschrift